NOV 16 1964

AN INVESTIGATION OF THE SHAPE, TEMPERATURE DISTRIBUTION AND TENSION OF A HEATED FREE JET FLOWING AT ULTRA LOW REYNOLDS NUMBERS

by

LEON R. GLICKSMAN

S.B., Massachusetts Institute of Technology (1959)
S.M., Stanford University (1960)

Submitted in Partial Fulfillment
of the Requirements for the
Degree of Doctor of Philosophy

at the

MASSACHUSETTS INSTITUTE OF TECHNOLOGY

September, 1964

Signature of Author.....
Department of Mechanical Engineering

Certified by.....
Thesis Supervisor

Accepted by.....
Chairman, Departmental Committee on
Graduate Students

TABLE OF CONTENTS

		Page
ABSTRACT		i
ACKNOWLEDGEMENTS		iii
LIST OF SYMBOLS		iv
LIST OF FIGURES		vii
CHAPTER 1:	INTRODUCTION	1
CHAPTER 2:	BACKGROUND	3
2.1	General	3
2.2	The Constant Viscosity Two-Dimensional Jet Region	6
CHAPTER 3:	DERIVATION OF THE GOVERNING EQUATION ON THE JET IN THE ONE-DIMENSIONAL REGION	10
3.1	General Considerations	10
3.2	The Assumptions Used in the One-Dimensional Equations	11
3.3	A General Outline of the Analysis Used for the One-Dimensional Region	14
3.4	The Central Jet Region	16
3.5	The Upper Jet	28
CHAPTER 4:	THE SOLUTION OF THE ONE-DIMENSIONAL EQUATIONS	34
4.1	The Laminar Boundary Layer	34
4.2	The General One-Dimensional Equations	36
4.3	The Solution of the Simplified Equations	39
CHAPTER 5:	THE TEMPERATURE AND VELOCITY GRADIENTS IN THE JET WHEN THE SLOPE OF THE BOUNDARY IS SMALL	46
5.1	The Velocity Distribution	46
5.2	The Temperature Distribution	48
CHAPTER 6:	THE SHEAR STRESS AND FILM COEFFICIENT OF HEAT TRANSFER FOR A LAMINAR BOUNDARY LAYER	52

TABLE OF CONTENTS (cont'd)

		Page
CHAPTER 7:	THE PREDICTION OF THE DRAG ON THE JET DUE TO A TURBULENT BOUNDARY LAYER	60
CHAPTER 8:	A DESCRIPTION OF THE EXPERIMENTAL EQUIPMENT USED FOR THE VARIABLE VISCOSITY EXPERIMENTS	65
8.1	Experimental Procedure	69
8.2	Quantities Which Could Not Be Measured	72
8.3	Properties of the Fluid	73
8.4	Data Reduction	74
CHAPTER 9:	A COMPARISON OF THE EXPERIMENTAL AND THE THEORETICAL RESULTS	80
9.1	The Jet Shape	80
9.2	The Temperature Distribution in the Jet	88
9.3	Tension in the Jet	94
CHAPTER 10:	THE EFFECT OF THE OPERATING VARIABLES ON JET FORMATION	104
10.1	The Environment	104
10.2	Criterion for Producing Jets of a Given Final Radius	109
10.3	Upper Jet Instability	114
CHAPTER 11:	CONCLUSIONS	117
CHAPTER 12:	RECOMMENDATIONS	119
REFERENCES		121
APPENDIX A:	TABULATED RESULTS AND ERROR ANALYSIS	A-1
APPENDIX B:	GOVERNING EQUATIONS, TWO DIMENSIONAL EQUATIONS AND BOUNDARY CONDITIONS FOR A CONSTANT VISCOSITY JET	B-1
B.1	Governing Equation	B-1
B.2	Boundary Conditions	B-3
B.3	Free Surface Boundary Conditions	B-6
B.4	Simplifications of the Boundary Conditions	B-16

TABLE OF CONTENTS (cont'd)

Page

APPENDIX C: A CONSIDERATION OF VARIOUS METHODS TO SOLVE THE GENERAL CONSTANT VISCOSITY DIFFERENTIAL EQUATION AND BOUNDARY CONDITIONS..... C-1

C.1 A Closed Form Solution..... C-1

C.2 Solution by Finite Differences Using the Relaxation Method..... C-3

C.3 Solution by Calculus of Variations..... C-4

C.4 Solution By Series..... C-5

C.5 Discussion of the Solution of the Differential Equation and Boundary Conditions..... C-8

APPENDIX D: THE EXPERIMENTS USING CONSTANT VISCOSITY FLUID..... D-1

D.1 General..... D-1

D.2 Qualitative Results..... D-1

D.3 Description of the Experimental Apparatus D-2

D.4 Further Results..... D-4

APPENDIX E: A STABILITY CRITERION FOR THE CONSTANT VISCOSITY JET..... E-1

APPENDIX F: COMPUTER PROGRAMS..... F-1

APPENDIX G: ADDITIONAL FIGURES..... G-1

BIOGRAPHICAL NOTE

AN INVESTIGATION OF THE SHAPE, TEMPERATURE DISTRIBUTION AND TENSION OF A HEATED FREE JET FLOWING AT ULTRA LOW REYNOLDS NUMBERS

by

LEON R. GLICKSMAN

Submitted to the Department of Mechanical Engineering on September 8, 1964, in partial fulfillment of the requirements for the degree of Doctor of Philosophy.

ABSTRACT

One method of spinning polymers or inorganic materials into fibers is based upon formation of the material into a viscous liquid jet. In many instances, a vertical jet is produced by forcing the molten material through a small nozzle. The jet is simultaneously cooled by convection and radiation and the jet radius is attenuated under mechanical tension.

The present study has been limited to the axi-symmetric flow of a hot jet of Newtonian fluid, the viscosity of the fluid changing rapidly with changes in temperature.

A one-dimensional analysis has been developed which predicts the shape, temperature distribution and tension in the jet as a function of fluid and environmental properties, flow rate, initial jet temperature, initial jet radius, initial jet slope, and final jet radius. Experimental verification of the shape and tension predictions has been made; temperature measurements have not been made because the size of the jets is extremely small.

The one-dimensional analysis has been found to be invalid within three to four nozzle diameters of the nozzle exit; below this point the theory and experimental results has been found to be in agreement. The radius predicted for any given position along the jet agrees with the measured radius within 15 per cent for cases where the initial jet radius has been attenuated by a factor of 100. The tension in the jet, measured where the jet has solidified agrees with the predicted tension within 20 per cent.

The theory predicts the limiting conditions under which a jet may be formed and indicates that laminar forced convection heat transfer occurring in the region where the jet is being attenuated and turbulent shear stress occurring below this region have a dominating influence on the jet.

Thesis Supervisor: Kenneth R. Wadleigh

Title: Professor of Mechanical Engineering

ACKNOWLEDGEMENTS

I am indebted to Professor Kenneth R. Wadleigh whose guidance and encouragement throughout the course of this investigation proved invaluable. I would like to thank the other members of my thesis committee, Professor George A. Brown and Professor Peter Griffith, for many helpful suggestions and thorough discussions of the work.

I would like to thank Drs. C. L. Roberson, R. Machlan and C. McKinnis of Owens-Corning Fiberglas for allowing me to draw on their wealth of experience while conducting all phases of the program.

I would also like to thank Miss Nancy Di Benedetto who typed the many drafts of the manuscript.

This program was supported by a Grant-in-Aid from the Owens-Corning Fiberglas Corporation. This work was done in part at the Computation Center at the Massachusetts Institute of Technology.

LIST OF SYMBOLS

A	non-dimensional $a_2(T_E - T_{ATM})$
a_1, a_2	terms in the expression for the fluid viscosity $\ln(\mu) = a_1 - a_2 T$
B	non-dimensional $r_E k_{ATM} C_L / w c_p$
C_F	drag coefficient $\tau_\infty / 1/2 \rho U_\infty^2$
C_L	non-dimensional shear stress $\tau_\infty 2\pi r_o / \mu_{ATM} U_\infty$
c_p	specific heat of the jet fluid
h	film coefficient of heat transfer
k	thermal conductivity of the jet fluid
L	length of the upper jet region
$(Nu)_z$	Nusselt Number, hz/k_{ATM}
p	pressure of the jet fluid
Po	percentage of the total radiation energy for which the material is opaque
p_T	percentage of the total radiation energy for which the material is transparent
Q	volume rate of flow
$\dot{q}$	heat flux
$\dot{q}/A$	heat flux per unit area

r	radial co-ordinate
r_{FINAL}	the final value of the jet radius
r_o	the radius of the jet
$(Re)_{r_o}$ $(Re)_z$	Reynolds Number, $v\ r_o/\nu$ and $v\ z/\nu$ respectively
R_1	radius of curvature of the jet surface in the r-z plane
R_o	the initial jet radius
T	the jet temperature
T_{ATM}	temperature of the environment far away from the jet
(Tension)	the axial tension in the jet
U_∞	the velocity of the jet surface, used to evaluate τ_∞
v_r	component of the velocity in the radial direction
v_z	component of the velocity in the axial direction
W_{B_λ}	monochromatic emmisive power of a black surface
w	mass rate of flow
z	axial co-ordinate
ν_λ	monochromatic absorption coefficient
γ_T	surface tension of jet fluid
δ	thickness of the velocity boundary layer
δ_T	thickness of the thermal boundary layer

ϵ	emmisivity of the jet surface
ϵ_m	eddy diffusivity
θ	angle between tangent to jet surface and axial direction
λ	wave length
μ	viscosity of the jet fluid
ν_{ATM}	kinematic viscosity of the environment
ρ	density of the jet fluid
σ	Stefan-Boltzmann constant
τ_∞	shear stress on the jet surface
ψ	stream function in cylindrical co-ordinates

Subscripts and Superscripts:

$( )_E$	conditions at the end of the upper jet region, the beginning of the central jet region
$( )_o$	conditions at the beginning of the jet, at the nozzle exit
$( )_{ATM}$	conditions of the environment, the properties are evaluated at the film temperature, the average of the jet surface temperature and environmental temperature, T_{ATM}
$\bar{( )}$	quantities non-dimensionalized by dividing by the same quantity evaluated at position E, e.g., $\bar{T} = T/T_E$

LIST OF FIGURES

Fig. No.		Page
2.1	THE JET	5
3.1	AN ELEMENT OF DIFFERENTIAL LENGTH IN THE CENTRAL JET REGION	18
3.2	VISCOSITY VS. TEMPERATURE FOR GLASS	23
3.3	ABSORPTION COEFFICIENT VS. WAVELENGTH DISTRIBUTION ASSUMED FOR GLASS	26
3.4	THE UPPER JET REGION	30
6.1	LAMINAR BOUNDARY LAYER SHEAR STRESS	56
6.2	THE STEADY STATE BOUNDARY LAYER ON A CYLINDER	58
7.1	DRAG COEFFICIENT VS. REYNOLDS NUMBER LAMINAR AND TURBULENT BOUNDARY LAYER FLOW ALONG THE AXIS OF A CYLINDER	63
8.1	SCHEMATIC OF EXPERIMENTAL SET UP	67
8.2	THE NOZZLE	68
8.3	THE TENSOMETER	70
8.4	VISCOSITY VS. TEMPERATURE FOR GLASS	75
8.5	PHOTOGRAPHS OF THE JET	76
8.6	PHOTOGRAPHS OF THE JET	77
9.1	JET RADIUS VS. DISTANCE	81
9.2	JET RADIUS VS. DISTANCE	82
9.3	JET RADIUS VS. DISTANCE	83

Fig. No.		Page
9.4	JET RADIUS VS. DISTANCE	85
9.5	JET RADIUS VS. DISTANCE	86
9.6	JET RADIUS VS. DISTANCE	89
9.7	JET RADIUS VS. DISTANCE	90
9.8	TEMPERATURE (THEORETICAL) VS. DISTANCE ASSUMING DIFFERENT VALUES FOR THE SPECIFIC HEAT OF THE GLASS	92
9.9	TEMPERATURE (THEORETICAL) VS. DISTANCE ASSUMING DIFFERENT VALUES FOR THE INITIAL TEMPERATURE	93
9.10	TEMPERATURE (THEORETICAL) VS. DISTANCE	95
9.11	TEMPERATURE (THEORETICAL) VS. DISTANCE	96
9.12	TENSION VS. DISTANCE	98
9.13	TENSION VS. DISTANCE	99
9.14	TENSION VS. DISTANCE	100
9.15	DRAG COEFFICIENT VS. REYNOLDS NUMBER	102
10.1	JET RADIUS VS. DISTANCE	105
10.2	TEMPERATURE VS. DISTANCE	106
Appendices:		
B-1	AN ELEMENT OF THE FLUID AT THE SURFACE	B-7
B-2	THE FORCES ACTING ON A FLUID ELEMENT	B-8
B-3	THE SURFACE "SKIN" SHOWING THE FORCES THAT ACT ON IT	B-12

Fig. No.		Page
E-1	THE TRANSITION FROM DRIPPING TO FLOWING.....	E-5
G-1	JET RADIUS VS. DISTANCE.....	G-2
G-2	JET RADIUS VS. DISTANCE.....	G-3
G-3	JET RADIUS VS. DISTANCE.....	G-4

CHAPTER I

INTRODUCTION

One method of spinning polymers or inorganic materials into fibers is based upon formation of the material into a viscous liquid jet. In many instances, a vertical jet is produced by forcing the molten material through a small nozzle. The jet is simultaneously cooled and the radius is attenuated under mechanical tension. The solidified jet is wound on a rotating pulling wheel, which maintains the tension in the fiber.

The object of this investigation is to develop an analysis, verified by experiments, which will predict the steady state shape, temperature distribution, axial tension in the jet and the stability of jet as a function of the fluid properties and the process variables, e.g., the pulling speed and the ambient conditions.

The present investigation is limited to the study of a single material, glass, which was processed under the following conditions for this research program: the glass was kept in an electrically heated reservoir at a temperature of 2200°F or above; it was forced through a single nozzle at the bottom of the reservoir by the application of a very low positive pressure on the reservoir, the pressure at the nozzle entrance being at most thirty inches of

water above atmospheric pressure; the nozzle was cylindrical in shape with a constant inner diameter of 0.067 inches; the diameter Reynolds number based upon conditions at the nozzle exit was less than one.

The hot fluid leaving the nozzle formed an axi-symmetric jet which was attenuated while simultaneously being cooled by radiation and forced convection. The jet was attenuated to radii as small as 2.5×10^{-4} inches with a final velocity as high as 170 ft/second.

The viscosity of the attenuating jet was a strong function of the fluid temperature, e.g., when the temperature dropped from 2400°F to 2300°F, the viscosity doubled.

CHAPTER 2

BACKGROUND

2.1 General

Although voluminous works appear on the subject of jets flowing at high Reynolds numbers and on the subject of submerged jets, see for example references (1) and (2)[1], the author was unable to find any published works dealing with the flow of a low Reynolds number free Newtonian jet of variable viscosity. Studies of a related subject, the spinning of polymers, which have appeared in textile journals (3), (4), are not applicable to the case at hand because polymers are not Newtonian fluids and the solutions presented in the literature are based upon unrealistic assumptions, e.g., assuming the viscosity is constant.

In the present work, the simplified case of a fluid jet with a constant viscosity was studied both experimentally and analytically as a first step to the solution of the actual case. Obviously, for the real case where the jet is cooled and attenuated, the assumption of a constant viscosity is far from correct. However, it was felt

---

[1] Numbers in parentheses refer to References given on page 121.

that the techniques developed to solve the constant viscosity case might be extended to the variable viscosity case. Attention was focused on obtaining the solution for the velocity distribution and shape of the constant viscosity jet immediately below the nozzle exit, referred to in Fig. 2.1 as the upper jet region. After writing the governing equation of motion for the upper jet with its associated boundary conditions, an unsuccessful attempt was made to solve the equations both in closed form and by approximate techniques.

Concurrently, constant viscosity jets were studied experimentally. The results only lead to an approximate empirical method for representing the shape of the upper jet.

Because of the difficulties in obtaining a solution for the upper jet region, it was later decided to ignore that region and to focus attention on a solution applicable to the region below the upper jet--the central jet region, where the governing equations can be simplified. Although the study of the constant viscosity upper jet did not bear fruitful results, a detailed discussion of the early work will demonstrate why the simpler solution for the central jet does not rigorously apply to the upper jet and why it was necessary to revert back to the simplified equations.

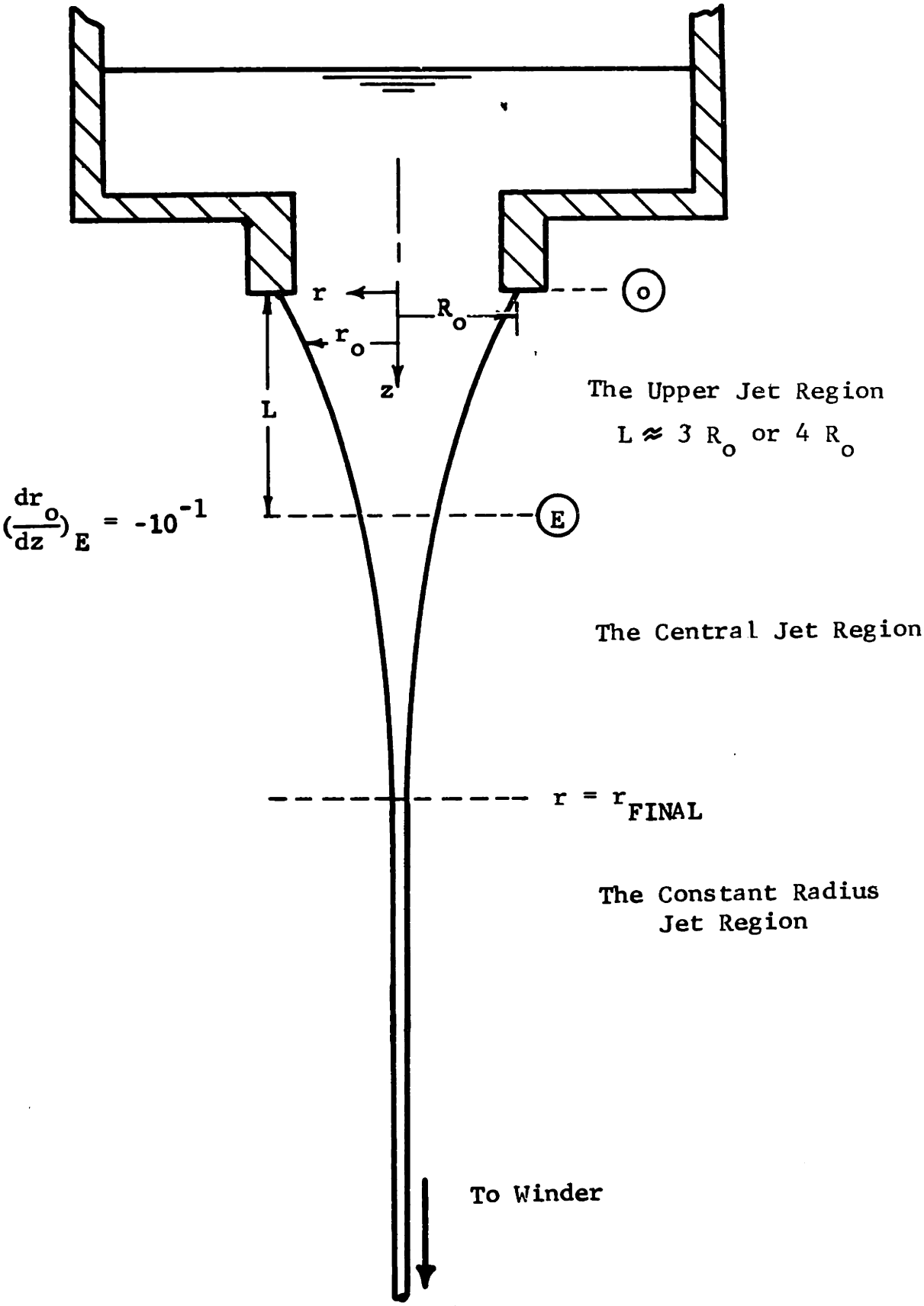

Fig. 2.1
THE JET

2.2 The Constant Viscosity Two-Dimensional Jet Region

In the upper jet region, consideration will be limited to cases where the Reynolds number is less than one. Therefore, in the governing dynamical equations, the Navier-Stokes equations, the inertial terms can be neglected in favor of the viscous terms. Generally, this condition can be described as creeping flow.

Assuming steady, axi-symmetric flow the equations can be written in cylindrical co-ordinates in terms of the stream function as:

$$E^2(E^2\varphi) = 0^* \tag{2.1}$$

where

$$E^2 = \frac{\partial^2}{\partial z^2} - \frac{1}{r}\frac{\partial}{\partial r} + \frac{\partial^2}{\partial r^2} \tag{2.2}$$

$$v_z = \frac{1}{r}\frac{\partial \varphi}{\partial r} \quad ; \quad v_r = -\frac{1}{r}\frac{\partial \varphi}{\partial z} \tag{2.3}$$

The associated boundary conditions for the free surface are non-linear and complex. In contrast to the simple no-slip conditions at a solid wall, the free surface boundary conditions must be written in terms of the forces acting on the boundary. At the

---

* For a complete list of symbols, please refer to page iv.

boundary between the fluid and its environment, the normal and shear forces in both mediums must be equal. The free surface boundary conditions, written in terms of the velocity components, are in the normal direction

$$p\left[1+\left(\frac{dr_o}{dz}\right)^2\right]+2\mu\left[-\frac{\partial v_r}{\partial r}+\frac{dr_o}{dz}\left(\frac{\partial v_r}{\partial z}+\frac{\partial v_z}{\partial r}\right)-\frac{\partial v_z}{\partial z}\left(\frac{dr_o}{dz}\right)^2\right] \qquad (2.4)$$
$$=\left[1+\left(\frac{dr_o}{dz}\right)^2\right]\left[p_{ATM}+\gamma_T\left(\frac{\cos\theta}{r_o}-\frac{1}{R_1}\right)\right]$$

In the tangential direction

$$\mu\left[\frac{\partial v_r}{\partial z}+\frac{\partial v_z}{\partial r}\right]\left[1-\left(\frac{dr_o}{dz}\right)^2\right]+\mu\frac{dr_o}{dz}\left(\frac{\partial v_r}{\partial r}-\frac{\partial v_z}{\partial z}\right) \qquad (2.5)$$
$$=\left[1+\left(\frac{dr_o}{dz}\right)^2\right]\left[\tau_\infty-\frac{\partial \gamma_T}{\partial z}\cos\theta\right]$$

where $dr_o/dz = v_r/v_z$.

For the cases to be studied, the contact angle between the liquid and the outside surface of the nozzle is small; thus, the initial slope of the jet boundary is large, i.e., the order of magnitude of dr_o/dz at the nozzle exit is one. Therefore, in the upper jet the radial component of the jet velocity near the jet surface is of the same order of magnitude as the axial component of the jet velocity. In addition, since the velocity on the surface of the free jet is not constrained to be zero, there is insufficient in-

formation to permit an estimation of the order of magnitude of the viscous terms in either the boundary conditions or the Navier-Stokes equations to be made. Consequently, for the upper jet, no simplifying assumptions to the creeping flow equations can be made, rather the equations must be solved in their general form.

The solution of the problem must also specify the location of the boundaries. All of the proposed methods of solution envisioned numerical techniques involving very lengthy digital computer solutions (see Appendix C).

For the actual case of a variable viscosity fluid additional complications arise because the Navier-Stokes equations are non-linear. In addition, the fluid dynamic and heat transfer equations must be solved simultaneously since the viscosity is a strong function of the fluid temperature, and the heat transfer from the jet depends upon the shape of the jet. In view of these complications, the attempt to find the exact solution for the upper jet was abandoned. Instead, an attempt was made to find an approximate technique which would qualitatively predict the upper jet shape and temperature distribution.

In conjunction with the search for an analytical solution for the constant viscosity upper jet region, a limited number of constant viscosity jet experiments were conducted (see Appendix D

for a complete description of the experiments). The experiments qualitatively indicated that once a steady axi-symmetric jet was established, the shape was smooth, i.e., the radius approached an axi-symmetric value without any discontinuities in the rate of change of the jet slope. Therefore, it was assumed that the shape of the upper jet could be approximated by a series of the form

$$r_o = C_o + \frac{C_1}{(z+z_o)} + \frac{C_2}{(z+z_o)^2} + \frac{C_3}{(z+z_o)^3} \qquad (2.6)$$

where the constants are determined by the initial radius and slope and the radius and slope at the end of the upper jet region. The use of such a technique ignores the equations of motion of the fluid. It will be shown later that a simpler and physically more plausible approach gives results for the upper jet region which are as good as the curve fitting technique.

In the region below the upper jet where the slope of the jet boundary is less than minus one-tenth, simplifying one-dimensional assumptions can be made which allow a solution to be obtained for the variable viscosity case.

The succeeding chapters will describe the one-dimensional solution. An overall analysis of the upper jet from the nozzle exit to the beginning of the one-dimensional solution will be used to obtain the initial conditions for the one-dimensional solution.

CHAPTER 3

DERIVATION OF THE GOVERNING EQUATION OF THE JET IN THE ONE-DIMENSIONAL REGION

3.1 General Considerations

In the preceding chapter, it was pointed out that an analytical solution of the two-dimensional variable viscosity case would be very lengthy and complex. Referring to Fig. 2.1, in the region defined as the upper jet region, extending a length equal to three or four initial jet radii from the nozzle exit, simplifications of the governing two-dimensional dynamical relations can not be justified. Below the upper jet where the slope of the jet boundary is small, defined as the central jet region in Fig. 2.1, the governing relations for the case of the variable viscosity jet can be simplified by assuming the velocity, pressure and temperature are uniform over any cross section, i.e., the distribution of velocity, pressure and temperature is one-dimensional. The one-dimensional equations will be solved to yield the jet shape, the velocity, temperature and tension distribution in the jet.

In the present chapter, the one-dimensional equations for the variable viscosity jet will be derived. In the next chapter a solution of the one-dimensional equations will be given when it is

further assumed that the environmental boundary layer on the jet surface is laminar.

In Chapter 5 it will be proved that when the slope of the jet boundary is less than or equal to one-tenth, the radial gradient of velocity is negligible compared to the axial velocity gradient and the calculated axial temperature gradient is in error by not more than 10 per cent when the temperature gradient in the radial direction is assumed to be zero.

Before the one-dimensional equations are presented, the assumptions used in writing the equations will be listed and an estimation of the variation of the tension in the upper jet will be made.

The tension is defined as the net normal force on a given cross section of the jet which tends to resist attenuation of the jet. The tension is composed of surface tension forces and viscous forces. Obviously, if a jet exists in an environment at a constant pressure, the level of the environmental pressure can not directly affect the attenuation process.

3.2 The Assumptions Used in the One-Dimensional Equations

As mentioned previously, the assumption that the fluid velocity and temperature are one dimensional will be shown in Chapter 5 to be

valid for the central jet region. It also will be assumed that the pressure distribution is one dimensional.

The analysis will be restricted to the axi-symmetric steady flow of a Newtonian fluid which has a constant specific heat, density, surface tension, and absorption coefficient versus wavelength. The viscosity is not constant, rather it will be shown that the variation of viscosity with temperature has an important influence on the jet flow.

In estimating the tension distribution in the upper jet, it is necessary to calculate the tension in the jet at its initial point, at the nozzle exit. A rigorous calculation of the tension in the upper jet depends upon a knowledge of the two-dimensional velocity and viscosity distributions at the nozzle exit. In order to find the two-dimensional distributions, the equation of motion and the energy equation must be solved for the region encompassing the nozzle exit and the upper jet. Since the two-dimensional solution is not available, the tension will be calculated in the upper jet assuming the velocity and viscosity distribution are one-dimensional.

The one-dimensional equations will be developed so that the jet shape, the velocity and temperature distribution and the tension in the jet can be found if the following quantities are specified:

(a) The physical properties of the fluid, e.g., the density, surface tension, and the viscosity versus temperature

(b) The physical properties of the environment, e.g., the density and the thermal conductivity,

(c) The flow rate

(d) The final jet radius

(e) The conditions at the nozzle exit:

the temperature

the initial jet radius

the initial slope of the jet surface

(f) The characteristics of the boundary layer which forms on the jet surface (given in Chapter 4).

The conditions at the nozzle exit, which are needed to calculate the tension can not be predicted at present for a given nozzle geometry, flow rate and reservoir temperature. The initial jet radius and the initial slope are dependent upon the contact angle phenomena between the fluid and the nozzle. In many cases, the fluid wets the nozzle and spreads out along the outside surface of the nozzle. Therefore, the contact angle and initial jet radius can only be found experimentally. To predict the initial jet temperature, a heat transfer analysis of the nozzle and the upper jet

is necessary. At present, it will be assumed that the initial fluid temperature equals the temperature of the outside nozzle surface, which can be measured. In cases where the initial conditions have not been measured, values measured in previous experiments performed at similar conditions will be used.

3.3 A General Outline of the Analysis Used for the One-Dimensional Region

In order to obtain a solution of the governing equations for the region where the one-dimensional assumptions apply, a consideration of many diverse topics must be made. As an aid to the reader, an outline of the analysis will be given below. The assumptions necessary for each step in the analysis will be included in the outline. Quantities will be classified as known if they are included in the list given on page 13 or if they can be obtained from the results of a previous step. All other quantities will be classified as unknown.

The equations of momentum and energy are written in differential form in Section 3.4 for the case of axi-symmetric, steady flow. It is assumed that the velocity, temperature and pressure are constant for any cross section. All fluid properties except the viscosity are assumed to be constant. In Chapter 5, the assumptions of one-

dimensional and temperature distribution will be proved to be valid when the slope of the jet surface is less than one tenth. The upper boundary of the one-dimensional region will be defined as the point where the slope is minus one-tenth, defined as position 'E'. The position where the jet radius becomes constant, defined as the final radius, will be taken as the lower boundary of the one-dimensional region. The one-dimensional equations and their associated boundary conditions are written in terms of the flow rate and fluid properties, known quantities, and in terms of the film coefficient of heat transfer and the shear stress at the jet surface, and the value of the jet radius and the temperature at position 'E', the latter four quantities are unknown.

In order to find one expression relating the unknown values of r_E and T_E to known quantities, a relationship between the tension at the nozzle exit and the tension at position E is found in Section 3.5. It is assumed that the initial tension can be calculated from the expressions derived when the velocity and temperature are one-dimensional. To calculate the initial tension, the flow rate, the initial jet radius, slope and temperature, all known quantities, are used. The results of the upper jet analysis show that the tension is a constant in the upper jet. Therefore, the initial tension can be set equal to the tension

at the end of the upper jet, point E; the tension at point E written in terms of r_E and μ_E.

In Chapter 4, the surface shear stress and film heat transfer coefficient are predicted based upon the assumptions that the environmental boundary layer on the jet surface is laminar and is analogous to the boundary layer on a solid right circular cylinder moving in the axial direction. A detailed discussion of the laminar boundary layer solution will be presented in Chapter 6. In succeeding sections of Chapter 4, two solutions for the one-dimensional equations will be presented, the general solution for the complete, non-linear equations and the closed form solution of the simplified, linear equations.

3.4 The Central Jet Region

In the present section, the momentum and energy equations for the jet will be derived for the case where the velocity, temperature and pressure are assumed to be constant across any given cross section. It will be shown in Chapter 5 that the one-dimensional assumption for velocity and temperature are valid when the slope of the jet is less than minus one-tenth. Therefore, the region of the jet where the one-dimensional equations will be applied, called the central jet region, will be defined to extend from the point where the slope is minus one-tenth down to the point

where the radius becomes constant. The solution of the equa indicates that the final radius is approached asymptotically therefore, the end of the central jet region will be alterna defined for numerical solutions as the point at which the je radius is within one half of one per cent of the final fiber radius and the slope of the jet surface is less than 10^{-4}.

Turning to the momentum equation first, assuming all fl properties except the viscosity are constant, the momentum equation in differential form is, referring to Fig. 3.1

$$\frac{d}{dz}(w\, v_z)dz = \frac{d}{dz}((F)_{viscous} - \int pdA)dz + \rho g\pi\, r_o^2 dz$$

$$+ \frac{d}{dz}(2\pi r_o \gamma_T \cos\theta)dz - \tau_\infty\, 2\pi r_o \cos\theta$$

$$+ p_{ATM}\, 2\pi r_o \sin\theta\, dz$$

Considering the term in (3.1) containing the viscous normal and the fluid pressure,

$$(F)_{viscous} - \int pdA = (F)_{viscous} - p\pi r_o^2$$

For cylindrical co-ordinates,

$$(F)_{viscous} - p\pi r_o^2 = (2\mu \frac{\partial v_z}{\partial z} - p)\pi r_o^2$$

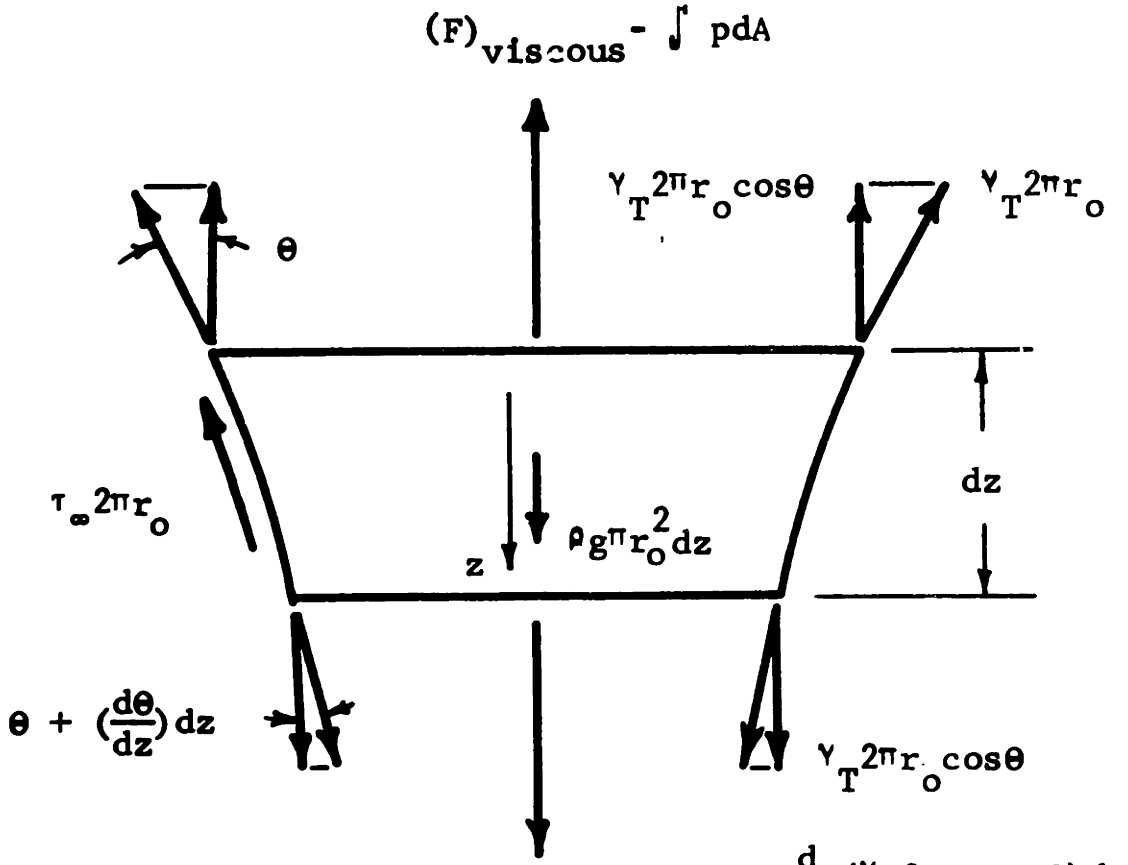

AN ELEMENT OF DIFFERENTIAL LENGTH
IN THE CENTRAL JET REGION

Fig. 3.1

The continuity equation for steady one-dimensional flow is

$$v_z = \frac{w}{\rho\pi r_o^2} \tag{3.4}$$

$$\frac{\partial v_z}{\partial z} = -\frac{2w}{\rho\pi r_o^3}\frac{dr_o}{dz} = -\frac{2v_z}{r_o}\left(\frac{dr_o}{dz}\right) \tag{3.5}$$

The pressure can be found from the boundary condition in the normal direction, Eq. (2.4), simplified for the case of small (dr_o/dz)

$$p = 2\mu\frac{\partial v_r}{\partial r} + p_{ATM} + \gamma_T\frac{\cos\theta}{r_o} \tag{3.6}$$

and from the continuity equation in differential form, at the jet boundary

$$\left(\frac{\partial v_r}{\partial r}\right)_{r_o} = -\left(\frac{\partial v_z}{\partial z}\right)_{r_o} - \frac{v_r}{r_o} = +\frac{2v_z}{r_o}\left(\frac{dr_o}{dz}\right) - \frac{v_z}{r_o}\frac{dr_o}{dz} = \frac{v_z}{r_o}\frac{dr_o}{dz} \tag{3.7}$$

using

$$\left(\frac{v_r}{v_z}\right)_{r_o} = \frac{dr_o}{dz} \tag{3.8}$$

Substituting Eq. (3.8) into the equation for the pressure 3.6,

$$p = \frac{2\mu v_z}{r_o}\frac{dr_o}{dz} + p_{ATM} + \gamma_T\frac{\cos\theta}{r_o} \tag{3.9}$$

Equation (3.3) can now be written as

$$F_{viscous} - p\pi r_o^2 = -\frac{6\mu v_z}{r_o}\frac{dr_o}{dz} - p_{ATM} - \gamma_T\left(\frac{\cos\theta}{r_o}\right) \tag{3.10}$$

The momentum equation can now be written as

$$\frac{d}{dz}\left(\frac{\rho Q^2}{\pi r_o^2}\right) = \frac{d}{dz}\left(-\frac{6\mu Q}{r_o}\frac{dr_o}{dz} - \gamma_T \pi r_o \cos\theta\right) + \rho g \pi r_o^2 + \frac{d}{dz}\left(2\pi r_o \gamma_T \cos\theta\right) - \tau_\infty 2\pi r_o \cos\theta \tag{3.11}$$

Combining the term containing the surface tension,

$$\frac{d}{dz}\left(\frac{\rho Q^2}{\pi r_o^2}\right) = \frac{d}{dz}\left(-\frac{6\mu Q}{r_o}\frac{dr_o}{dz} + \pi r_o \gamma_T \cos\theta\right) + \rho g \pi r_o^2 - \tau_\infty 2\pi r_o \cos\theta \tag{3.12}$$

The term $(-6\mu Q/r_o \; dr_o/dz + \pi r_o \gamma_T \cos\theta)$ is the net force acting normal to the cross section and is therefore the expression for the tension when the velocity is assumed to be one-dimensional.

The boundary conditions for Eq. (3.12) are,

at $z = o$ defined as the point where

$dr/dz = -1/10$

$r_o = r_E$

$\mu = \mu_E$

and as

$$z \longrightarrow \infty$$

$$r_o \longrightarrow r_{FINAL}$$

At the present stage of the analysis r_E and μ_E must be considered unknowns along with the shear stress on the jet surface, τ_∞. Since $\left|dr_o/dz\right| \leq 10^{-1}$ or $\theta \leq 6°$ for the central jet, small angle approximations will be used

$$\frac{-2\rho Q}{\pi r_o^3}\frac{dr_o}{dz} = -\frac{6Q}{r_o}\frac{dr_o}{dz}\frac{d\mu}{dz} + \frac{6\mu Q}{r_o^2}\left(\frac{dr_o}{dz}\right)^2 - \frac{6\mu Q}{r_o}\frac{d^2r_o}{dz^2} \qquad (3.13)$$

$$+ \rho g \pi r_o^2 + \gamma_T \pi \cos\theta \frac{dr_o}{dz} - \gamma_T \pi r_o \frac{dr_o}{dz}\left(\frac{d^2r_o}{dz^2}\right)$$

$$- \tau_\infty 2\pi r_o$$

The equations will now be written in non-dimensional form using the definitions

$$\bar{r} = r/r_E \qquad (\bar{r} = 1 \text{ when } dr_o/dz = -1/10) \qquad (3.14)$$

$$\bar{z} = z/r_E$$

$$\bar{\mu} = \mu/\mu_E$$

The momentum equation becomes:

$$\frac{d^2\bar{r}}{d\bar{z}^2}\left[1+\left(\frac{\gamma_T \pi r_E^2}{6\mu_E Q}\right)\frac{\bar{r}^2}{\bar{\mu}}\frac{d\bar{r}}{d\bar{z}}\right]=\left(\frac{\rho g \pi r_E^4}{6\mu_E Q}\right)\frac{\bar{r}^3}{\bar{\mu}}-\frac{\pi r_E^3}{3\mu_E Q}\frac{\bar{r}^2}{\bar{\mu}}\tau_\infty$$
$$+\frac{d\bar{r}}{d\bar{z}}\left[\frac{1}{\bar{r}}\frac{d\bar{r}}{d\bar{z}}+\left(\frac{\gamma_T \pi r_E^2}{6\mu_E Q}\right)\frac{\bar{r}}{\bar{\mu}}+\left(\frac{\rho Q}{3\pi r_E \mu_E}\right)\frac{1}{\bar{r}^2\bar{\mu}}-\frac{d\ln\bar{\mu}}{d\bar{z}}\right] \tag{3.15}$$

The boundary conditions associated with Eq. (3.15) are:

$$\text{at } \bar{z}=0 \tag{3.16}$$
$$\bar{\mu}=1$$
$$\bar{r}=1$$
$$d\bar{r}/d\bar{z}=-1/10$$
$$\text{at } z\to\infty$$
$$\bar{r}\to\bar{r}_{FINAL}=r_{FINAL}/r_E$$

The last term in Eq. (3.15) contains the rate of change of the viscosity of the fluid. Since the viscosity is related to the temperature for the fluid under consideration, by an expression of the form, (Fig. 3.2)

$$\ln\mu=a_1-a_2 T \tag{3.17}$$

the last term serves to couple the equation of motion to the temperature distribution in the jet. To find the temperature, the energy equation must be solved.

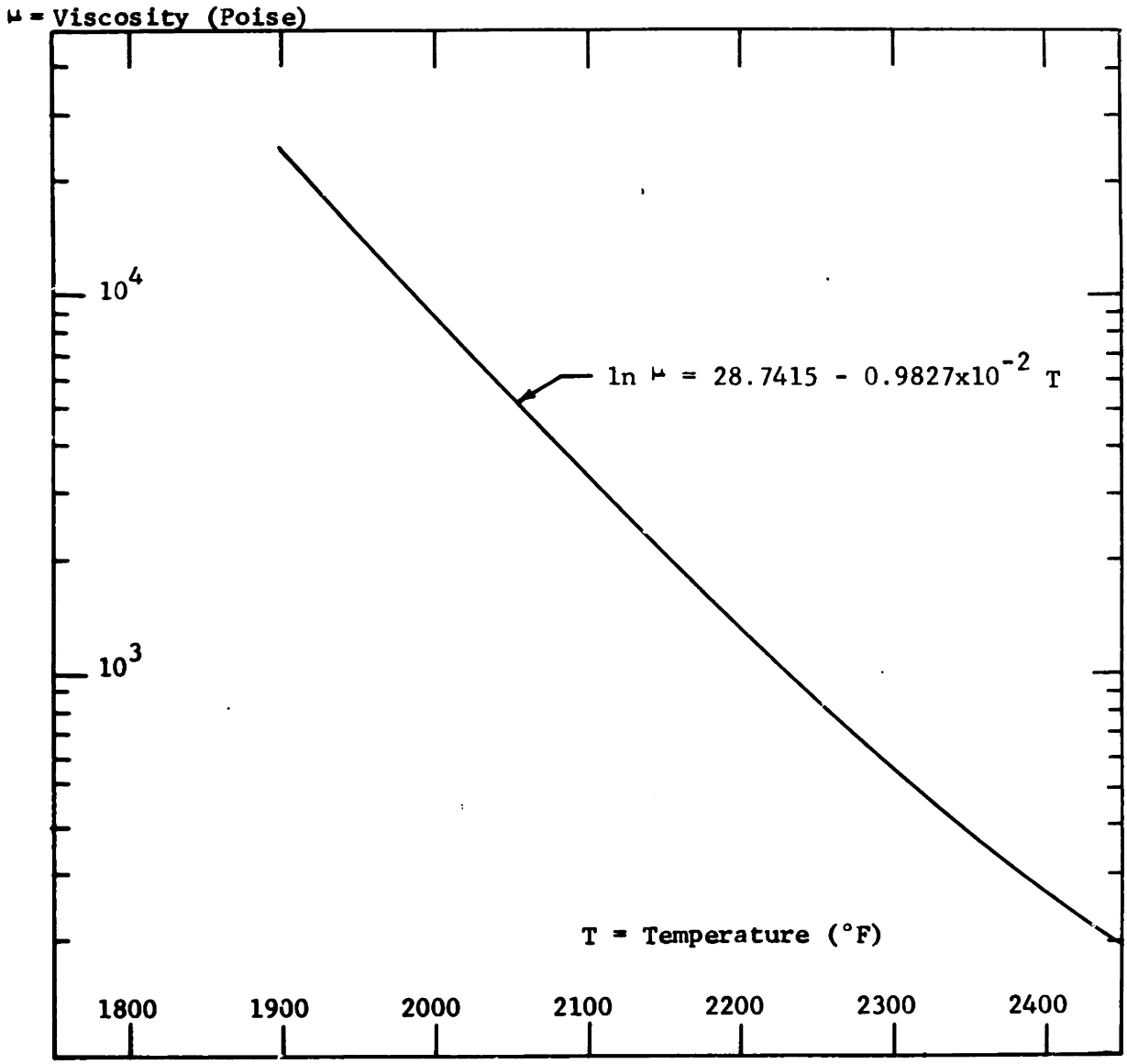

VISCOSITY VS. TEMPERATURE FOR GLASS

Fig. 3.2

The Energy Equation

Assuming a steady flow, the energy equation in the central jet region can be written for an element of differential length as

$$\frac{d}{dz}(w\, c_p T)dz = k\frac{d}{dz}(\pi r_o^2 \frac{dT}{dz})dz - h\, 2\pi r dz(T-T_{ATM}) \qquad (3.18)$$

$$- (\dot{q})_{RADIATION}$$

The radiation heat transfer is composed of both surface radiation and radiation from the fluid volume to the environment. For wavelengths where the fluid is opaque, surface radiation occurs. A body is opaque when the absorption coefficient times the distance it must travel, in this case the jet radius, is much larger than one:

$$\text{when } \gamma_\lambda r_o \gg 1 \qquad (3.19)$$

$$\lambda = \lambda_{OPAQUE}$$

$$(\dot{q})_{OPAQUE} = 2\pi r_o dz \int_{\lambda=\lambda_{OPAQUE}} \epsilon_\lambda w_{B\lambda} d\lambda_{OPAQUE}$$

For wavelengths where the absorption coefficient-radius product is small, volume radiation occurs

$$\gamma_\lambda r_o \ll 1 \quad ; \quad \lambda = \lambda_{TRANSPARENT} = \lambda_T \qquad (3.20)$$

$$\dot{q} = \pi r_o^2 dz \int_{\lambda_T} 4\, \gamma_\lambda w_{B\lambda} d\lambda_T$$

When the product of absorption coefficient and radius is of the order of one, volume radiation still occurs but expression (3.20) cannot be used. All of the radiation emitted in the volume is not transmitted to the outside of the jet, some of it is absorbed in other parts of the jet before it reaches the boundary. Fortunately, from published absorption coefficient data on the material in question, glass, references (5) and (6) indicate that a very small percentage of the total radiant energy falls within this case. Therefore, it will be assumed that all of the radiant energy transmitted to the surrounding area from the jet can be described by either equation (3.19) or (3.20), and the absorption coefficient versus wavelength will be assumed to vary as shown in Fig. 3.3.

The energy equation (3.18), can now be written as

$$w\, c_p \frac{dT}{dz} = 2\pi r_o k \frac{dr}{dz}\frac{dT}{dz} + \pi r_o^2 k \frac{d^2T}{dz^2}$$

$$- h\, 2\pi r_o (T - T_{ATM}) - 2\pi r_o \int \epsilon_\lambda w_{B\lambda} d\lambda_{OPAQUE} \qquad (3.21)$$

$$- 4\pi r_o^2\, dz \int \gamma_\lambda\, w_{B\lambda}\, d\lambda_T$$

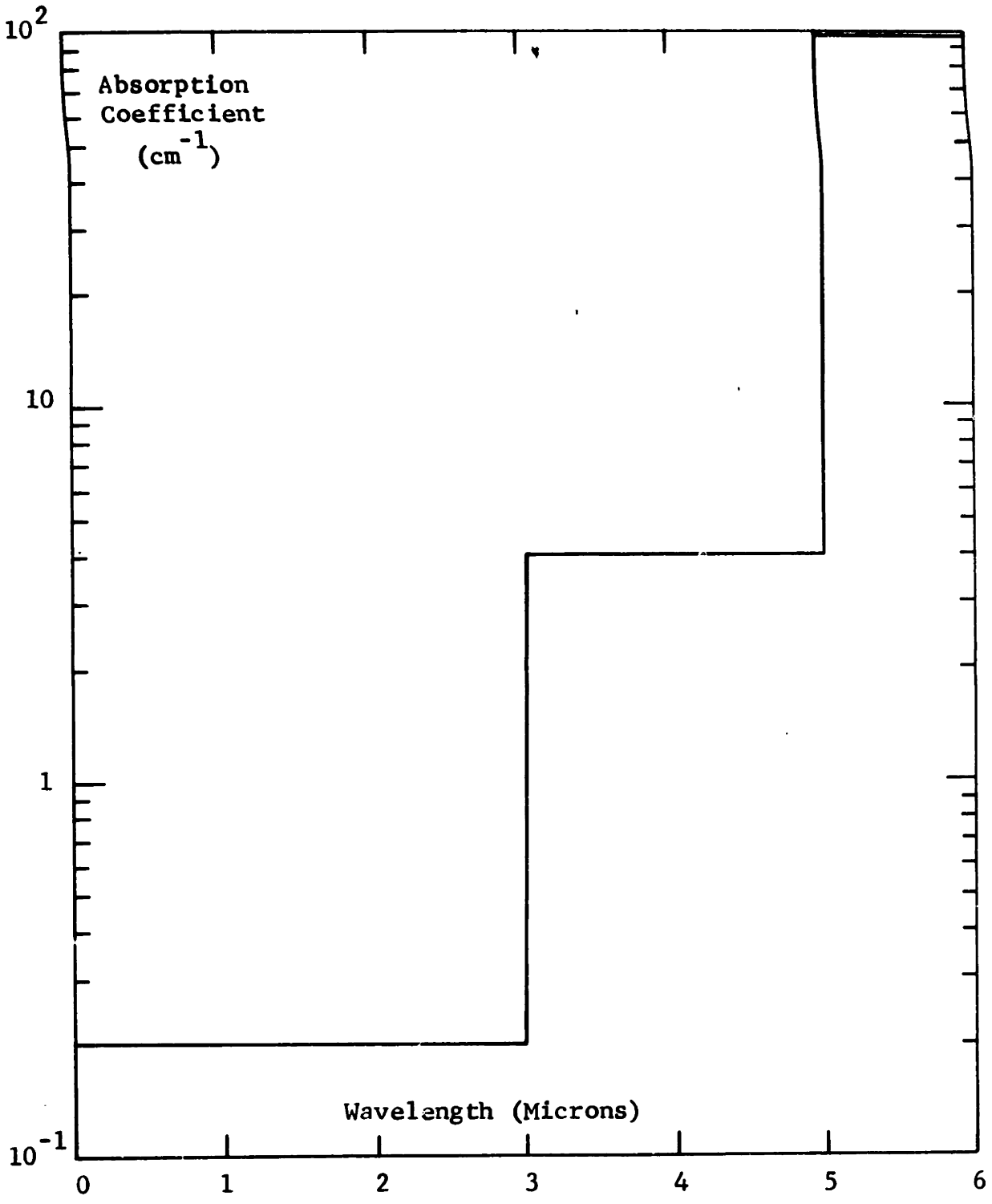

Absorption Coefficient
Versus
Wavelength
Distribution Assumed For Glass

Fig. 3.3

For the central jet region, the second derivative of temperature is negligible in the energy equation. Rearranging Eq. (3.21) and non-dimensionalizing the equation using the same definitions used in the energy equation plus

$$\bar{T} = T/T_E \tag{3.22}$$

The energy equation becomes:

$$\frac{d\bar{T}}{d\bar{z}}\left[1 - \frac{2\pi k r_E}{w\, c_p}\bar{r}\,\frac{d\bar{r}}{d\bar{z}}\right] = -\left(\frac{2\pi r_E^2}{w\, c_p}\right)h\bar{r}\left[\bar{T} - \bar{T}_A\right]$$
$$-\left(\frac{T_E^3 2\pi r_E^2 \sigma}{w\, c_p}\right)\left[\left(\bar{T} + \frac{459}{T_E}\right)^4 - T_{ATM}^4\right]\bar{r}\,\epsilon\, p_o \tag{3.23}$$
$$-\left(\frac{4T_E^3 \pi r_E^3 \sigma}{w\, c_p}\right)\bar{r}^2\left[\left(\bar{T} + \frac{459}{T_E}\right)^4 - T_{ATM}^4\right]\int \gamma_\lambda dp_T$$

where p_o is the percentage of the total radiant energy in the wavelengths where the material is opaque, ϵ is the average surface emissivity over the opaque wavelengths. p_T is the percentage of radiant energy over the wavelengths where $\gamma \times r_o$ is much less than one.

The initial condition associated with (3.23) is:

$$\text{at } \bar{z} = o$$
$$\bar{T} = 1 \tag{3.24}$$

The energy equation as formulated contains the assumption that the specific heat and the thermal conductivity of the fluid are constants. Assuming the fluid properties including absorption coefficient versus wavelength are known, the energy equation contains three unknowns, the radius at the beginning of the central jet region, r_E, the temperature at the same point, T_E, and an expression for the forced convection film coefficient of heat transfer, h.

3.5 The Upper Jet

By considering the order of magnitude of the forces in the upper jet, one relation between the unknown values at position 'E' and the known values at the nozzle exit can be found.

The details of the two-dimensional velocity and temperature distribution in the upper jet are unknown because the governing equations have not been solved for this region. It has been assumed that the temperature, radius and slope at the nozzle exit, designated state 0 in Fig. 2.1, are known. The lower end of the upper jet region designated state E, is defined as the point at which the slope of the jet boundary equals minus one-tenth, the point where the one-dimensional approximations are valid. The length, L, from state 0 to state E is unknown although an estimate of its magnitude will be made from physical observations.

Assuming the jet is axi-symmetric and steady, one can write the momentum equation in the axial direction for a control volume enclosing the entire upper jet, from state 0 to state E, Fig. 3.4. The pressure of the environment, assumed constant, will not appear in the momentum equation.

The momentum equation in the axial direction for the upper jet is

$$(\text{Tension})_E - (\text{Tension})_0 + \rho g(\text{Volume}) - \int_{\text{surface area}} \tau_\infty \cos\theta \, dA \tag{3.25}$$

$$= \int_{A_E} v_z dw - \int_{A_0} v_z dw$$

The order of magnitude of the gravity force, the shear force on the jet surface and the inertial force will be compared to the order of magnitude of the initial tension. As pointed out previously, the exact expression for the initial tension can only be found by a solution of the general two-dimensional equations for the nozzle and the upper jet. Since this has yet to be done, it will be assumed that the initial tension can be calculated by the one-dimensional expression developed in the last section,

$$(\text{Tension})_0 = -\frac{6\mu_0 Q}{R_o}\left(\frac{dr_o}{dz}\right)_o + \pi R_o \gamma_T \cos\theta_o \tag{3.26}$$

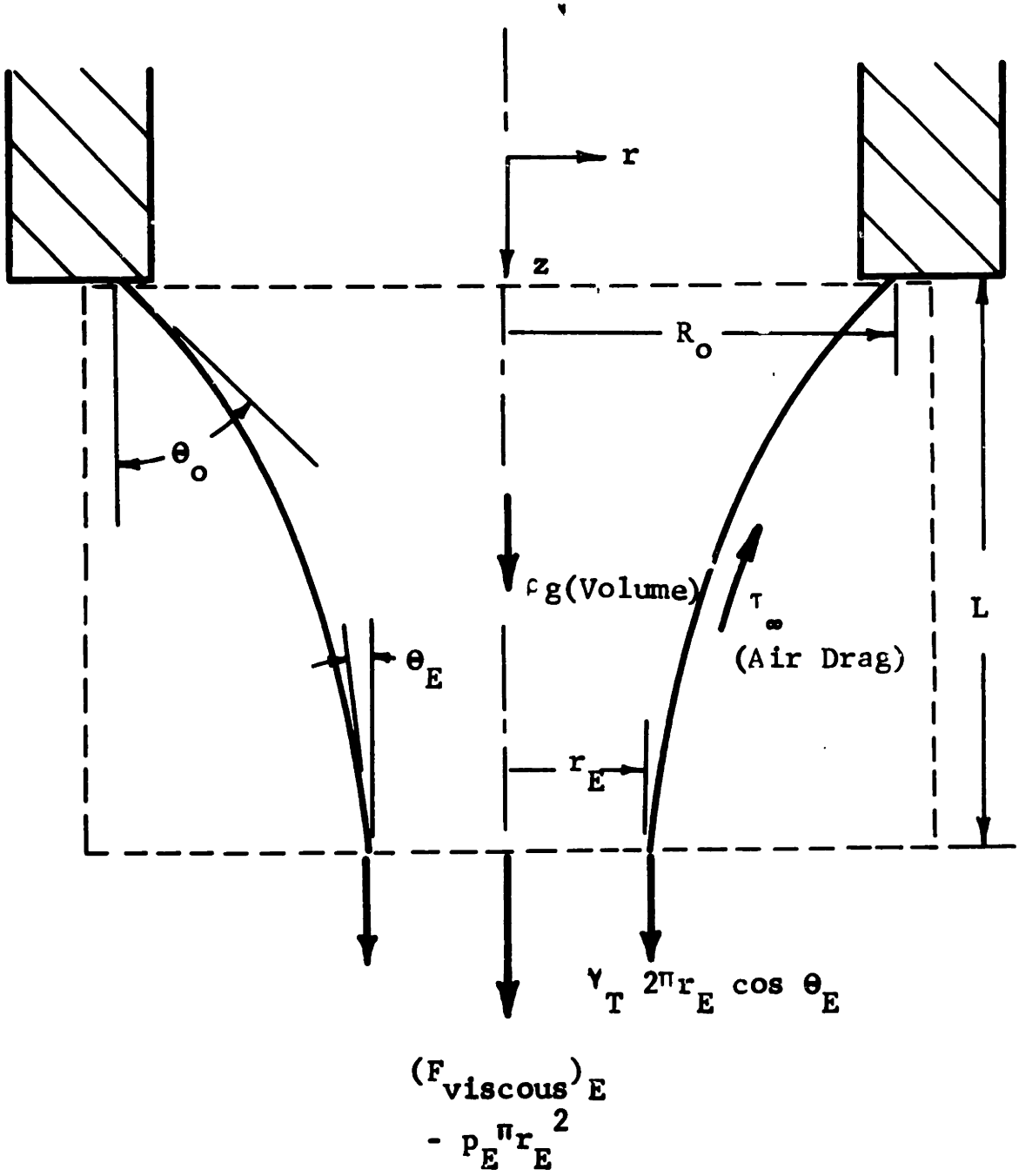

THE UPPER JET REGION

Fig. 3.4

The slope of the jet surface is always negative so that the two terms comprising the tension will always be additive. To simplify the order of magnitude considerations which follow, only the term containing the surface tension in (3.26) will be used to estimate the order of magnitude of the tension, this simplification will not affect the conclusions.

The ratio of the forces on the upper jet to the initial tension are:

$$\frac{\text{Gravity Force}}{(\text{Tension})_o} = \frac{\rho g(\text{Volume})}{\gamma_T \pi R_o \cos\theta_o} \approx \frac{\rho g \pi R_o^2 L}{\gamma_T \pi R_o \cos\theta_o} = \frac{\rho g R_o L}{\gamma_T \cos\theta_o} \qquad (3.27)$$

$$\frac{\text{Inertia Force}}{(\text{Tension})_o} = \frac{\rho Q^2}{\pi r_E^2 \gamma_T \pi R_o \cos\theta_o} = \frac{\rho Q^2}{\pi^2 r_E^2 R_o \gamma_T \cos\theta_o} \qquad (3.28)$$

Using those approximate values which make the ratios as large as possible for the fluid used in the experiment (glass):

γ_T = 320 dynes/cm

w = 1/60 gm/sec

ρ = 2.5 gm/cm^3

$(R_o)_{MAX}$ = 0.10 cm

$(R_o)_{MIN}$ = .05 cm

$$(r_E)_{MIN} = 0.02 \text{ cm}$$

$$L = 2\,R_o$$

$$(\cos\theta_o)_{MIN} = 0.8$$

one finds:

$$\left(\frac{\text{Gravity}}{\text{Surface Tension}}\right)_{MAX} \leq 0.2$$

$$\left(\frac{\text{Momentum Flux}}{\text{Surface Tension}}\right)_{MAX} \leq 10^{-2} \qquad (3.29)$$

In some cases, the viscous normal force is larger than the surface tension force making the ratios even smaller. To estimate the shear force on the jet surface a solution of the environmental boundary layer on the jet surface is necessary. The boundary layer solution given in Chapters 6 and 7 for laminar and turbulent boundary layers respectively indicates that, at most, the ratio of the shear force to the initial tension is 0.05. Therefore, for the upper jet the influence of gravity, shear stress and momentum change is small and the tension at the start of the central jet region equals the tension at the nozzle exit.

$$(\text{Tension})_o = \pi R_o \gamma_T \cos\theta_o - \frac{6\mu_o Q}{R_o}\left(\frac{dr_o}{dz}\right)_o = (\text{Tension})_E \qquad (3.30)$$

$$= \pi r_E \gamma_T \cos\theta_E - \frac{6\mu_E Q}{r_E}\left(\frac{dr}{dz}\right)_E$$

With this additional information, the central jet region can now be solved without a detailed solution of the upper jet region if the shear stress and film heat transfer coefficient can be predicted.

CHAPTER 4

THE SOLUTION OF THE ONE-DIMENSIONAL EQUATIONS

In order to solve the one-dimensional equations derived in the last chapter, a prediction of the film heat transfer coefficient and the shear stress on the jet surface is necessary. In the present chapter, the film coefficient and the shear stress is predicted using the assumptions that the boundary layer on the jet surface is analogous to that on a solid right circular cylinder and the boundary layer is laminar.

Two cases will be presented: first, the general non-linear one-dimensional equations with a laminar boundary layer requiring a numerical solution for each specific set of conditions; second, a simplification of the general equations yielding a closed form solution for the jet shape and the temperature distribution. The general non-linear equations contain the assumptions made in Sections 3.4 and 3.5.

4.1 The Laminar Boundary Layer

The results of this study show that the shear stress and the film heat transfer coefficient, especially the latter, are the controlling parameters of the central jet. Because of their

importance, a separate chapter is entirely devoted to a discussion of the prediction of the air drag and film coefficient.

Anticipating the results of the following chapters, for a laminar boundary layer on a cylinder moving in the axial direction, the relationship between the non-dimensionalized air drag on the cylinder and the Reynolds number and length to radius ratio can be predicted.

The local air drag is non-dimensionalized as $\tau_\infty 2\pi r_o/\mu_{ATM}U_\infty$ which will be defined as C_L (no relationship to the lift coefficient) and it is a function of $\nu_{ATM}z/U_\infty r_o^2$ the length Reynolds number divided by the radius Reynolds number squared, also equal to z/r_o divided by the radius Reynolds number. Further, for the central jet region, C_L is a very weak function of z/r_o $/(Re)_{r_o}$, in fact, C_L is approximately a constant. The air drag may be written as

$$\tau_\infty = \frac{U_\infty \mu_{ATM}}{2\pi r_o} C_L = \frac{Q\,\mu_{AIR}\,C_L}{2\pi^2 r_o^3} \qquad (4.1)$$

(Assuming a one-dimensional jet velocity)

$$C_L = F\left[(Re)_z/(Re)_{r_o}^2\right] = F\left[(z/r)(1/(Re)_{r_o})\right]$$

lying Reynolds Analogy for laminar flow one finds for the local
selt number

$$Nu_z = (Re)_z \frac{\tau_\infty}{\rho U_\infty^2} \tag{4.2}$$

$$h = \frac{k_{AIM}}{2\pi r_o} C_L \tag{4.3}$$

2 The General One-Dimensional Equations

Substituting relations (4.1) and (4.3) into the momentum and
ergy equation, one finds for the momentum equation

$$\frac{d^2\bar{r}}{d\bar{z}^2}\left[1 + \left(\frac{\gamma_T \pi r_E^2}{6\mu_E Q}\right)\frac{\bar{r}^2}{\bar{\mu}}\frac{d\bar{r}}{d\bar{z}}\right] = \left(\frac{\rho g \pi r_E^4}{6\mu_E Q}\right)\frac{\bar{r}^3}{\bar{\mu}} \tag{4.4}$$

$$- \left(\frac{1}{6\pi\mu_E}\right)\frac{C_L}{\bar{\mu}}\frac{\mu_{AIR}}{\bar{r}}$$

$$+ \frac{d\bar{r}}{d\bar{z}}\left[\frac{1}{\bar{r}}\frac{d\bar{r}}{d\bar{z}} + \left(\frac{\gamma_T \pi r_E^2}{6Q\mu_E}\right)\frac{\bar{r}}{\bar{\mu}} + \left(\frac{\rho Q}{3\pi r_E \mu_E}\right)\frac{1}{\bar{r}^2\bar{\mu}} - \frac{d \ln \bar{\mu}}{d\bar{z}}\right]$$

itial conditions

at $\bar{z} = 0$

$\bar{r} = 1$

$d\bar{r}/d\bar{z} = -1/10$

at $z \to \infty$

$\bar{r} \to r_{FINAL}/r_E = \bar{r}_{FINAL}$

and for the energy equation

$$\frac{d\bar{T}}{d\bar{z}}\left[1-2\,\frac{\pi k r_E}{w\,c_p}\,\bar{r}\,\frac{d\bar{r}}{d\bar{z}}\right]=-\left(\frac{k_{ATM}\,r_E\,C_L}{w\,c_p}\right)(\bar{T}-\bar{T}_{ATM}) \qquad (4.5)$$

$$-\left(\frac{T_E^{\,3}\,2\,\pi r_E^{\,2}\sigma}{w\,c_p}\right)\left[\left(\bar{T}+\frac{459}{T_E}\right)^4-\bar{T}_{ATM}^{\,4}\right]\bar{r}\,\epsilon\,p_o$$

$$-\left(\frac{T_E^{\,3}\,\pi r_E^{\,3}\,4\sigma}{w\,c_p}\right)\left[\left(\bar{T}+\frac{459}{T_E}\right)^4-\bar{T}_{ATM}^{\,4}\right]\int \gamma_\lambda\, dp_T$$

Initial conditions

at $\bar{z}=0$

$\bar{T}=1$

$A_{1,2}$ is known from the estimation of the order of magnitude of the forces acting on the upper jet, Section 3.5,

$$(\text{Tension})_o=(\text{Tension})_E=\pi r_E\gamma_T\cos\theta_E-\frac{6\mu_E Q}{r_E}\left(\frac{dr_o}{dz}\right)_E \qquad (4.6)$$

and from the properties of the fluid

$$\ln\mu=a_1-a_2\,T \qquad (4.7)$$

Since Eqs. (4.4) and (4.5) are non-linear, the equations can be written as difference equations which can be solved numerically. The unknowns in the above equations are r_E and μ_E, since T_E can be found from μ_E using Eq. (4.7). The initial tension is calculated using the one-dimensional relationship, Eq. (3.26).

The solution of the equations requires an iterative process once the flow rate, fluid properties, environmental properties, R_o, $(dr_o/dz)_o$, T_o and r_{FINAL} are known.

1. A value of r_E is chosen.
2. μ_E is calculated from Eq. (4.6).
3. The momentum and energy equations are solved simultaneously.
4. The predicted radius approaches an asymptotic value with increasing z, if the asymptotic value is within 0.5% of $\bar{r}_{FINAL}$, the solution is completed, if it is not, a new value of r_E is chosen and the analysis is repeated starting at Step 2.

Since Eqs. (4.4) and (4.5) are non-linear, the equations were written as difference equations and solved numerically on a digital computer. The details of the computer program are given in Appendix F.

In order to gain a better insight into the effect a specific variable such as the specific heat of the fluid has on the solution, the governing equations will be simplified allowing a solution to be obtained in closed form.

Aside from the assumptions used in deriving the general one-dimensional equation, it will be further assumed that: (i) the tension is a constant, in the one-dimensional region, (ii) the surface tension is negligible compared to the viscous normal force, (iii) heat transfer by radiation and conduction is negligible compared to heat transfer by convection, and (iv) the temperature of the environment at which the film coefficient, h, is evaluated at is a constant.

4.3 The Solution of the Simplified Equations

Considering the energy equation first, in all of the cases studied conduction heat transfer is negligible compared to forced convection in the central jet region. If one further assumes that radiation heat transfer is negligible, an assumption which is borne out by the results in the central jet region, the energy equation (4.5) becomes

$$\frac{d\bar{T}}{d\bar{z}} = - \frac{r_E C_L k_{ATM}}{w\, c_p} \left[\bar{T} - \bar{T}_{ATM} \right] \tag{4.8}$$

or

$$\frac{dT}{dz} = - \frac{C_L k_{ATM}}{w\, c_p} \left[T - T_{ATM} \right]$$

Fortuitously, the simplified energy equation is independent of the momentum equation since neither $\bar{r}$ nor its derivatives appear in Eq. (4.8). If one assumes C_L does not vary with z, a valid assumption for the central jet region and that K_{ATM} is a constant, a questionable assumption since K_{ATM} actually varies with the jet temperature, Eq. (4.8) can be solved yielding:

$$T = T_{ATM} + (T_E - T_{ATM})e^{-Bz} \tag{4.9}$$

$$B = k_{ATM} C_L / w c_p$$

which satisfies the inition condition

at $z = 0$

$T = T_E$

The jet temperature's asymptotic approach toward the ambient air temperature as predicted by (4.9), seems correct by intuition.

The viscosity temperature relation for the fluid can be represented by

$$\ln \mu = a_1 - a_2 T \tag{4.10}$$

which combined with (4.9) yields

$$\frac{d \ln \mu}{dz} = - a_2 \frac{dT}{dz} = a_2 B (T_E - T_{ATM}) e^{-Bz} \tag{4.11}$$

Defining a new constant

$$\Lambda = a_2 (T_E - T_{ATM}) \tag{4.12}$$

Equation (4.11) becomes

$$\frac{d \ln \mu}{dz} = A B e^{-Bz} \tag{4.13}$$

integrating

$$\mu = c e^{-(\Lambda e^{-Bz})} = \mu_E e^{\Lambda} e^{-(\Lambda e^{-Bz})} \tag{4.14}$$

which satisfies the condition

at $z = 0$

$\mu = \mu_E$

If one assumes that the tension is constant in the central jet region and that the viscous normal force is the dominant tension term the momentum equation simply states that the viscous normal force must not change with distance:

$$\frac{d}{dz} \left(- \frac{6 \mu Q}{r_o} \frac{dr_o}{dz}\right) = 0 \tag{4.15}$$

This is most easily seen by referring to Eq. (3.12).

Integrating Eq. (4.15) once,

$$-\frac{6\mu Q}{r_o}\frac{dr_o}{dz} = (\text{Tension})_E = \text{constant} \tag{4.16}$$

Since the upper jet analysis has indicated that the tension is constant in the upper jet, (4.16) can be written as,

$$-\frac{6\mu Q}{r_o}\frac{dr_o}{dz} = -6\mu Q\frac{d\ln(r_o)}{dz} = (\text{Tension})_o \tag{4.17}$$

$$\therefore \ln(r_o) = -\frac{(\text{Tension})_o}{6Q}\int \frac{1}{\mu}\,dz \tag{4.18}$$

The last equation shows the importance of the viscosity gradient on the resultant jet shape. The viscosity can be found from Eq. (4.14) yielding,

$$\ln(r_o) = -\frac{(\text{Tension})_o}{6\mu_E Q e^A}\int e^{(A e^{-Bz})}\,dz \tag{4.19}$$

In order to integrate the right hand side of Eq. (4.19), the following definition will be introduced

$$y = A e^{-Bz} \tag{4.20}$$

$$\therefore dy = -A B e^{-Bz} \tag{4.21}$$

$$\frac{dy}{y} = -B\,dz \tag{4.22}$$

and

$$\frac{e^y\, dy}{y} = -\, B\, e^{Ae - Bz}\, dz \tag{4.23}$$

Therefore, integrating from z = 0 to any other value of z, (4.19) can be written as

$$\ln\left(\frac{r_o}{r_E}\right) = + \frac{(\text{Tension})_o}{6B\mu_E Q\, e^A} \int_{z=0}^{(y)} \frac{e^y}{y}\, dy \tag{4.24}$$

Using the exponential integral (see references (7) and (8)) defined as

$$E_i^*(x) = \int_{-\infty}^{x} \frac{e^u}{u}\, du \tag{4.25}$$

Equation (4.24) can be written as

$$r_o = r_E\, e^{+\left\{\frac{(\text{Tension})_o}{6B\mu_E Q\, e^A}\left[E_i^*(A\, e^{-Bz}) - E_i^*(A)\right]\right\}} \tag{4.26}$$

r_E can be found from the relation

$$(\text{Tension})_E = -\frac{6\,\mu_E Q}{r_E}\left(\frac{dr_o}{dz}\right)_E = (\text{Tension})_o \tag{4.27}$$

where $\left(\frac{dr_o}{dz}\right)_E = -\,1/10$

$$\therefore\ r_E = \frac{0.6\,\mu_E Q}{(\text{Tension})_o} \tag{4.28}$$

Therefore,

$$r_o = \frac{0.6\ \mu_E Q}{(\text{Tension})_o}\ e^{+\left\{\frac{(\text{Tension})_o}{6B\mu_E Q\ e^A}\left[E_i^*(A\ e^{-Bz}) - E_i^*(A)\right]\right\}} \quad (4.29)$$

$$A = a_2(T_E - T_{ATM})$$

$$B = k_{ATM}\ C_L / w\ cp$$

To find the unknown value of μ_E in Eq. (4.29) the condition at the end of the central jet region is used

$$\text{at } z \to \infty$$

$$r_o \to r_{FINAL} \quad (4.30)$$

$$r_{FINAL} = \frac{0.6\ \mu_E Q}{(\text{Tension})_o}\ e^{-\left[\frac{(\text{Tension})_o}{6B\mu_E Q\ e^A}\ E_i^*(A)\right]}$$

For large values of A, the usual case for the present conditions

$$E_i^*(A) \approx e^A/A \quad (4.31)$$

and replacing A and B by their definitions

$$r_{FINAL} \approx \frac{0.6\ \mu_E Q}{(\text{Tension})_o}\ e^{-\left[\frac{\rho\ c_p\ (\text{Tension})_o}{6\ a_2(T_E - T_{ATM})\mu_E k_{ATM} C_L}\right]} \quad (4.32)$$

Raising the value of T_E, lowering μ_E causes the final jet radius to decrease for the same value of the flow rate, initial tension, etc. The effect of changing the fluid properties can

also be easily seen. The results of the approximate solution will be discussed in greater detail in Chapter 10.

It must be kept in mind that some of the simplifying assumptions are not strictly correct. The thermal conductivity of air is not a constant as assumed, it decreases with decreased jet temperature. Also, near the beginning of the central jet the viscous normal force is not a constant and for some cases radiation may not be negligible. However, it is the assumption of a constant air conductivity, used in the calculation of the film coefficient of heat transfer which introduces the largest error in the solution.

A more accurate solution may be obtained by subdividing the central jet region into zones of arbitrary length or zones which cover a given temperature change. The temperature distribution and shape of each zone are solved for separately. The solutions are linked by equating the temperature, radius and slope at the divisions between zones. For each zone the value of air conductivity for that zone's particular temperature range is used. It is obvious that as the number of zones increases, both the accuracy and the time for a given solution increase.

Rather than following the above mentioned approach, the detailed numerical solution of the general equations was made.

CHAPTER 5

THE TEMPERATURE AND VELOCITY GRADIENTS IN THE JET WHEN THE SLOPE OF THE BOUNDARY IS SMALL

It will be demonstrated that when the slope of the jet boundary is small, the radial gradients of velocity and temperature may be neglected in favor of the axial gradients.

5.1 The Velocity Distribution

The velocity distribution will be considered first. A comparison of the radial gradient of the axial velocity, $\partial v_z/\partial r$, to the axial gradient, $\partial v_z/\partial z$, will be made.

When the dr_o/dz is less than minus one-tenth, the free surface boundary condition in the tangential direction, given in Appendix B assuming a constant surface tension, is

$$\mu\left(\frac{\partial v_r}{\partial z} + \frac{\partial v_z}{\partial r}\right) = \tau_\infty \tag{5.1}$$

From symmetry, the radial velocity and $\partial v_z/\partial r$ are zero at the center line. Assuming that the velocity distributions do not have any discontinuities, v_r and $\partial v_z/\partial r$ should have their maximum values at the jet boundary. At the boundary,

$$v_r/v_z = dr_o/dz \tag{5.2}$$

$$\therefore \frac{\partial v_r}{\partial z} = \frac{\partial v_z}{\partial z}\left(\frac{dr_o}{dz}\right) + v_z\left(\frac{d^2 r_o}{dz^2}\right) \approx \frac{\partial v_z}{\partial z}\left(\frac{dr_o}{dz}\right) + \frac{v_z}{R_1} \qquad (5.3)$$

From the laminar boundary layer theory, evaluating C_L for the upper jet

$$\tau_\infty = \frac{U_\infty \mu_{ATM} C_L}{2\pi r_o} = \left[0\right] \frac{\mu_{ATM} U_\infty}{r_o} \qquad (5.4)$$

where the symbol $\left[0\right]$ means "the order of magnitude of".

Combining (5.3) and (5.4) with Eq. (5.1) and solving for $\partial v_z/\partial r$,

$$\frac{\partial v_z}{\partial r} = -\frac{\partial v_z}{\partial z}\left(\frac{dr_o}{dz}\right) - \frac{v_z}{R_1} + \left[0\right]\left(\frac{\mu_{ATM}\, U_\infty}{\mu\ r_o}\right) \qquad (5.5)$$

Using the continuity equation the average axial velocity is

$$\bar{v}_z = Q/\pi r_o^2 \qquad (5.6)$$

$$\frac{\partial \bar{v}_z}{\partial z} = -\frac{2Q}{\pi r_o^3}\frac{dr_o}{dz} = -\frac{2\bar{v}_z}{r_o}\left(\frac{dr_o}{dz}\right) \qquad (5.7)$$

U_∞ the velocity of the jet surface is at most equal to $\bar{v}_z$, therefore,

$$\therefore \frac{\partial v_z}{\partial r} = -\frac{\partial v_z}{\partial z}\left(\frac{dr_o}{dz}\right) - \frac{v_z}{R_1} + \left[0\right]\left[\frac{\mu_{ATM}}{\mu}\ \frac{Q}{10\ r_o^3}\right] \qquad (5.8)$$

Assuming that the order of magnitude of the gradient of the average axial velocity and the local axial velocity at any point is the same, Eq. (5.8) can be divided by $\partial \bar{v}_z/\partial z$ to yield

$$\frac{\partial v_z/\partial r}{\partial \bar{v}_z/\partial z} = + \left[0\right] \left(\frac{dr_o}{dz}\right) + \left[0\right] \left[\frac{r_o}{R_1 \left(\frac{dr_o}{dz}\right)} \right] - \left[0\right] \left[\frac{\mu_{ATM}}{\mu \frac{dr_o}{dz}} \right] \quad (5.9)$$

At the highest jet temperatures, about 2400°F or 1200°F film temperature, where the air viscosity is a maximum and the jet viscosity is a minimum, the ratio of the environmental viscosity to the jet fluid viscosity is 10^{-6}. From experimental results it is found that the ratio of the jet radius to R_1 is always at least one order of magnitude smaller than dr_o/dz.

$$\frac{\partial v_z/\partial r}{\partial \bar{v}_z/\partial z} = - \left[0\right] \left[\frac{dr_o}{dz}\right] + \left[0\right] \left[10^{-1}\right] + \left[0\right] \left[\frac{10^{-6}}{dr_o/dz} \right] \quad (5.10)$$

Proceeding down the jet, the ratio of air to the fluid viscosity decreases rapidly due to the drop in the temperature of the jet. Therefore, in the region of interest, since $\partial v_z/\partial r$ is negligible compared to $\partial \bar{v}_z/\partial z$

$$v_z \approx \bar{v}_z = F(z) \quad (5.11)$$

5.2 The Temperature Distribution

In the region where the volume radiation from the jet to the exterior can be neglected, the boundary conditions at the jet surface is

$$k \frac{\partial T}{\partial n} = (\dot{q}/A) \tag{5.12}$$

and

$$\frac{\partial T}{\partial n} = \frac{\partial T}{\partial r} \frac{dr}{dn} + \frac{\partial T}{\partial z} \frac{dz}{dn} \tag{5.13}$$

When dr_o/dz is less than -10^{-1}

$$\dot{q}/A = k \frac{\partial T}{\partial n} \approx k \frac{\partial T}{\partial r} \tag{5.14}$$

For most of the jet length the principle form of heat transfer is due to laminar forced convection

$$\dot{q}/A = [0]\left[h(T - T_{ATM})\right] = [0]\left[\frac{k_{ATM} C_L}{2\pi r_o} (T - T_{ATM})\right] \tag{5.15}$$

$$\dot{q}/A = [0]\left[(\frac{k_{ATM}}{\pi r_o})(T - T_{ATM})\right] \tag{5.16}$$

Combining (5.14) and (5.16)

$$k \frac{\partial T}{\partial r} = \frac{k_{ATM}}{\pi r_o} (T - T_{ATM}) \tag{5.17}$$

The temperature difference from the jet centerline to outside surface can be estimated as

$$T_{\ell} - T_{r_o} = \Delta T = [0]\left[(r_o \frac{\partial T}{\partial r})\right] = [0]\left[(\frac{k_{ATM}}{k})(T - T_{ATM})\right] \tag{5.18}$$

Using the maximum value of the air thermal conductivity

$$\frac{\Delta T}{T-T_{ATM}} = \left[0\right] \left[\frac{k_{ATM}}{k}\right] = \left[0\right] \left[10^{-1}\right] \tag{5.19}$$

Equation (5.19) states, at worst, the value of $T-T_{ATM}$ used for convection heat transfer is in error by 10 per cent. At 2000°F the value of T^4 used in the radiation calculation has a maximum error of 36 per cent. When radiative heat transfer exceeds forced convection heat transfer, Eq. (5.16) must be modified to include the addition $\dot{q}/A$ causing an even larger difference between the center line temperature and the surface temperature. Fortunately, numerical calculations show that forced convection is the dominant form of heat transfer in the central jet region. The results also indicate the error in using the one dimensional temperature profile in the upper jet where radiation is large.

It has not been proved that in the central jet region the radial temperature gradient is negligible compared to the axial gradient; rather it has been shown that the assumption of a constant temperature at any cross-section causes, at most, a 10 per cent error in the calculated heat transfer from the jet to the environment. Since in the simplified case the axial gradient of the temperature is related to the heat transfer by

$$w\, c_p \frac{\partial T}{\partial z} = (\dot{q}/A)\, 2\pi r_o \qquad (5.20)$$

A 10 per cent error in the heat transfer caused by neglecting the radial gradient of the temperature produces a 10 per cent error in the calculated axial temperature gradient.

CHAPTER 6

THE SHEAR STRESS AND FILM COEFFICIENT OF HEAT TRANSFER FOR A LAMINAR BOUNDARY LAYER

As shown in the solution for the one-dimensional equations, a prediction of the forced convection heat transfer is of principle importance. When the radius has reached a final value which remains constant down to the pulling wheel, the momentum equation becomes

$$\frac{d(\text{Tension})}{dz} = \tau_\infty \, 2\pi r_o \tag{6.1}$$

Obviously, a theory which correctly predicts the air drag is necessary to determine the tension increase in the constant radius region. This chapter will cover the prediction of the laminar boundary layer and the next chapter will cover the turbulent boundary layer. All of the results will be for the case of a solid right-circular cylinder moving at constant speed in the axial direction only. For the laminar boundary layer, the results for the shear stress will be converted to film coefficient results using Reynolds analogy.

In the solutions that follow, the properties of the air will be evaluated at the film temperature, the average of the jet and the ambient temperature.

Seban and Bond (9) and Kelly (10) analytically studied the case of a laminar boundary layer on an unheated cylinder of finite length aligned parallel to the direction of the flow. A solution for a non-dimensionalized shear stress, displacement thickness, etc., were found as universal functions of $\nu_{ATM} z/U_\infty r_o^2$, equal to $(Re)_z/(Re)_{r_o}^2$ or $(z/r)/(Re)_{r_o}$. The shear stress is non-dimenalized as $\tau_\infty 2\pi r_o/U_\infty \mu_{ATM}$, equal to the drag coefficient x $(Re)_{r_o}$ x 2π. The solution, a series type, is only valid for relatively small values of $\nu_{ATM} z/U_\infty r_o^2$.

Glauert and Lighthill (11) later used the Pohlhausen method to expand the solution to large values of $\nu_{ATM} z/U_\infty r_o$. They showed that their solution agreed with Seban and Bond's for low values of $\nu_{ATM} z/U_\infty r_o^2$, in the limit it approaches Blasius flat plate solution as $\nu_{ATM} z/U_\infty r_o^2$ approaches zero, i.e., when the boundary layer thickness is very small compared to the cylinder radius. For large values of $\nu_{ATM} z/U_\infty r_o^2$ Glauert and Lighthill show that the Pohlhausen solution approaches a more exact asymmptotic series solution they have derived.

The velocity distribution used with the Pohlhausen solution is

$$u = \frac{U_\infty}{\sigma} \ln (1 + y/r_o) \qquad y \leq \delta \tag{6.2}$$

$$u = U_\infty \qquad y > \delta \tag{6.3}$$

where

$$\sim = \sim (\nu_{ATM} z / U_\infty r_o^2)$$

It is interesting to note that the shear stress at any location along the wire falls off as the reciprocal of the distance from the axis.*

No experimental measurement of the drag of a cylinder in axial flow in the laminar region could be found. Measurements of the film coefficient of heat transfer were found in works by Jakob (12) and NACA (13). Using Reynolds analogy for laminar flow where the Prandtl Number is approximately one,

$$\dot{q}/A = - k_{ATM} \left(\frac{\partial T}{\partial y}\right)_{y=o} = h(T_w - T_{ATM}) \tag{6.4}$$

$$h = - \frac{k_{ATM} (\partial T/\partial y)_o}{T_w - T_{ATM}} \tag{6.5}$$

$$\tau_\infty = \mu_{ATM} \left(\frac{\partial u}{\partial y}\right)_{y=o} \tag{6.6}$$

$$\left(\frac{\partial T}{\partial y}\right)_o = - C_o \left(\frac{T_w - T_{ATM}}{\delta_T}\right) \tag{6.7}$$

$$\left(\frac{\partial u}{\partial y}\right)_o = - C_1 \frac{U_\infty}{\delta} \tag{6.8}$$

---

* This shear stress behavior is the assumption used by Sparrow et al. (14) in analyzing the turbulent boundary layer on a cylinder and certainly seems correct at least for the "laminar sublayer" in view of Glauert and Lighthill's results.

Schlicting (15) states that in the cases of gases with a Prandtl number unity δ_T and δ as well as C_o and C_1 are nearly equal

$$\therefore \quad \frac{\partial T}{\partial y} \approx - \frac{T_w - T_{ATM}}{U_\infty} \left(\frac{\partial u}{\partial y}\right)_o \tag{6.9}$$

$$h = \frac{k_{ATM}}{U_\infty} \left(\frac{\partial u}{\partial y}\right)_o = \frac{k_{ATM}\, \tau_\infty}{U_\infty\, \mu_{ATM}} \tag{6.10}$$

defining

$$C_L = \frac{\tau_\infty 2\pi r_o}{U_\infty \mu_{ATM}} = F \left[(Re)_z / (Re)_{r_o}^2 \right]$$

Then

$$h = \frac{k_{atm}\, C_L}{2\pi r_o} \tag{6.11}$$

The converted heat transfer data are shown on Fig. 6.1 compared to Glauert and Lighthill's theory and the agreement is remarkably good.

Since Glauert and Lighthill's theory closely agrees with the experimental film coefficient data converted to shear stress using Reynolds analogy, the reverse procedure, using the shear stress theory and Reynolds analogy to predict film coefficients, should also yield valid results.

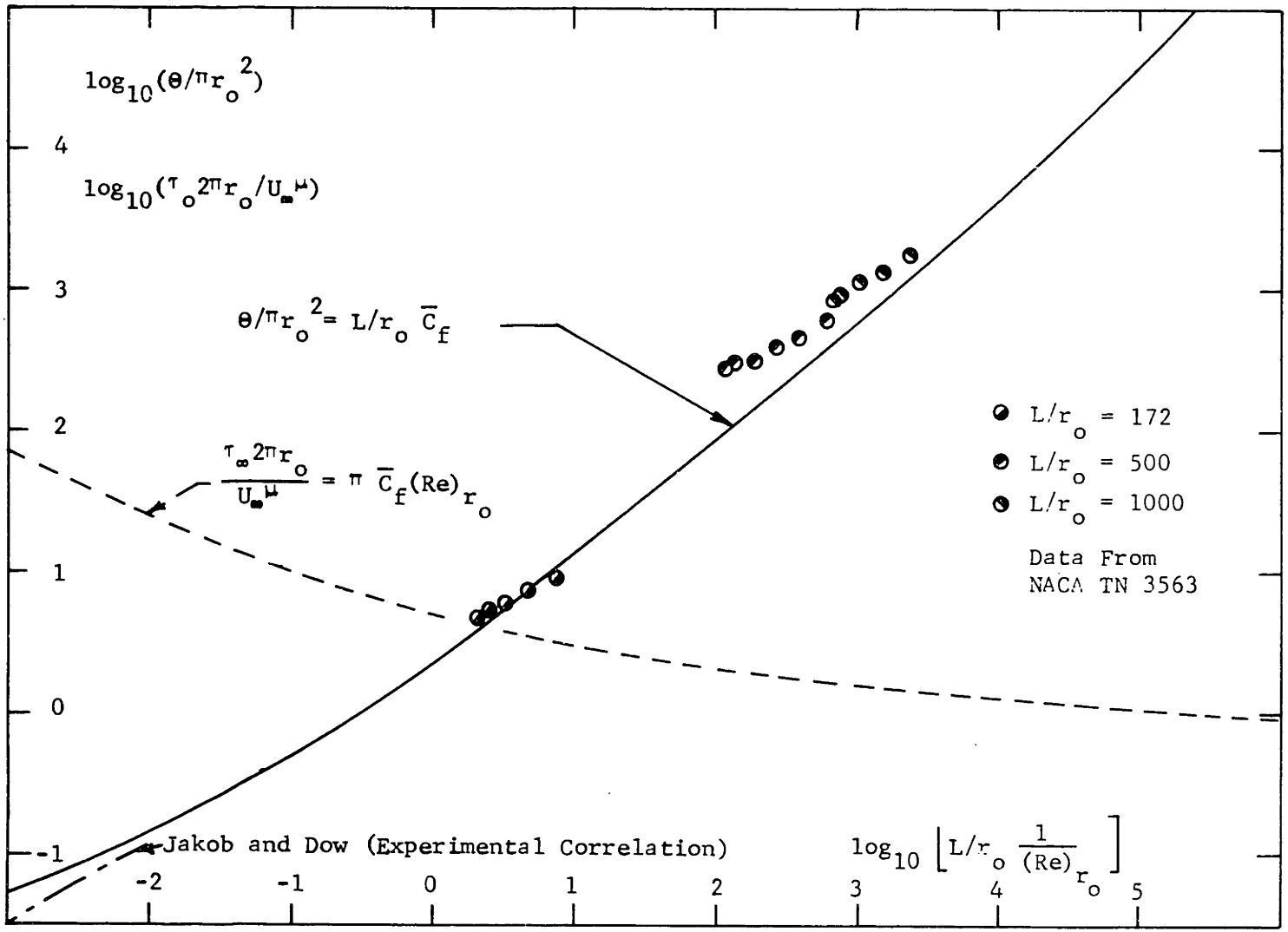

Fig. 6.1

LAMINAR BOUNDARY LAYER SHEAR STRESS

A COMPARISON OF GLAUERT AND LIGHTHILL'S THEORY WITH
HEAT TRANSFER DATA CONVERTED TO SHEAR STRESS USING REYNOLDS ANALOGY

The case under study, a continuous cylinder without a definite "leading edge" moving through still air is not exactly analogous to the case Glauert and Lighthill have studied.

Referring to Fig. 6.2, situation b would be the direct analogy to Glauert and Lighthill's situation. For the case of an infinite wire drawn from a nozzle or hole in a wall, situation c is the only steady state possibility. The boundary layer has zero thickness at the hole since the condition along the surrounding wall requires the velocity to be zero (no slip). The boundary layer must grow in the z direction since a stationary control volume drawn around the cylinder experiences a shear force from the cylinder in the positive z direction causing an acceleration of the fluid flowing through the control volume. Notice, for this case the fluid entering the control volume from above contributes no net momentum flux in the z direction.

Sakiadis (16) has studied the laminar boundary layer illustrated by Fig. 6.2C. He used an approach identical to Glauert and Lighthill only changing the assumed velocity profile to meet the new boundary conditions. The velocity profile Sakiadis used for the Pohlhausen technique was:

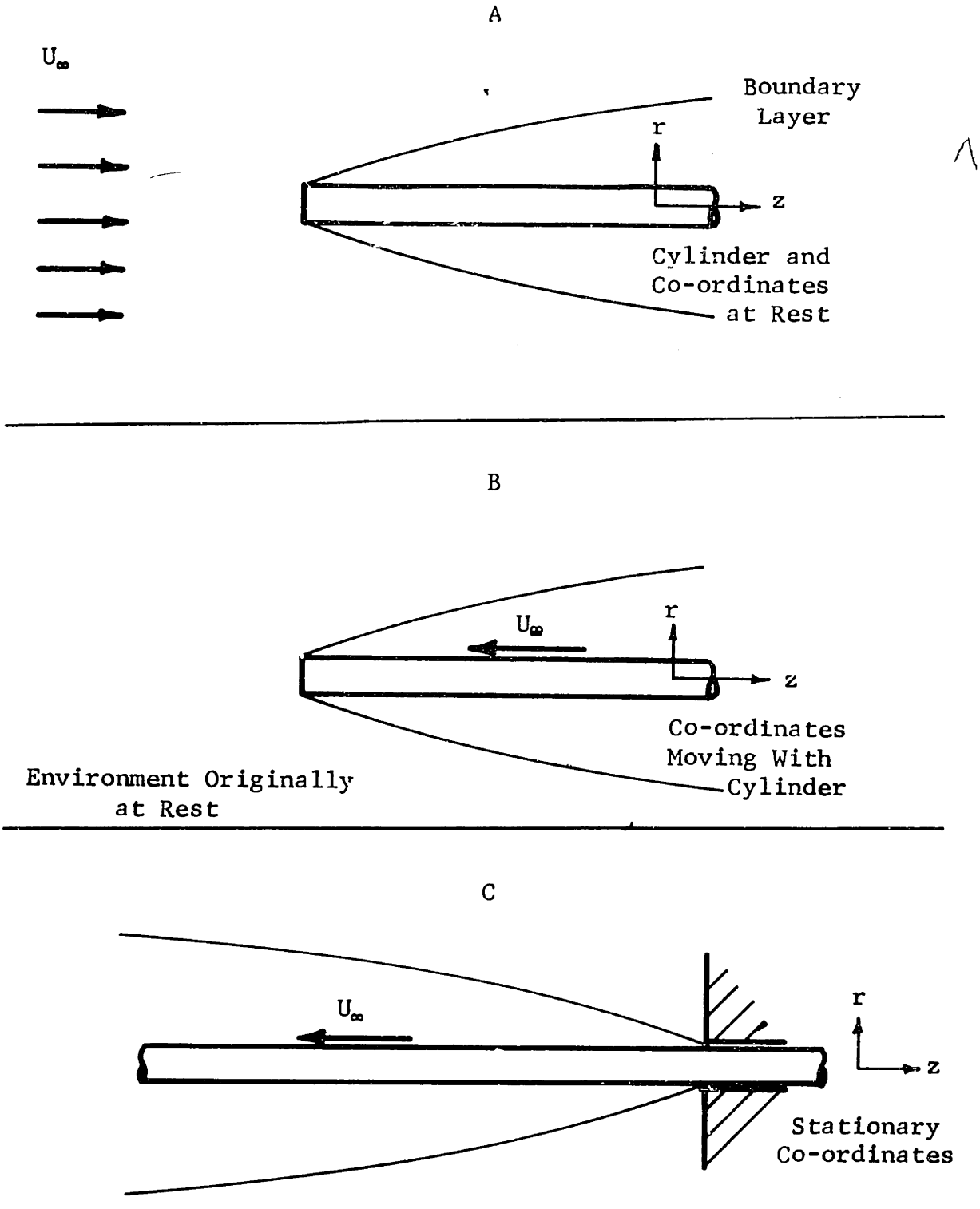

Fig. 6.2

THE STEADY STATE BOUNDARY LAYER ON A CYLINDER

A and B: Cylinders With Definite Leading Edges
C: A Continuous Cylinder (Steady State Condition)

$$u = U_\infty \left[1 - 1/\alpha \ln (1 + y/r_o)\right] \qquad y \leq \delta \tag{6.12}$$

$$u = 0 \qquad y > \delta \tag{6.13}$$

Sakiadis's results agreed with Glauert and Lighthill's results within 5 per cent in the range of $\nu_{ATM} z/U_\infty r_o^2$ considered.

In the case presently studied, the jet is not cylindrical rather the jet radius decreases with increasing axial distance. Instead of solving this more complicated boundary layer problem, it is assumed that at any axial position the shear stress is equal to the shear stress on a right circular cylinder with a radius equal to the local jet radius under consideration and length equal to the distance to the nozzle exit.

CHAPTER 7

THE PREDICTION OF THE DRAG ON THE JET DUE TO A TURBULENT BOUNDARY LAYER

In the preceding chapter, a theory for the laminar boundary layer was presented. In this chapter, the turbulent boundary layer will be studied. The results of this study will prove very important in the discussion of the experimentally measured tension in the jet.

Several authors have attempted to theoretically predict the skin friction on a cylinder subject to a turbulent boundary layer flow in the axial direction (17), (18), (19). The most recent and the most accurate is the work of Sparrow, Eckert and Minowycz (14). The other proposed theories when applied to the case at hand, predict turbulent friction factors which are less than the predicted laminar friction factors.

Sparrow, et al., made use of the expressions for eddy diffusivity for momentum derived by Deissler. The expressions were derived for the turbulent boundary layer on a flat plate, but Sparrow assumes that they may be used for the turbulent boundary layer on a cylinder. Using the definitions:

$$u^+ = u/(\tau_\infty/\rho)^{1/2} \tag{7.1}$$

$$y^+ = y(\tau_\infty/\rho)^{1/2} \qquad (7.2)$$

y is the radial distance from the cylinder wall. The expressions for the eddy diffusivity and shear stress are near the wall

$$\epsilon_m/\nu = (.109)^2 u^+ y^+ \qquad (7.3)$$

$$\tau = (\mu + \rho\, \epsilon_m)\, du/dy \qquad (7.4)$$

and away from the wall, defined by the condition $u^+ \geq 12.9$

$$\epsilon_m/\nu = \frac{(0.36)^2 (du^+/dy^+)^3}{(d^2u^+/dy^{+2})^2} \qquad (7.5)$$

$$\tau = \rho\, \epsilon_m\, du/dy \qquad (7.6)$$

The latter expressions originated from Von Karman's similarity hypothesis.

For the flat plate, Deissler assumed that the shear stress was a constant, for the cylinder Sparrow assumes the shear stress is inversely proportional to the distance from the cylinder

$$\tau/\tau_\infty = \frac{r_o}{r_o + y} \qquad (7.7)$$

Expression (7.5) agrees with Glauert and Lighthill's results for the variation of the laminar shear stress near the cylinder and when the cylinder radius is very large, Eq. (7.7) reduces to the case of the flat plate.

Expressions (7.4) and (7.6) were then integrated to yield the radial velocity distribution and the wall shear stress. Sparrow presents the results for the friction factors for the values of radius Reynolds numbers from 10^3 to 10^6 and length Reynolds numbers from 5×10^4 to 5×10^8.

For the present case, the radius Reynolds numbers are of the order of one to ten. Therefore, the author used Sparrow's theory to predict friction factors for the lower values of radius Reynolds numbers.

As the radius Reynolds number decreases, the ratio of the boundary layer thickness to the cylinder radius increases and the boundary layer tends to deviate further from the flat plate boundary layer. The validity of Sparrow's theory becomes questionable as the case under consideration deviates further from the case of the flat plate.

Data taken by Selwood (20) who measured the drag on a continuous nylon filament drawn through air was found. The data presented in dimensional form, was non-dimensionalized by the author assuming the experiments were run at standard conditions (60°F and 14.7 psia). The extended theory of Sparrow and the experimental data are shown on Fig. 7.1. The agreement is very good even though the theory is for a cylinder of finite length,

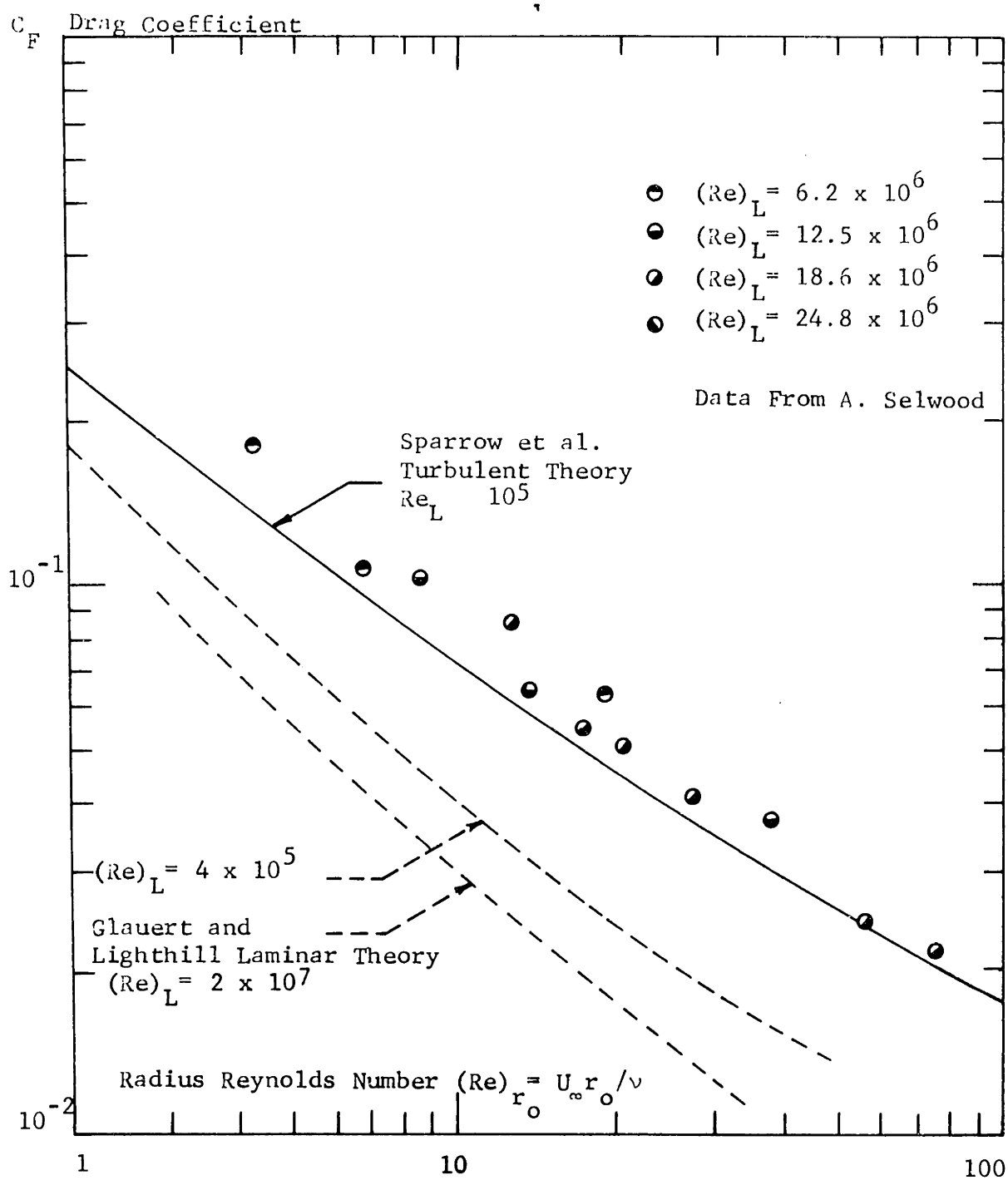

Drag Coefficient Versus Reynolds Number
Laminar and Turbulent Boundary Layer Flow
Along the Axis of a Cylinder

Fig. 7.1

with a definite leading edge, and the data is for the case of a continuous filament, the filament being unwound from one wheel and wound on another.

CHAPTER 8

A DESCRIPTION OF THE EXPERIMENTAL EQUIPMENT USED FOR THE VARIABLE VISCOSITY EXPERIMENTS

In order to check the results of the analysis, experiments were conducted using glass as the variable viscosity medium. The shape and tension distribution of the jet were measured for given values of the flow rate, the reservoir temperature, and the final fiber radius.

A description of the experimental equipment, test procedures, and data reduction procedure is presented below. A discussion of why measurements could not be made of such quantities as the velocity and temperature distributions will also be included.

Figure 8.1 shows a schematic of the test setup used for the case of the variable viscosity fluid, glass. The molten glass flowed from a resistance heated platinum reservoir through an axisymmetric nozzle. The cold, solidified jet was wound on a rotating steel drum. The drum and driving motor were mounted on a sliding base so that the jet could be wound at different positions on the drum. The reservoir was pressurized with air, the air pressure measured by a water manometer. The temperature of the reservoir was held constant using a Foxboro controller reading a platinum-platinum-rhodium thermocouple imbedded in the wall of the reservoir.

The temperature was checked with an identical thermocouple which was recorded using a Leeds and Northrup millivolt potentiometer. A Latronics Coloratio two color pyrometer was used to find the temperature of the nozzle tip. The speed of the steel drum was measured by both a strobatac and a mechanical tachometer.

The jet was photographed through a Gaertner tele-microscope which had a working distance, the distance from the front lens to the object viewed, of 5 inches of more. Magnifications used in the tests ranged from 5.4X to 33X. The large working distance was needed to keep the microscope sufficiently far away from the hot platinum so that the microscope would not overheat. As additional protection from unheating, a flat vycore window was mounted in front of the microscope and the microscope was surrounded by a water cooling coil. The tele-microscope was placed on a vertical traversing stand, the distance traversed was measured by a dial indicator. On the opposite side of the jet a strobotac was positioned without its reflector, to give approximately a point source of light. The strobotac was electrically connected to the camera so that depressing the shutter release also activated the strobotac light. The strobotac light was necessary since vibrations of the pulling wheel were transmitted to the fiber causing the jet to oscillate. The oscillations were very noticeable in the region where the jet

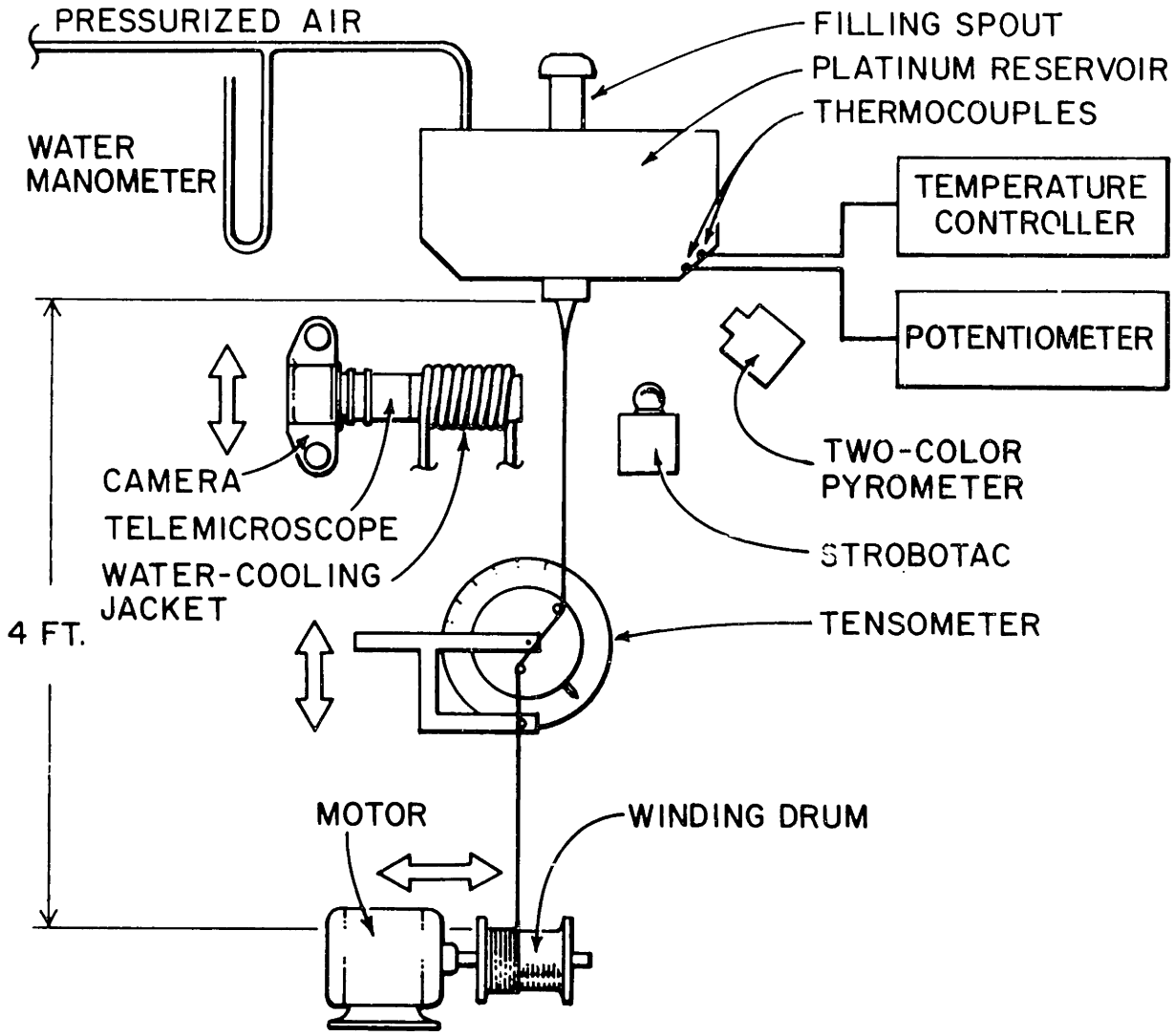

FIG. 8.1 SCHEMATIC OF EXPERIMENTAL SET UP

SIDE VIEW

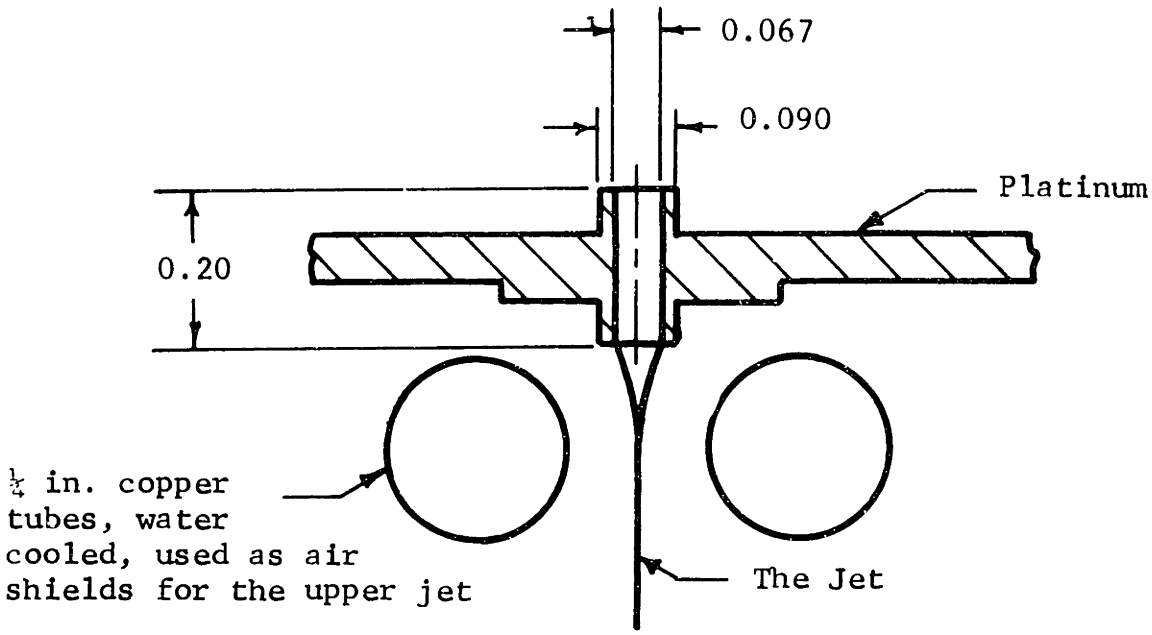

BOTTOM VIEW

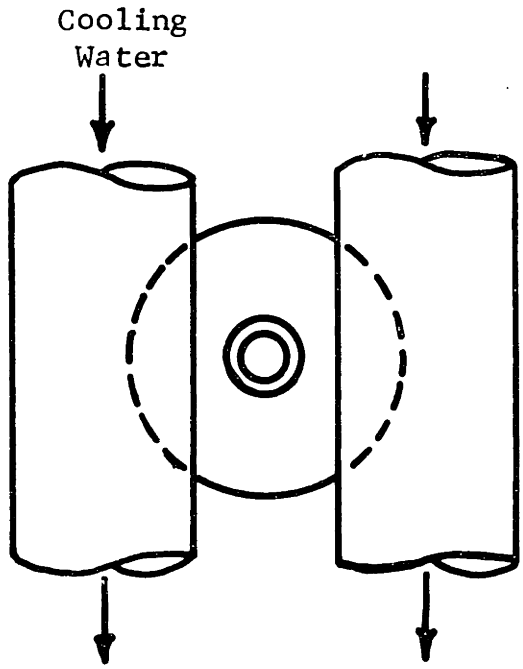

Fig. 8.2

THE NOZZLE

had reached its final radius. The amplitude of the motion would often be an order of magnitude larger than the local jet radius, the frequency varied with changes in the pulling wheel speed.

The tension was measured using a "tensometer", (see Fig. 8.3) developed by Owmes-Corning Fiberglas, which could be traversed to known vertical positions. The solidified jet was threaded on a graphite pin mounted on the end of a pivot arm. The torque on the pivot arm was transmitted to a hair spring mounted on the same shaft as the arm. The pointer, on an independent axis, was connected to the other end of the hair spring. When the pointer was rotated, the hair spring was extended until the pivot arm returned to its original position. The amount the pointer must be rotated in order to bring the pivot arm to its null position is therefore proportional to the torque or force on the pivot arm. The other two pins guide the solidified jet so that it leaves the tensometer radially from the pivot point causing no additional moments on the pivot arm.

If one draws a control volume about the tensometer, it may be seen that the force measured is the jet tension less the momentum flux of the jet and the air drag on the first pin.

8.1 Experimental Procedure

For each experiment, the flow rate, reservoir temperature, and winding speed were measured. Photographs were taken of the

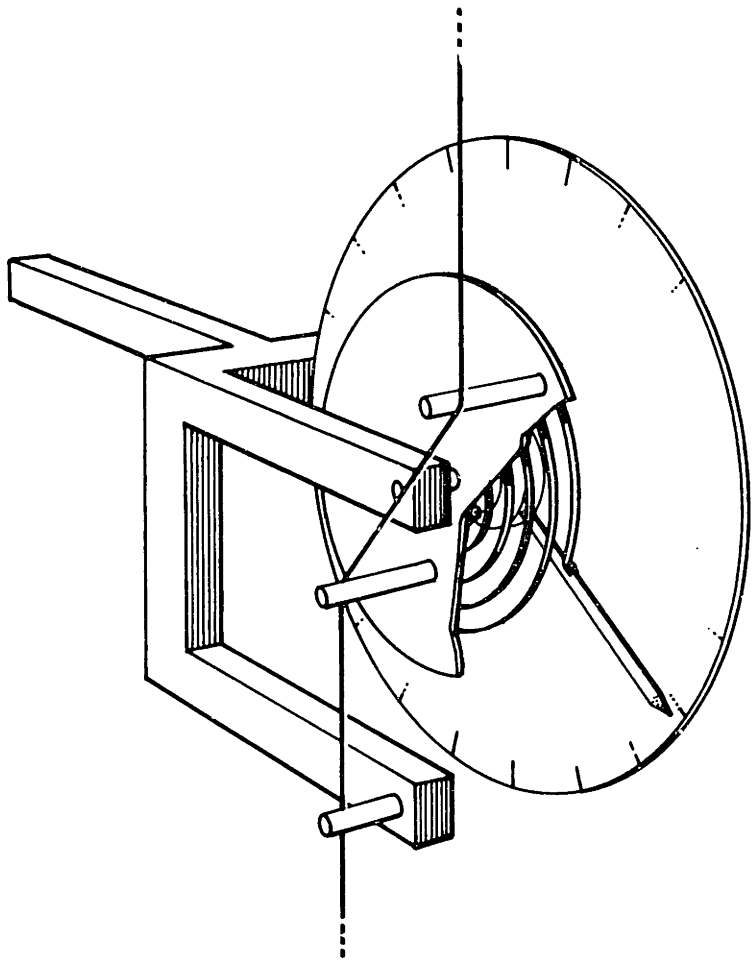

FIG. 8.3 THE TENSOMETER

jet starting at the nozzle exit and traversing the camera down to the region where the jet radius became constant. Because the jet vibrated it was difficult to keep the jet in focus at the high magnification used for the small radii. At least three photographs were taken at each camera position. For each magnification a photograph was taken of a stage micrometer (ruled to 0.01 mm) to serve as a reference. The tension was measured at seven or more different positions.

The flow rate was found by weighing the amount of fluid which had flowed during a given time interval. Since the fluid supply could not be continually replenished during a test, the flow rate was measured periodically during an experiment to be sure it did not vary more than 3 per cent.

The depth of fluid in the reservoir could not be measured while running the experiment; therefore, the total amount of glass which had been drawn was weighed and an equal amount of glass was put into the reservoir.

The final jet radius was calculated from the continuity relation, knowing the flow rate, drawing speed and the density of the fluid. The calculated radius agreed with the radius measured from the photographs within 5.2 per cent for all test runs except one, where the error was 9.6 per cent.

8.2 Quantities Which Could Not Be Measured

As previously mentioned, the temperature of the nozzle tip was measured using a two color pyrometer. This tip temperature was assumed to be approximately the same as the temperature of the fluid leaving the nozzle. The temperature of the fluid could not be measured with the pyrometer since the radiation from the fluid was partially volume radiation and partially surface radiation and the percentage of the surface radiation to the total radiation energy varied with varying temperature. Because of the small dimensions of the jet and the existence of volume radiation, it was felt that a thermocouple suspended in the flow would materially alter the temperature distribution in the fluid. The thermocouple would not measure the local fluid temperature due to the radiant exchange between the thermocouple and the long range surroundings.

No technique could be devised to measure the velocity distribution of the fluid either in the nozzle or in the jet. Again, this is due to the very small diameter of the jet (the nozzle I.D. for this test was .067"). Any velocity measuring device inserted in the flow would be of sufficient size to alter the flow pattern by obstructing the flow and also altering the temperature distribution as described above. Since the dynamical equations are linked to the temperature distribution by the strong viscosity-

temperature dependence, any change in the temperature distribution would cause a change in the velocity distribution.

The velocity distribution might be found by optically following the path of air bubbles or impurities in the flow. However, the image distortion at the fluid-air interface would extremely complicate this technique.

8.3 Properties of the Fluid

Very few properties of the jet fluid, glass, have been accurately measured at high temperatures. The specific heat and thermal conductivity are among the properties poorly known at high temperatures. No adequate technique has been developed to measure absorption coefficients at high wavelengths especially at high temperatures. At high wavelengths, the absorption coefficient is high, causing "normal sized" glass samples to appear opaque at these wavelengths, e.g., since the intensity of transmitted radiation decays as $e^{-\gamma x}$ a 1/8 inch thick sample would appear opaque to radiation if γ were 10^2 (cm^{-1}) or 10^5 (cm^{-1}).

Figure 3.3 shows the absorption coefficient versus wavelength distribution assumed for the glass. This was found from references on plate glass which probably has different optical properties than the glass used in the present experiments.

The viscosity is known and the viscosity-temperature relationship is shown on Fig. 8.4. There is a large change of viscosity with varying temperatures.

Since the accurate measurement of any of the above-mentioned properties would constitute a major effort in itself, no attempt was made by the author. Whenever a property value we needed in the calculations, the best value which could be found in the literature or by private communication was used. However, the reader should bear in mind that the accuracy of such values is questionable.

8.4 Data Reduction

The shape of the jet was found by mounting the negatives on glass slides and projecting the slides on an optical comparator. Examples of the pictures are shown on Figs. 8.5 and 8.6. The measurement was made by traversing a micrometer slide which held the negative. Positive prints and enlargements of the negative were not used in the measurement for fear of distorting the images when enlarged or printed.

The photographs of the stage micrometer scale were measured to determine the exact magnification factor used.

Three or four measurements of the diameter were made for each picture at a given axial position. For the smaller jet radii, two different pictures taken at the same camera location were measured.

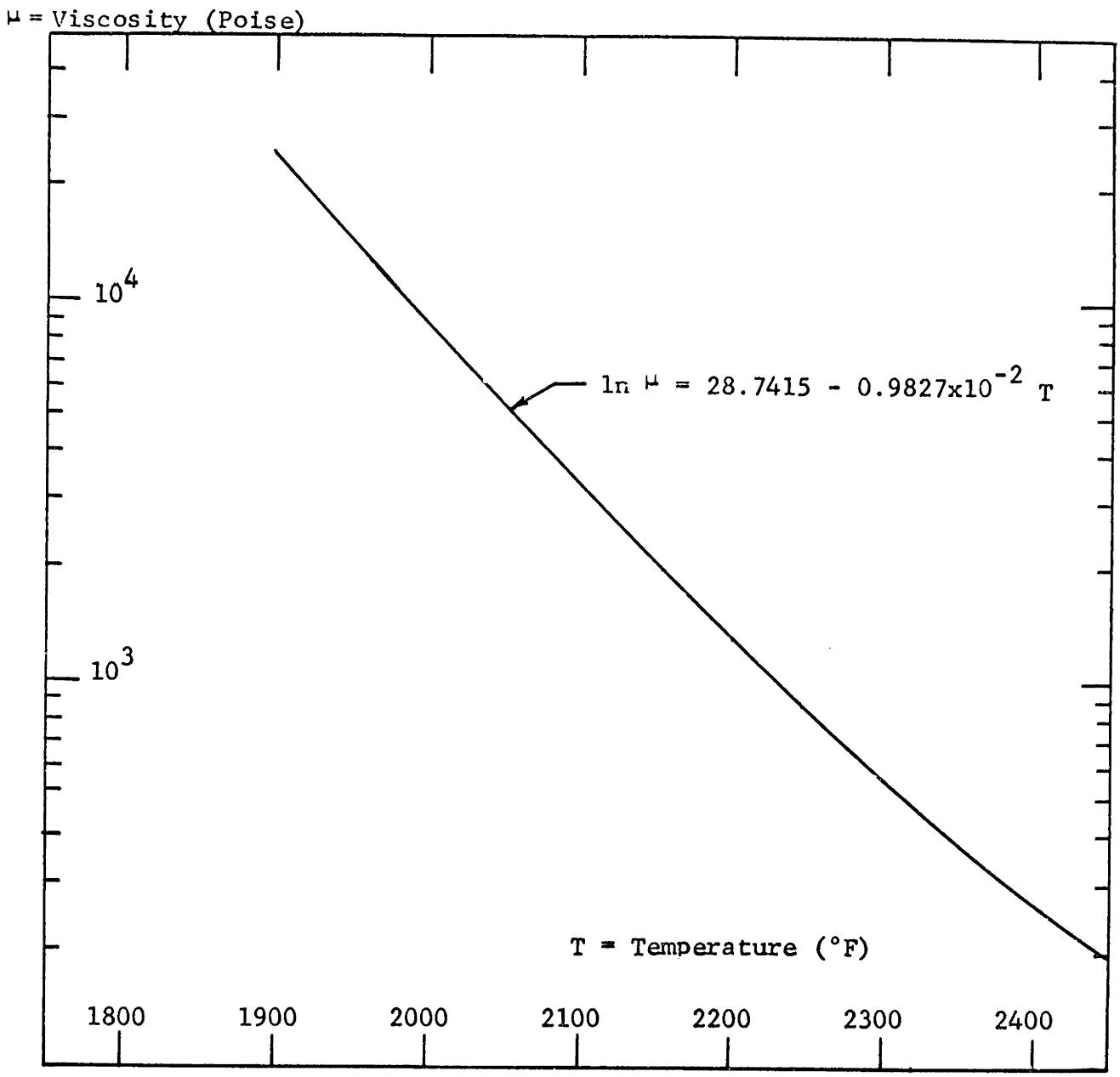

VISCOSITY VS. TEMPERATURE FOR GLASS

Fig. 8.4

0.1 In.
z = 0.0 in.
$R_o = 33.88 \times 10^{-3}$ in.

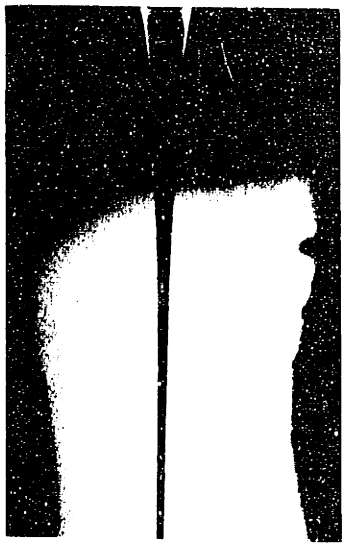

0.1 In.
z = 0.13 in.

0.1 In.
z = 0.26 in.

0.02 In.
z = 0.36 in.
$r_o = 0.98 \times 10^{-3}$ in.

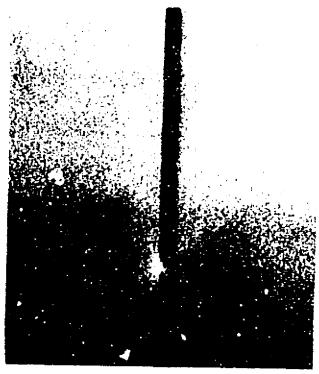

0.02 In.
z = 0.46 in.
$r_o = 0.774 \times 10^{-3}$ in.

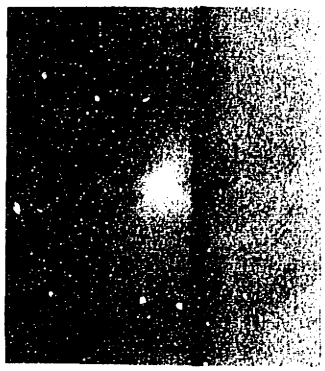

0.02 In.
z = 1.05 in.
$r_o = 0.478 \times 10^{-3}$ in.

Fig. 8.5

PHOTOGRAPHS OF THE JET

Test M8 - $w = 1.83 \times 10^{-5}$ (lbs)m/sec ; $T_o = 2160°F$

0.1 Inch
z = 0.0 in.
$R_o = 33.26 \times 10^{-3}$ in.

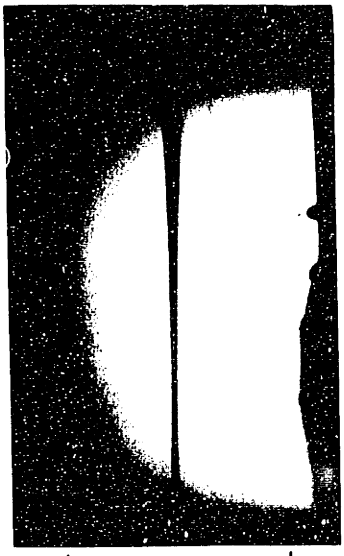

0.1 Inch
z = 0.133 in.

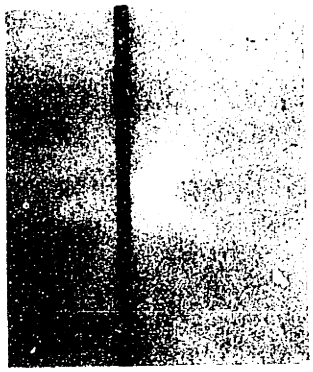

0.02 In.
z = 0.36 in.
$r_o = 0.622 \times 10^{-3}$ in.

0.02 In.
z = 0.46 in.
$r_o = 0.471 \times 10^{-3}$ in.

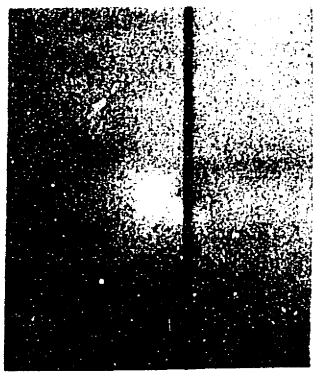

0.02 In.
z = 0.85 in.
$r_o = 0.331 \times 10^{-3}$ in.

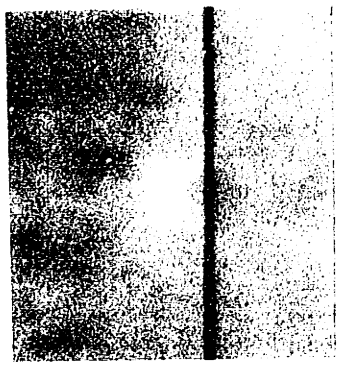

0.01 In.
z = 1.65 in.
$r_o = 0.248 \times 10^{-3}$ in.

Fig. 8.6

PHOTOGRAPHS OF THE JET

Test M7 - $w = 1.82 \times 10^{-5}$ (lbs)m/sec ; $T_o = 2160°F$

By calibrating the tensometer beforehand, the values read from the tensometer could be converted into units of force. The calibration did not change throughout the experiment. The resulting values were added to the momentum flux of the fiber. No accurate way to determine the air drag on the tensometer pin could be found. By using the boundary layer solutions to estimate the thickness of the boundary layer, a very crude approximation of the air drag was found. It was found that the magnitude of the air drag was, at most, equal to the momentum flux. This work was not pursued further, because one is principally concerned in using the slope of the tension versus distance curve to predict the drag coefficient. Assuming that the boundary layer does not change appreciably in the region of interest, the shear stress will be the same for all vertical positions. Therefore, the slope of the tension versus distance curve will not be effected if the correction for drag is not included.

The assumption that the shear stress does not vary with axial distance is a good one since the boundary layer theory applicable to this region is almost independent of the distance Reynolds number. The solution only depends upon the radius Reynolds number and in the region where the tension was mesured, the fiber radius is a constant.

The slope and position of the straight line to represent the tension data was calculated by the principle of least squares. Assuming that the "true" tension versus distance function is a straight line, the error in the calculated slope was estimated.

Appendix A presents all of the experimental data for glass in tabular form.

CHAPTER 9

A COMPARISON OF THE EXPERIMENTAL AND THE THEORETICAL RESULTS

The experimentally measured tension in the jet and the measured jet shape will be presented below. The data will be compared with the results of the theoretical analysis described in Chapters 3 and 4.

9.1 The Jet Shape

Figures 9.1, 9.2 and 9.3 show the measured jet shape along with the corresponding theoretical curves for three different test conditions. The theoretical curves are taken from the results of the numerical solutions of the complete one-dimensional equations, Eqs. (4.31) and (4.33). Since the specific heat is not accurately known, two theoretical curves are shown on each figure. The two curves were calculated using values for the specific heat of 0.25 BTU/lb°F and 0.30 BTU/lb°F respectively. The two values represent the approximate limits within which the value of the specific heat is known.

The one dimensional solution has been shown to be valid only when the boundary of the jet has a slope of less than one-tenth, defined as the central jet region.

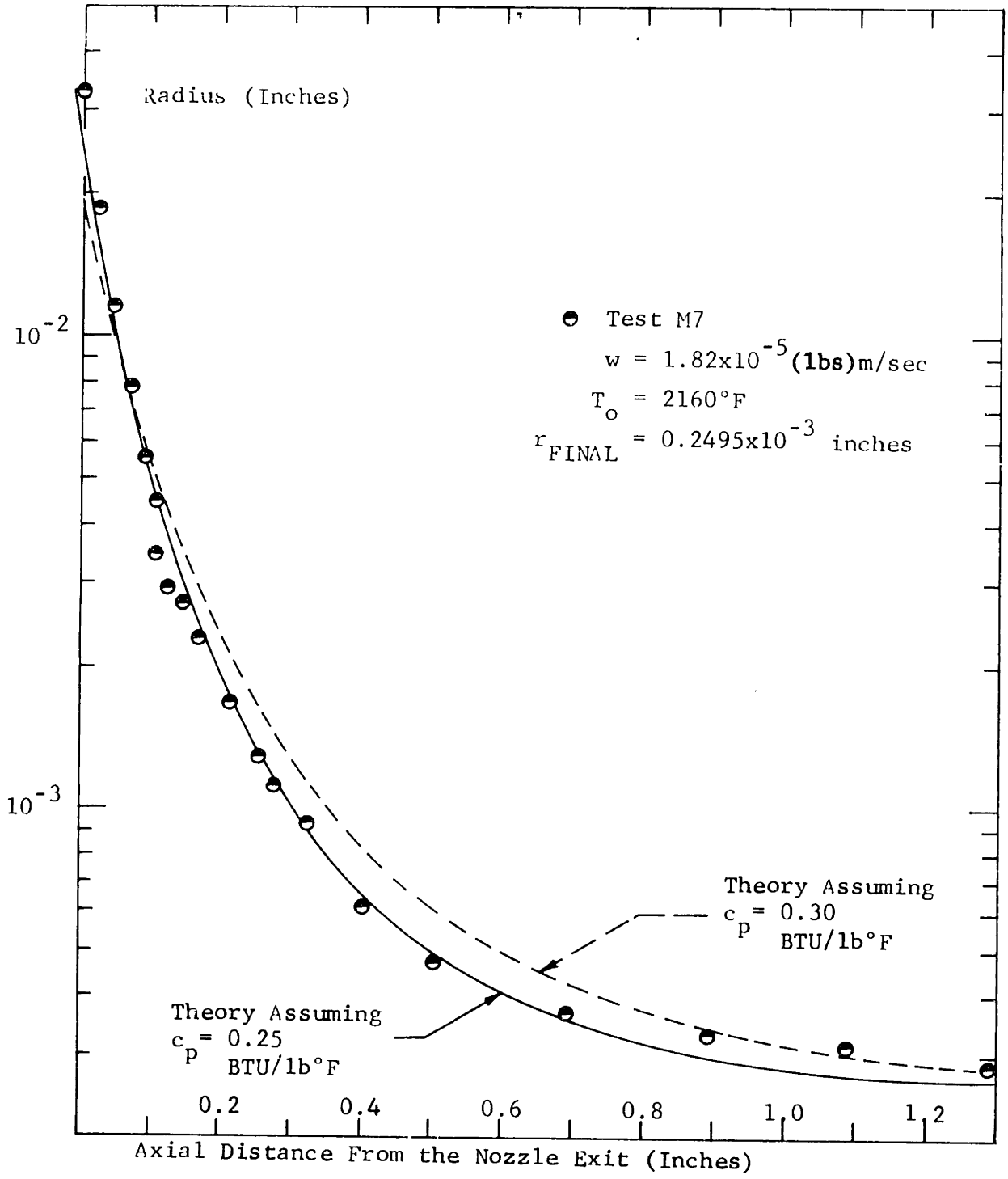

JET RADIUS VERSUS DISTANCE
THEORETICAL AND EXPERIMENTAL RESULTS

Fig. 9.1

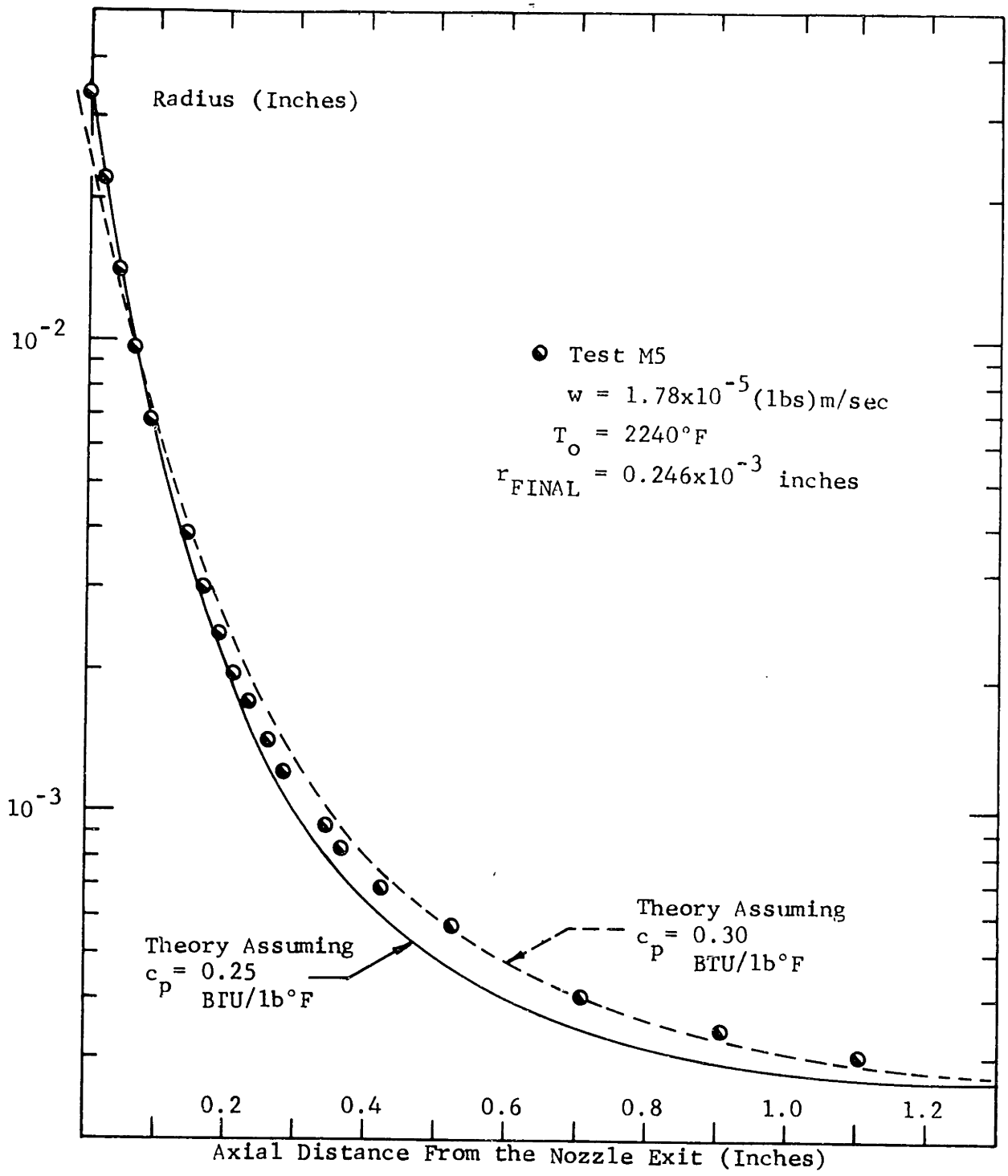

JET RADIUS VERSUS DISTANCE
THEORETICAL AND EXPERIMENTAL RESULTS

Fig. 9.2

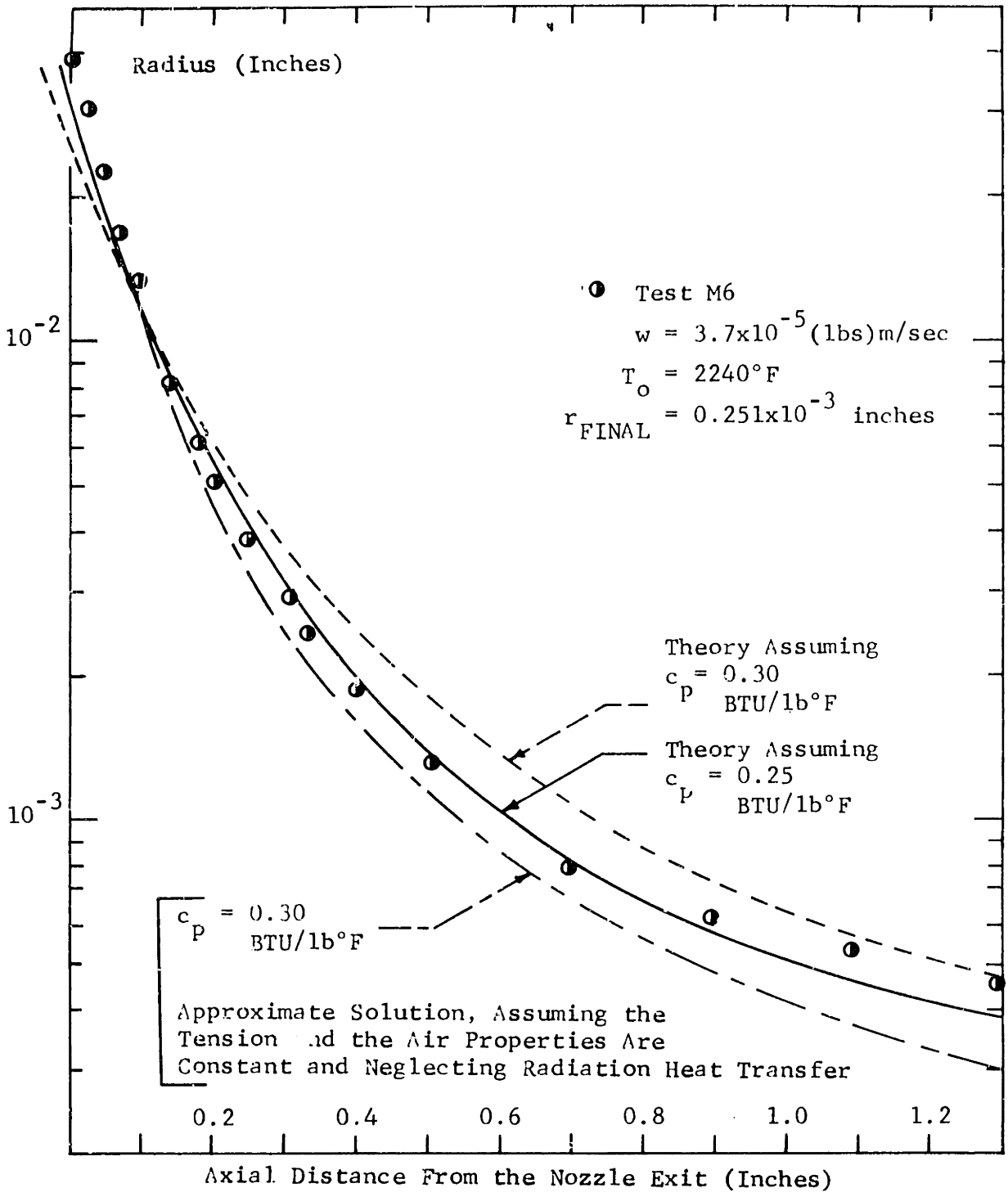

JET RADIUS VERSUS DISTANCE
THEORETICAL AND EXPERIMENTAL RESULTS

Fig. 9.3

Therefore, the theoretical curves were started at the data point where the slope is minus one-tenth. The theoretical curves were also extended to larger radii to see how much the upper jet deviated from the one-dimensional approximations. The data and theoretical curves were matched at the point where the slope was one-tenth rather than at the initial jet radius because in the latter method agreement between the data and the theory in the central jet region would be penalized by errors in the upper jet region.

The agreement between the data and the theory in the central jet region is very good. In the upper jet region the agreement is surprisingly good. See Figs. G-1 through G-3 in Appendix G for similar curves for other test conditions.

Figures 9.4 and 9.5 show the influence of various parameters on the theoretical model; the test condition is the same as in Fig. 9.3.

In Fig. 9.4 the theoretical curves are plotted assuming the initial temperature is 2280°F and 2200°F instead of 2240°F as measured. Although the initial tension for the two cases is 264 dynes and 381 dynes respectively, it can be seen that the change in the level of the tension or the initial temperature does not alter the shape in the central jet region. The third curve was calculated assuming that the absorption coefficient

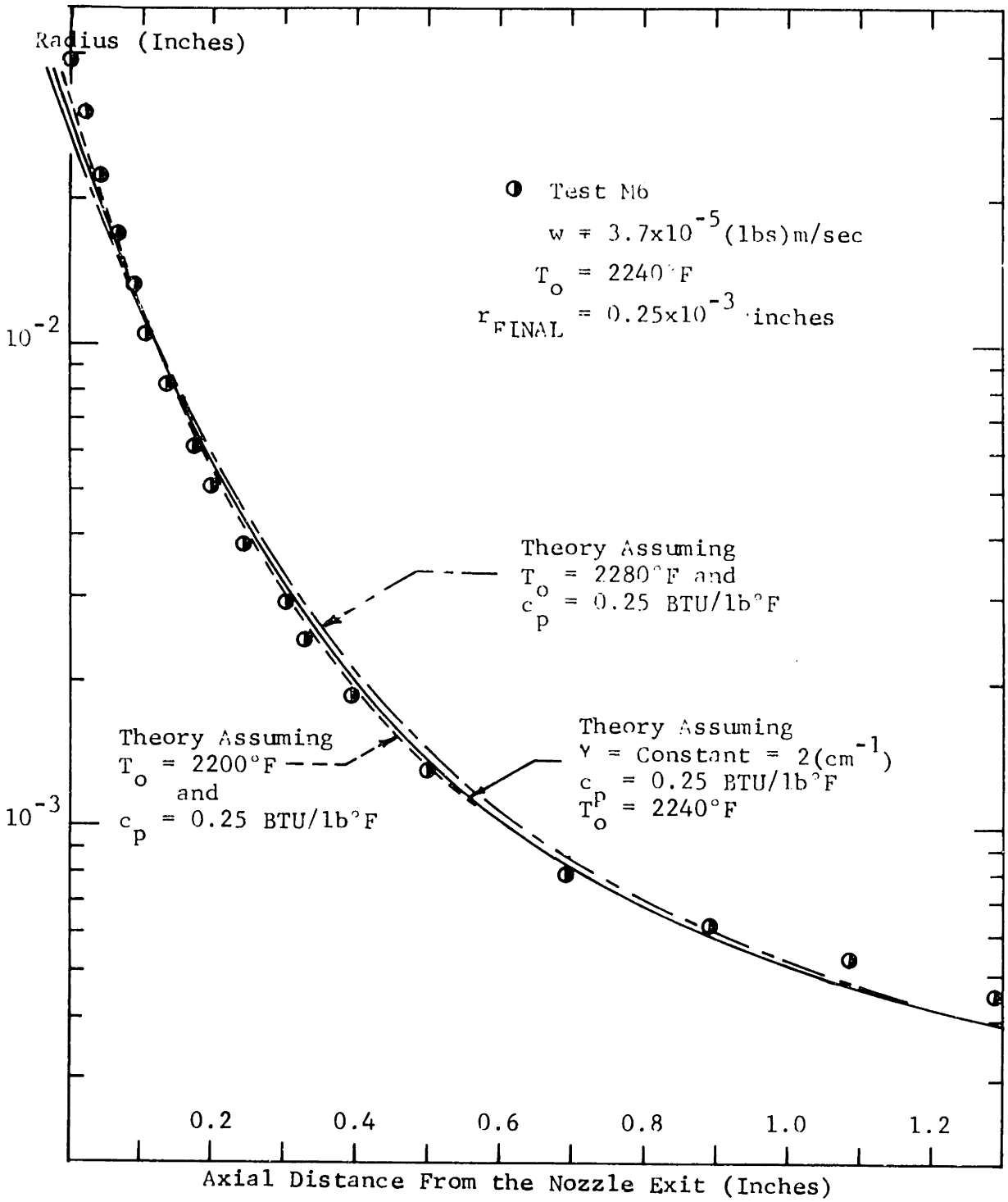

JET RADIUS VERSUS DISTANCE
THEORETICAL RESULTS ASSUMING DIFFERENT VALUES
OF THE INITIAL JET TEMPERATURE
AND ASSUMING A CONSTANT ABSORPTION COEFFICIENT

Fig. 9.4

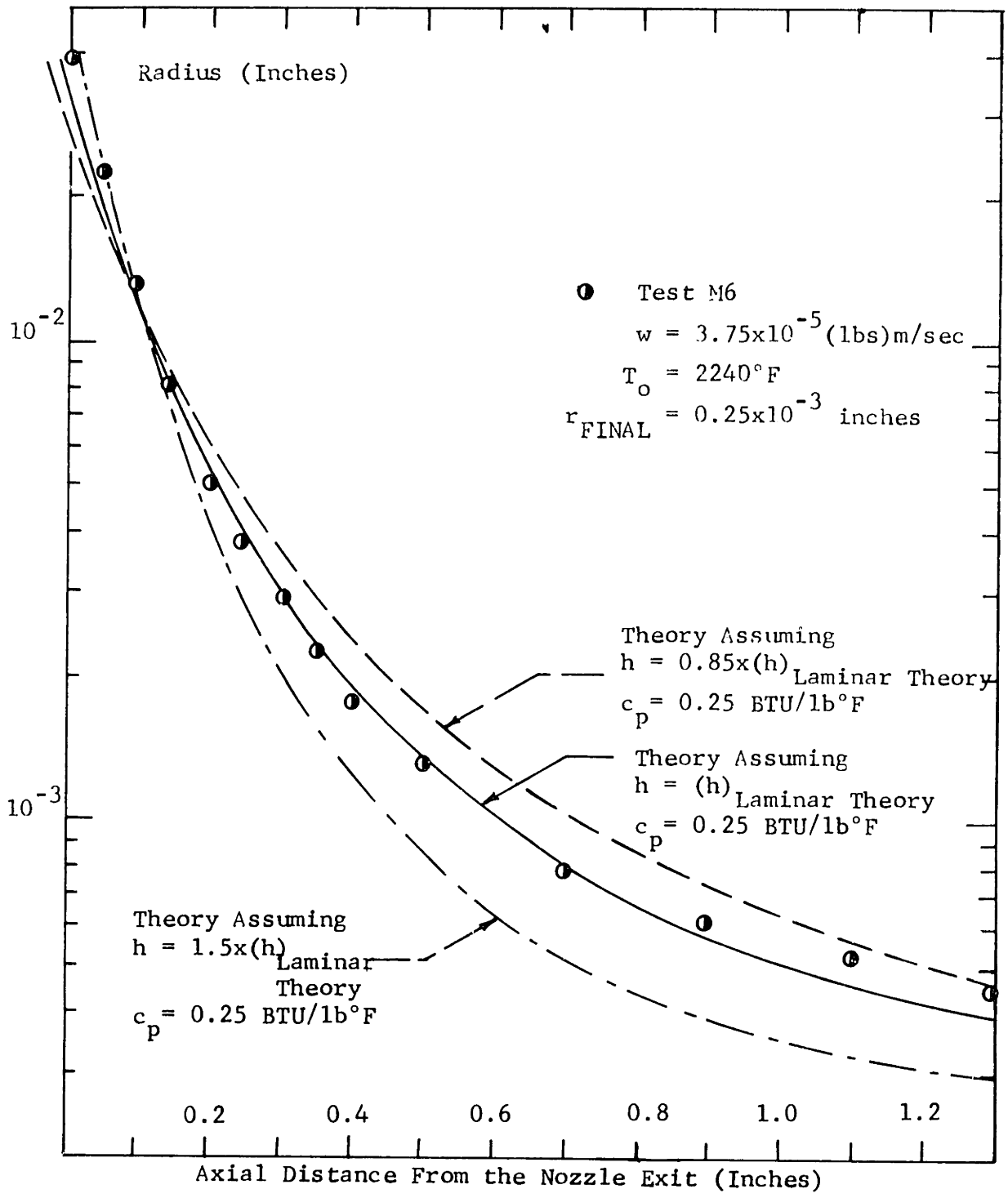

JET RADIUS VERSUS DISTANCE
THEORETICAL RESULTS ASSUMING DIFFERENT VALUES
FOR THE FILM HEAT TRANSFER COEFFICIENT, h ,
OTHER THAN THOSE PREDICTED BY GLAUERT AND LIGHTHILL'S THEORY

Fig. 9.5

was constant and equal to 2 (cm^{-1}) instead of the variation shown in Fig. 3.3. For this case the product $\gamma \times r_o$ is less than one and the radiation is all of the volume type. The figure shows that this does not affect the central jet shape materially but it does affect the upper jet shape.

In Fig. 9.5 the curves were calculated for two cases, assuming the laminar film coefficient of heat transfer is 0.85 and one and one half times the value predicted by Glauert and Lighthill's theory. It can be concluded that laminar forced convection has a dominating influence on the jet. If the value of specific heat used in this case, 0.25 BTU/lb°F is correct, the results also indicate that Glauert and Lighthill's results are correct and that the boundary layer on the central jet is laminar for these particular test conditions.

The following figures, 9.6 and 9.7, show the compiled results of the test runs along with the corresponding theoretical curves. In Fig. 9.6 the experimental results of first changing the final fiber radius by a factor of two and secondly changing the flow rate by a factor of two are shown. Examining the results of changing the final radius while keeping all other variables constant, one sees that there is no noticeable change in the shape of the upper jet. Comparing two cases where the final jet

radius is the same and only the flow rate is changed, e.g., tests M1 and M4, it is seen that the shape is much "fuller" for the higher flow rate which is to be expected. The higher flow rate requires a larger surface area for heat transfer to achieve the same temperature decrease in the region where radiation heat transfer is important.

Figure 9.7 illustrates the effect of experimentally changing the initial temperature by 80°F. Although the tests at the high temperatures have a "fuller" jet shape the difference between the jet shapes is small. Note that the solid and dotted curves in Fig. 9.8 are not theoretical curves, they were drawn only to aid the reader follow the data points for a particular test condition. Also, the axial distance scale has been increased so that only the upper part of the central jet region is shown.

9.2 The Temperature Distribution in the Jet

As mentioned previously, the temperature of the jet was not experimentally measured. Since the solution of the temperature distribution is an integral part of the solution of the jet shape for the one-dimensional case, the validity of the calculated temperatures is confirmed by the excellent jet shape results. The theoretically calculated temperature versus distance distributions for the jet will be presented.

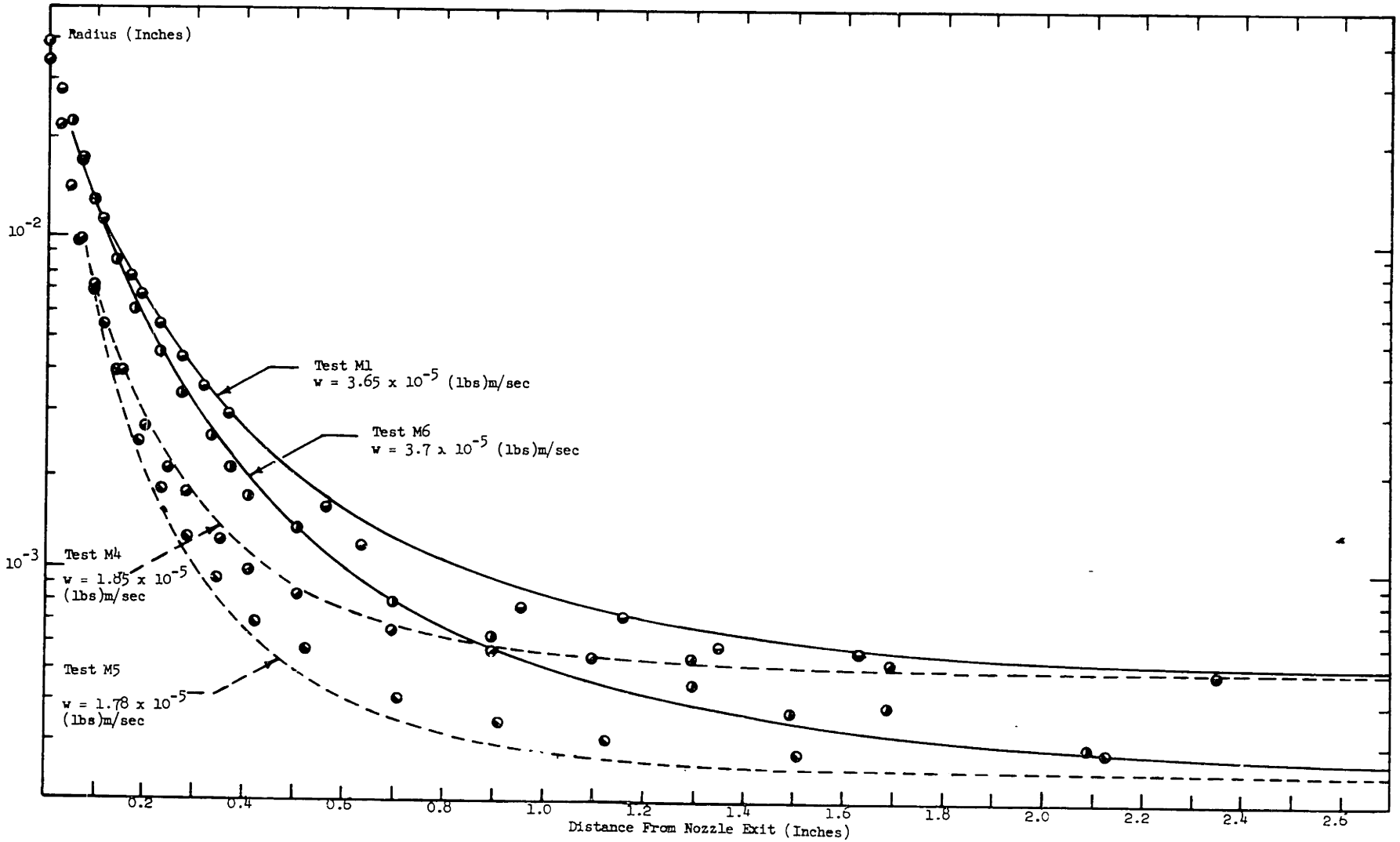

JET RADIUS VERSUS DISTANCE
THEORETICAL AND EXPERIMENTAL RESULTS
THE EFFECT OF DIFFERENT FLOW RATE AND FINAL FIBER RADII
FOR ALL CASES T_o = 2240°F, c_p = 0.25 BTU/lb°F FOR ALL THEORETICAL CURVES

Fig. 9.6

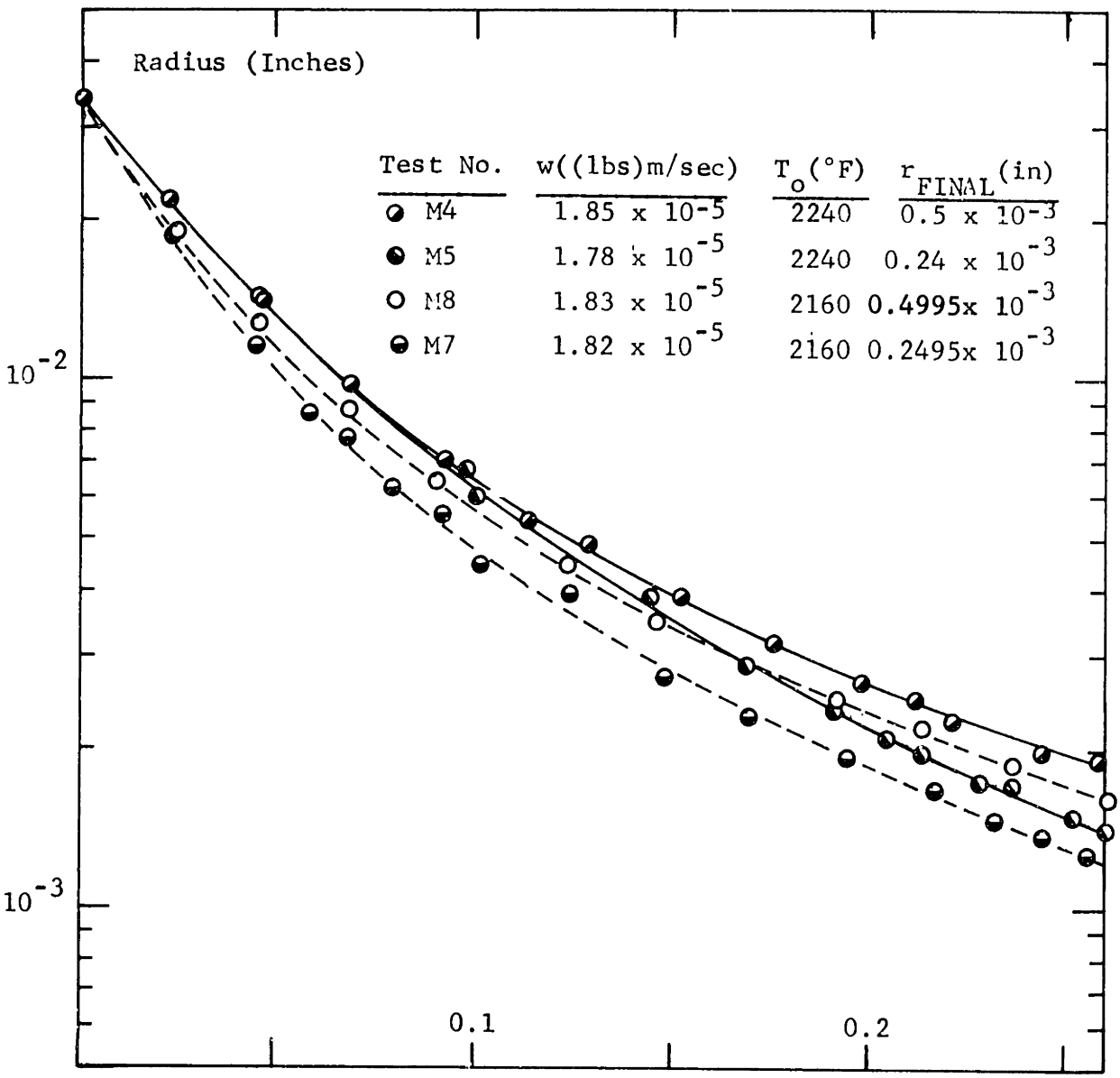

JET RADIUS VERSUS DISTANCE
EXPERIMENTAL RESULTS ONLY
THE EFFECT OF CHANGING THE INITIAL TEMPERATURE
AND CHANGING THE FINAL RADIUS ON THE SHAPE OF THE UPPER JET
WHILE THE FLOW RATE IS APPROXIMATELY CONSTANT

Fig. 9.7

Figure 9.8 shows the temperature distribution for the same conditions shown on Fig. 9.5. The temperature curves were positioned so that the temperature equaled T_E at the position below the nozzle exit where the slope equaled minus one tenth. The curves were extended into the upper jet region to the point where the calculated radius equaled the initial jet radius. Notice that the principle difference between the temperature curves for a specific heat of 0.25 BTU/lb°F and 0.30 BTU/lb°F is the slope of the curves. The temperature gradient in the jet determines the viscosity gradient which in turn effects the jet shape.

Figure 9.9 shows the effect of assuming different values of the initial jet temperature. The temperature level is different but the temperature gradient at any given distance below the nozzle exit has approximately the same value. The shape in the one-dimensional region is unaffected by a change in the initial jet temperature. Consequently, the fact that the experimentally measured shape agrees with the predicted shape can not be used to confirm that the measured value of the initial jet temperature is correct.

Notice also on Fig. 9.9 that for all three cases the temperature calculated at the initial jet radius, at the upper end of the temperature curves, is less than the assumed initial jet

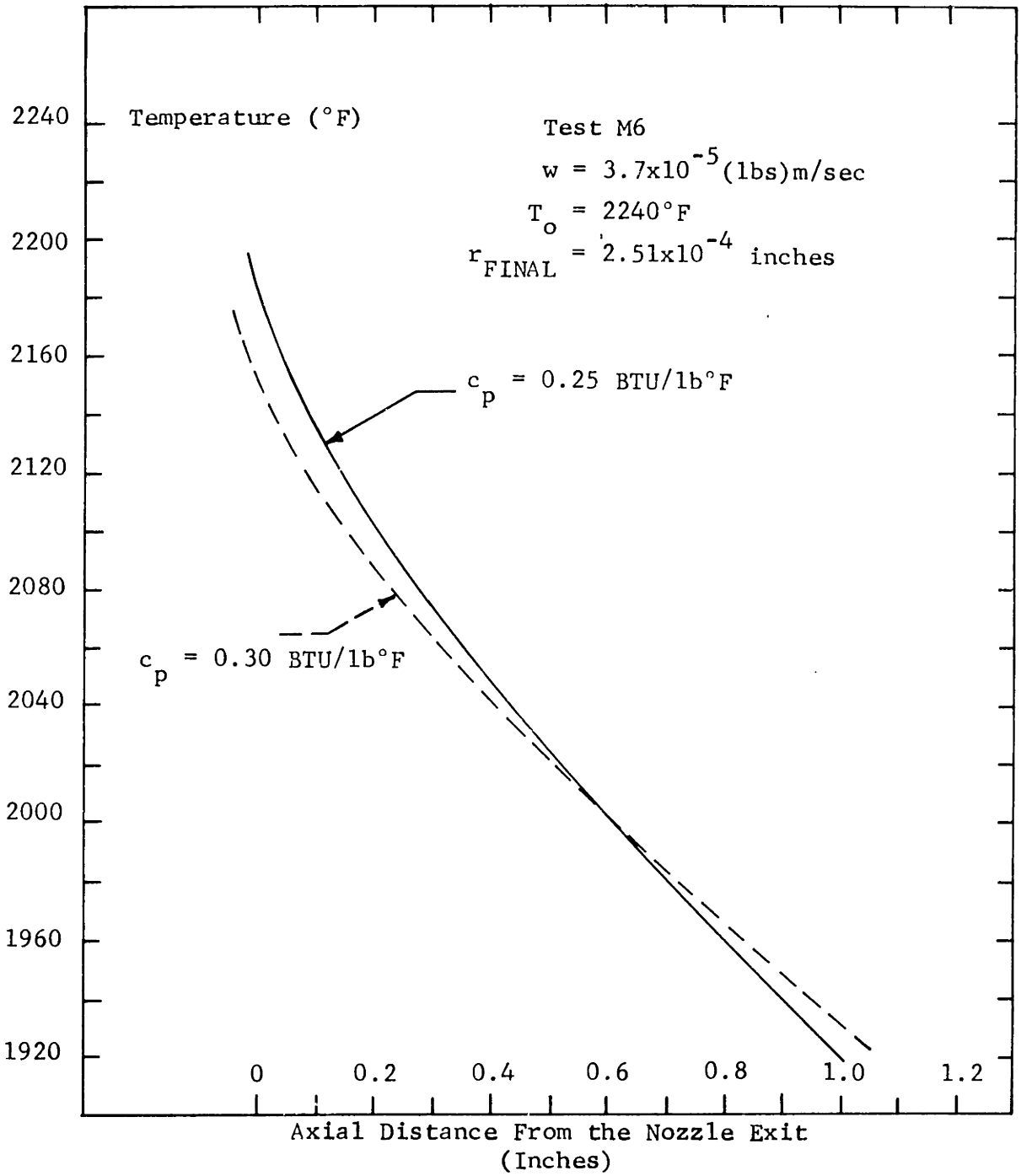

TEMPERATURE (THEORETICAL) VERSUS DISTANCE
ASSUMING DIFFERENT VALUES FOR THE SPECIFIC HEAT OF THE GLASS

Fig. 9.8

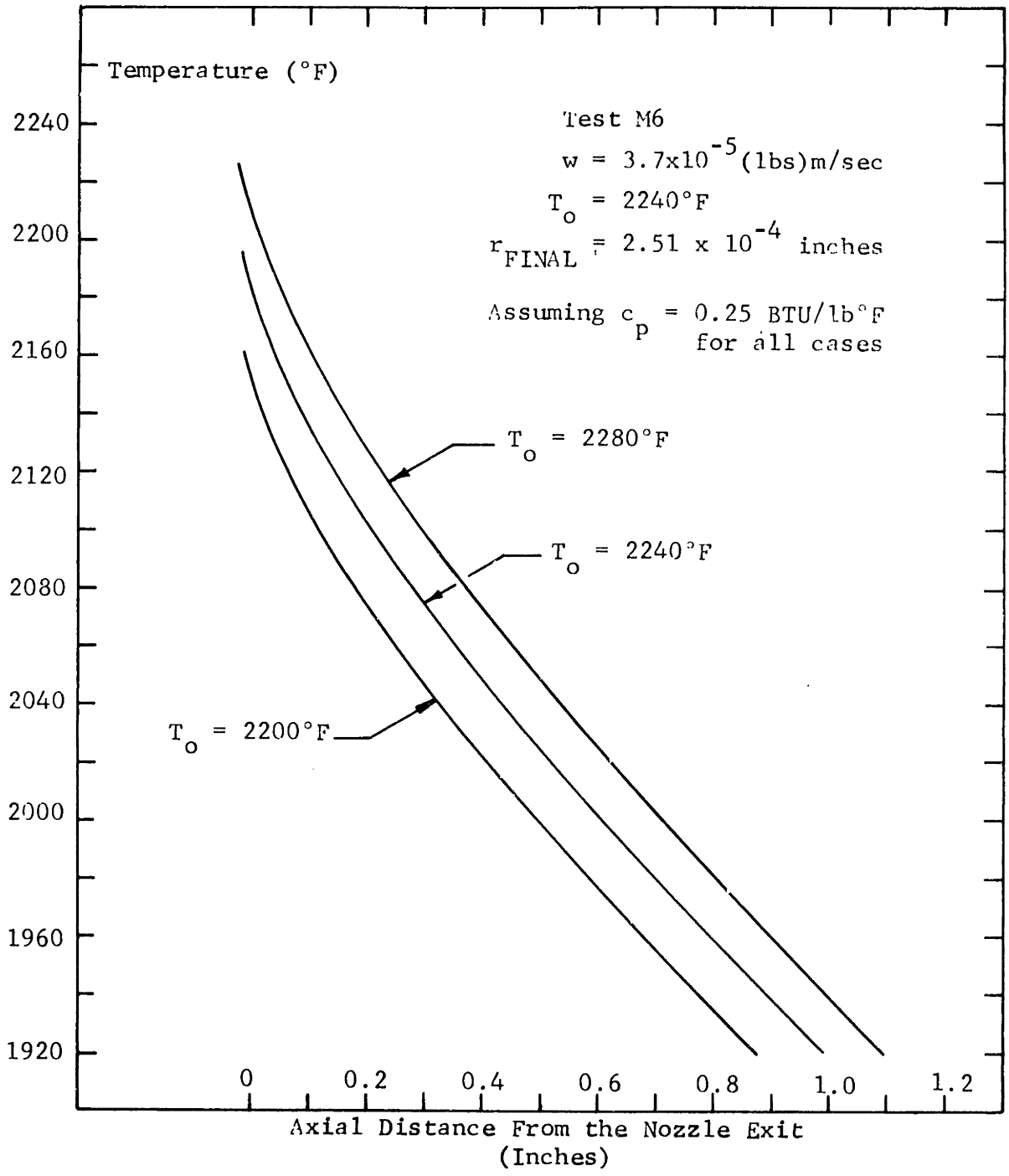

TEMPERATURE (THEORETICAL) VERSUS DISTANCE
ASSUMING DIFFERENT VALUES FOR THE INITIAL TEMPERATURE

Fig. 9.9

temperature. This confirms the fact that the one-dimensional temperature and velocity assumptions in the upper jet are not correct.

In Fig. 9.10 are shown the temperature distributions corresponding to the cases shown on Fig. 9.5 plus the case where the absorption coefficient is assumed to be a constant. For the case where the absorption coefficient of the glass is assumed a constant small value, the curve is only changed in the upper jet region.

Finally, Fig. 9.11 shows the calculated temperature distributions when the final fiber radius is varied and when the flow rate is varied, the latter having a large effect on the temperature gradient. For cases where only the final fiber radius is altered, the temperature is approximately the same at any axial distance. The temperature distribution is only shown for the central jet region since there is a transition to a turbulent boundary layer below this region, as explained in the next section.

9.3 Tension in the Jet

In the region where the jet has achieved its final radius, the tension versus distance was measured. Figures 9.13, 9.14 and 9.15 show the results of the measurements. The position of the straight line through the data points was found by the method of least squares. Also shown is the theoretical curve of tension

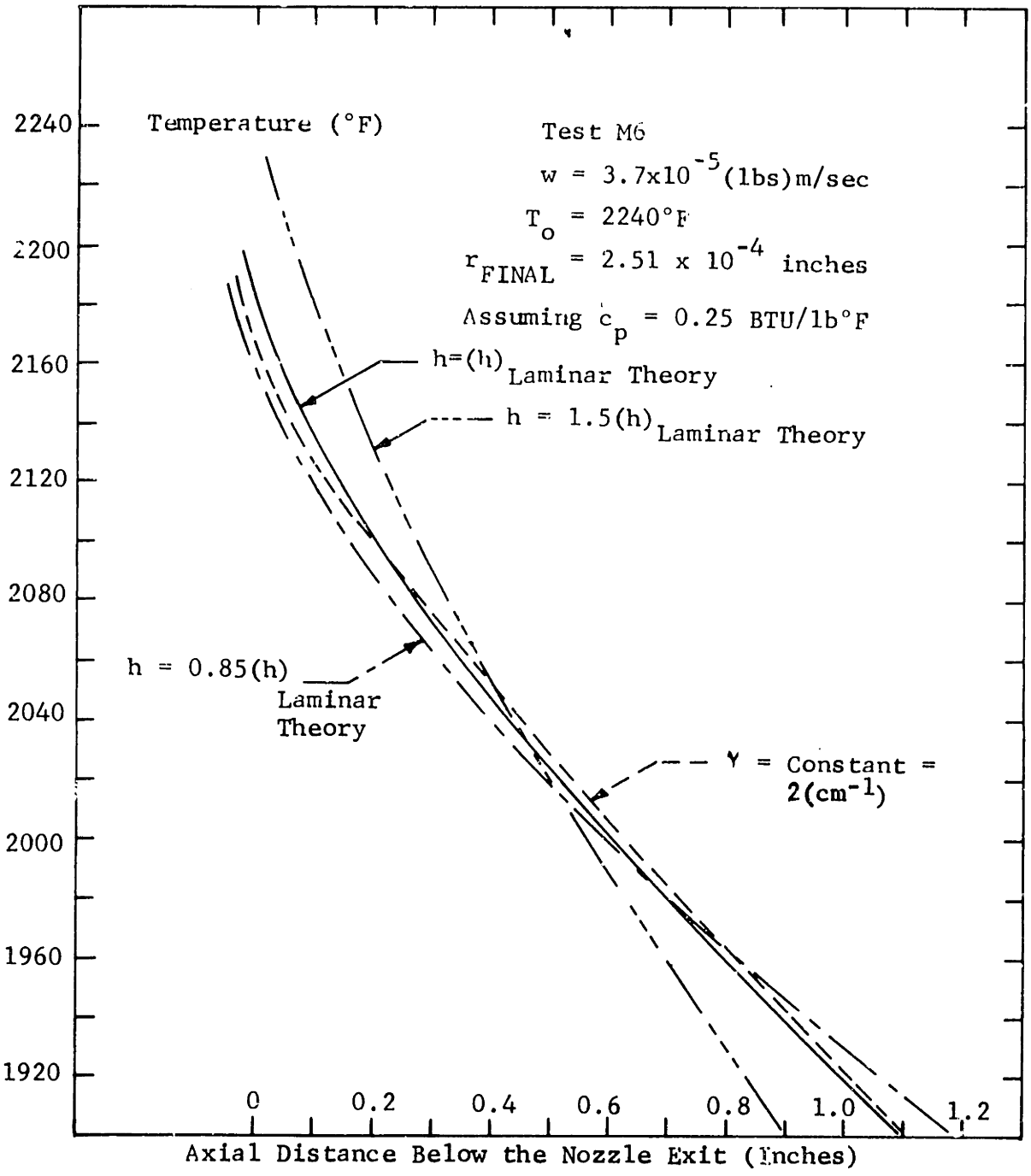

TEMPERATURE (THEORETICAL) VERSUS DISTANCE
ASSUMING VALUES OF THE FILM HEAT-TRANSFER COEFFICIENT, h, OTHER THAN THOSE PREDICTED BY GLAUERT AND LIGHTHILL'S THEORY
IN ADDITION, THE EFFECT OF ASSUMING A CONSTANT VALUE FOR THE ABSORPTION COEFFICIENT OF THE GLASS

Fig. 9.10

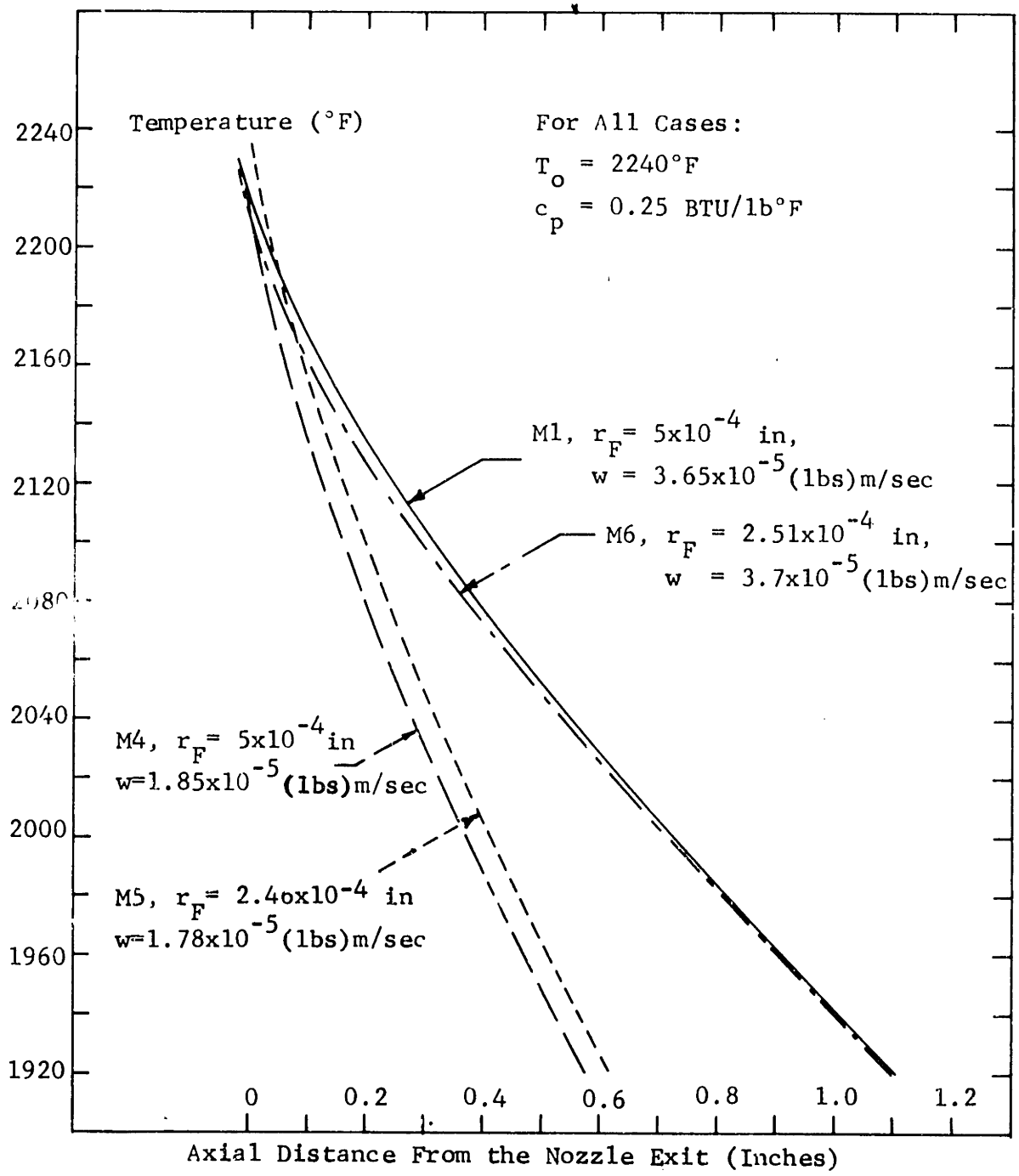

TEMPERATURE (THEORETICAL) VERSUS DISTANCE
THE EFFECT OF VARYING THE FLOW RATE AND FINAL FIBER RADIUS

Fig. 9.11

versus distance. The extreme left hand portion of the theoretical tension curve which is almost horizontal corresponds to the upper jet. The rapid rise is due to the increase in tension needed to accelerate the jet as it is attenuated. The final straight portion of the curve represents tension increase due to shear stress on the jet surface.

Also shown on Figs. 9.12 through 9.14 is the amount the initial jet temperature would have to be changed so that predicted and measured tension would coincide at the end of the central jet region, where the radius has just reached its final value. The small amount the initial temperature must be changed in all of the cases except M7 and M8 within the experimental error, $\pm$ 20°F, indicate that the one-dimensional expression used for the initial tension Eq. (3.6) is valid.

On the other hand, it could be assumed that an error in the measurement of the initial jet slope or angle caused the disagreement between the predicted and measured tension. The initial angle enters the formula for the predicted initial tension in the term $\gamma_T \pi R_o \cos\theta_o$. It is found that the error in measuring θ_o, the initial angle, would have had to be unreasonably large in most cases to make the theoretical and experimental tension agree, e.g., for test M5, θ_o would have had to be 55° instead of

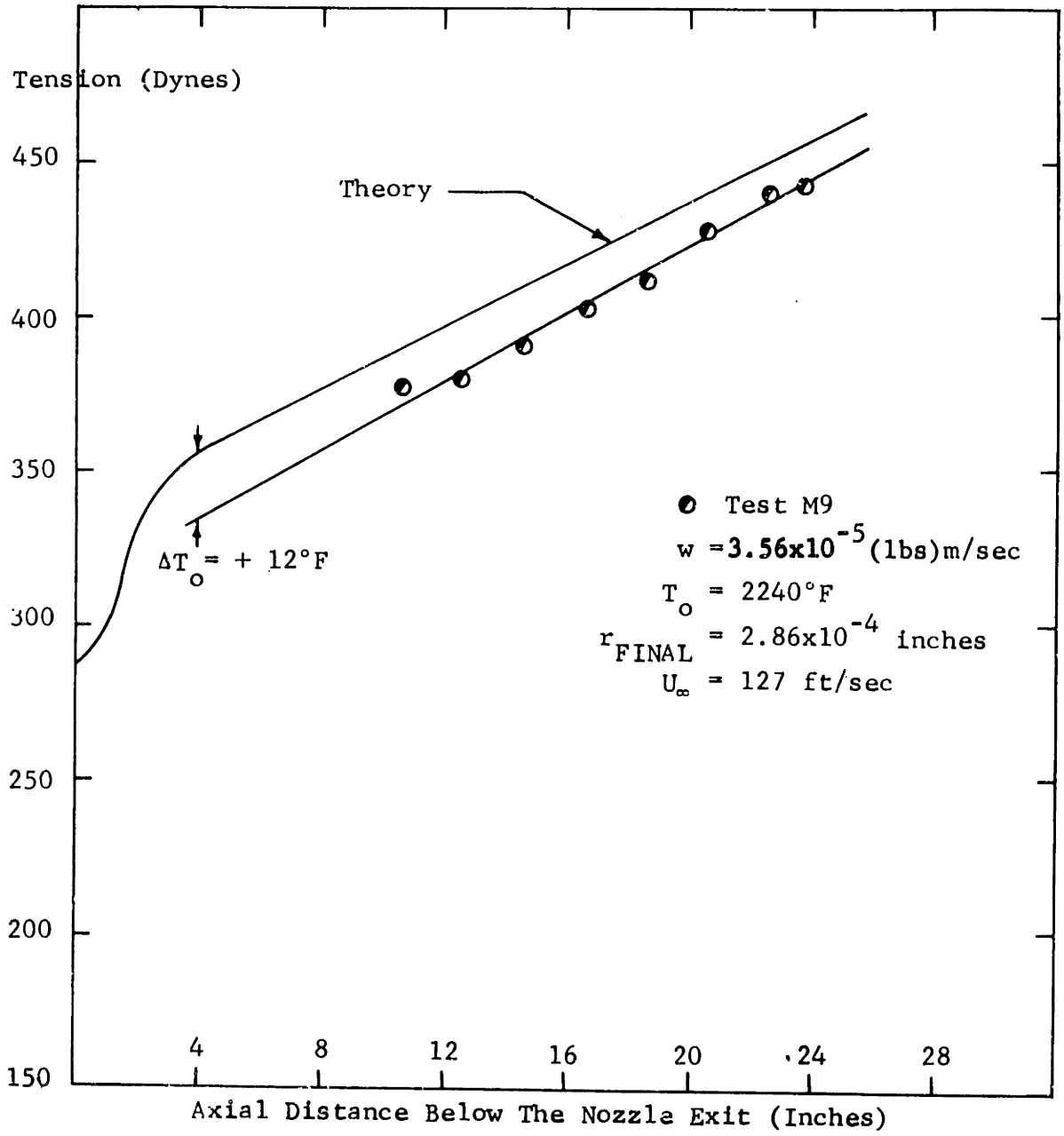

TENSION VERSUS DISTANCE
THEORY AND DATA

Fig. 9.12

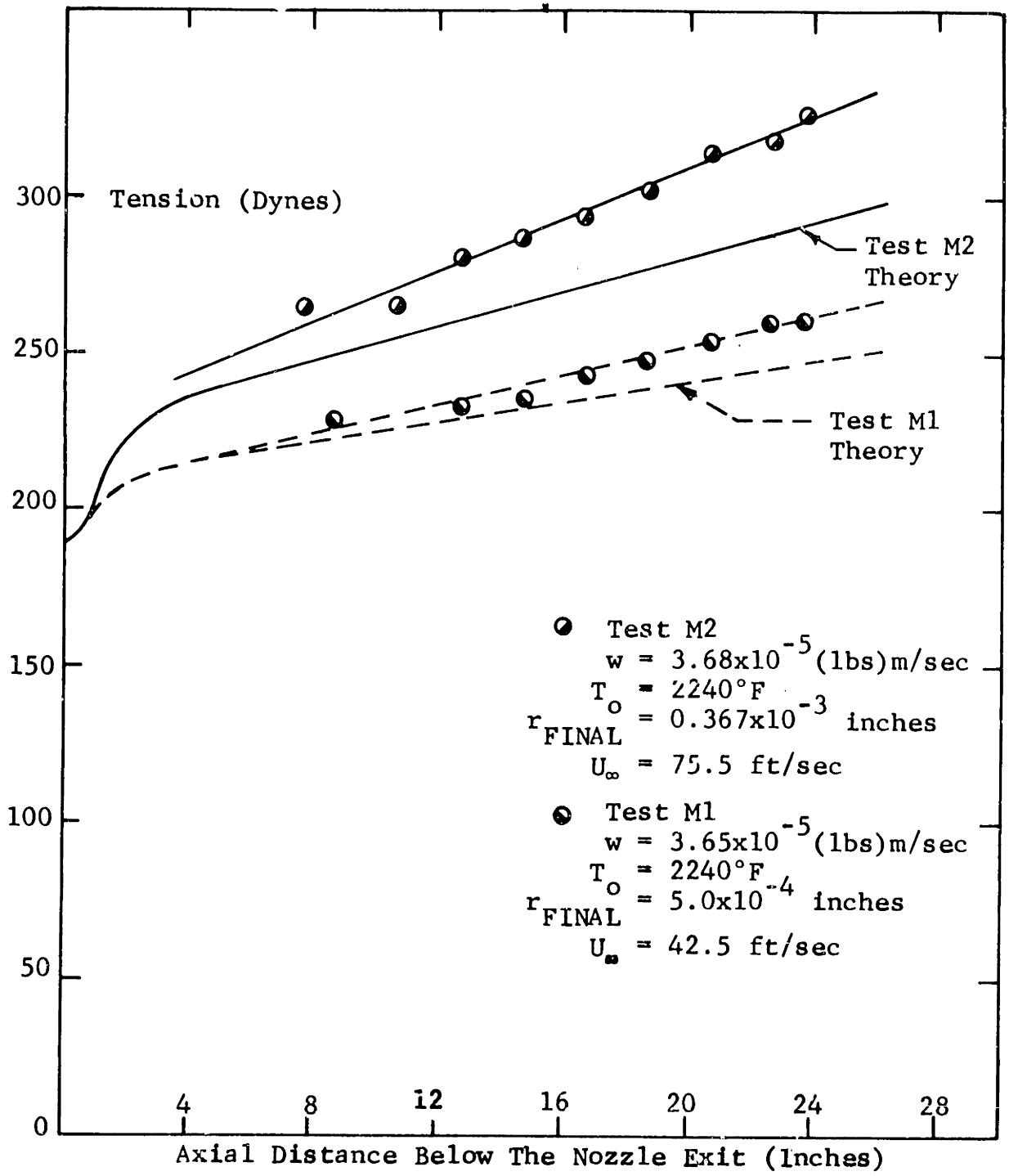

TENSION VERSUS DISTANCE
THEORY AND DATA
THE EFFECT OF CHANGING THE FINAL FIBER RADIUS

Fig. 9.13

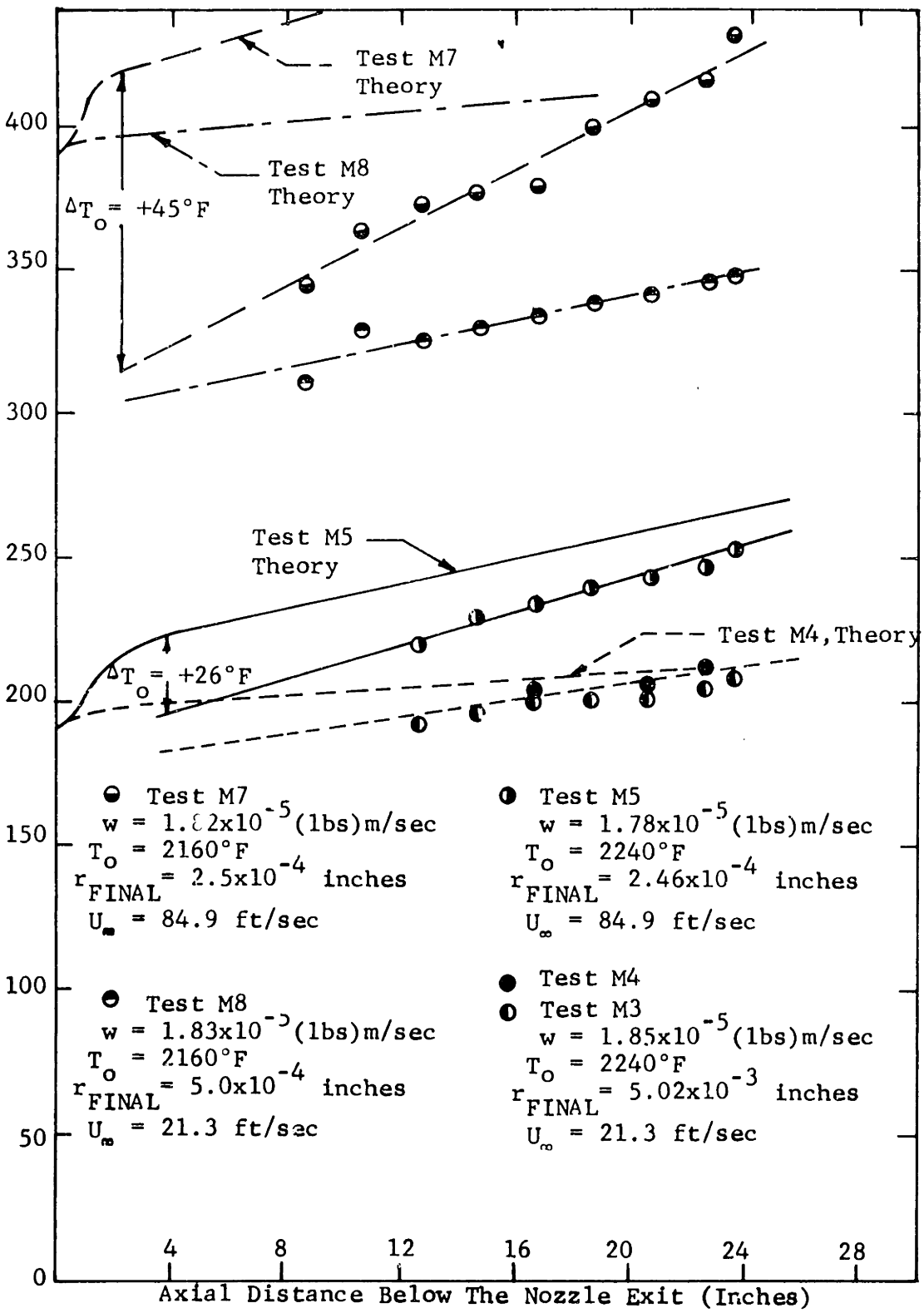

TENSION VERSUS DISTANCE
THEORY AND DATA
THE EFFECT OF CHANGING THE INITIAL TEMPERATURE AND
THE FINAL FIBER RADIUS

Fig. 9.14

the measured 32.3°, for test M7 even if θ_o was 90°, the predicted tension would still be 15 dynes higher than the measured value at the beginning of the constant radius region.

The experimental data were put in non-dimensional form to yield the drag coefficient versus Reynolds number. The data along with the error limits are plotted on Fig. 9.15 which also shows the theories and data presented previously on Fig. 7.1. The data agrees well with Sparrow, et al.'s turbulent theory. The points at the lowest radius Reynolds number deviate from it, although they have such large limits of error that it is impossible to reach any conclusions concerning the low Reynolds number points. The error is probably due to the fact that the jet vibrated causing an unsteady boundary layer. It is also interesting to note that at the smaller jet radii, the Knudsen number approaches 10^{-2}, indicating that the flow is at the onset of the slip flow regime.

The data points indicate that the boundary layer is turbulent in the region where the final fiber radius has been reached. The theoretical curves in Figs. 9.12 through 9.14 were plotted using Sparrow's turbulent theory for the constant radius region.

It must be emphasized that the author has used a single criterion to determine that the boundary layer is laminar in the central jet region and that it is turbulent when the jet has

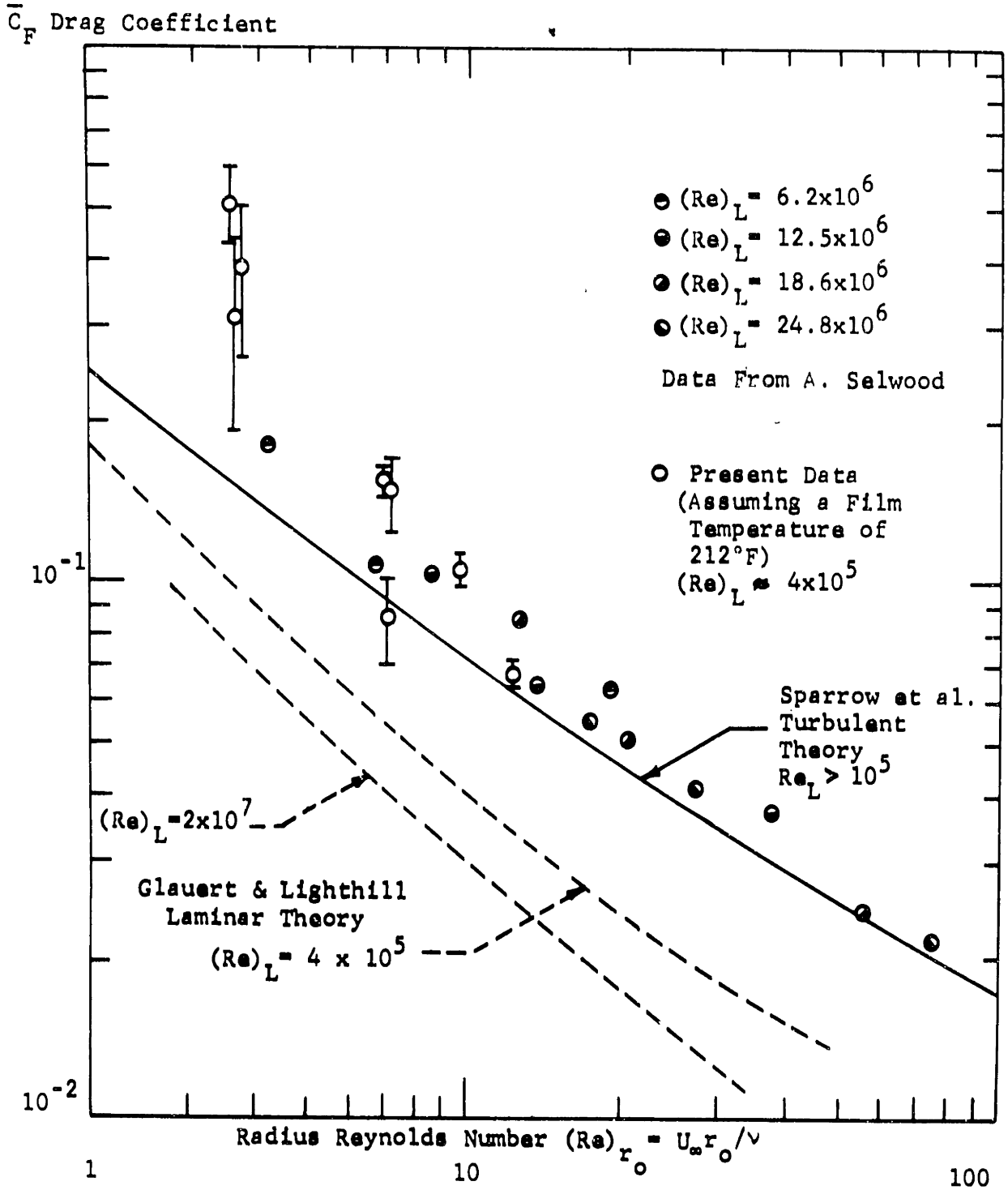

DRAG COEFFICIENT VERSUS REYNOLDS NUMBER
LAMINAR AND TURBULENT BOUNDARY LAYER FLOW
ALONG THE AXIS OF A CYLINDER

Fig. 9.15

reached a constant r radius. The criterion is to determine which form of the boundary layer, laminar or turbulent, causes the experimental and analytical results to agree. No information as to the length or radius Reynolds number at which transition occurs is available. It may well be that for test conditions differing from those used in this work, the boundary layer might stay laminar for a large portion of the constant radius region or at the other extreme, the boundary layer might be turbulent in the central jet region.

CHAPTER 10

THE EFFECT OF THE OPERATING VARIABLES ON JET FORMATION

The last chapter has presented the theoretical results for the shape, tension, and temperature distribution in the jet for the conditions encountered in the experiment. The analysis will now be extended to predict the behavior of the jet under different operating conditions.

Specifically, the effect of changing the environment of the jet will be investigated. A criterion is also presented which predicts the necessary changes in the values of the governing parameters in order to achieve very large or very small values of the final jet radius.

10.1 The Environment

Figure 10.1 compares the simplified theory described in Chapter 4 along with the exact numerical theory for the same experimental case as shown in Figs. 9.3, 9.4 and 9.5. The simplified theory gives an adequate prediction of the central jet shape; it was not extended to the upper jet since the theory neglects radiation heat transfer and would obviously be in error.

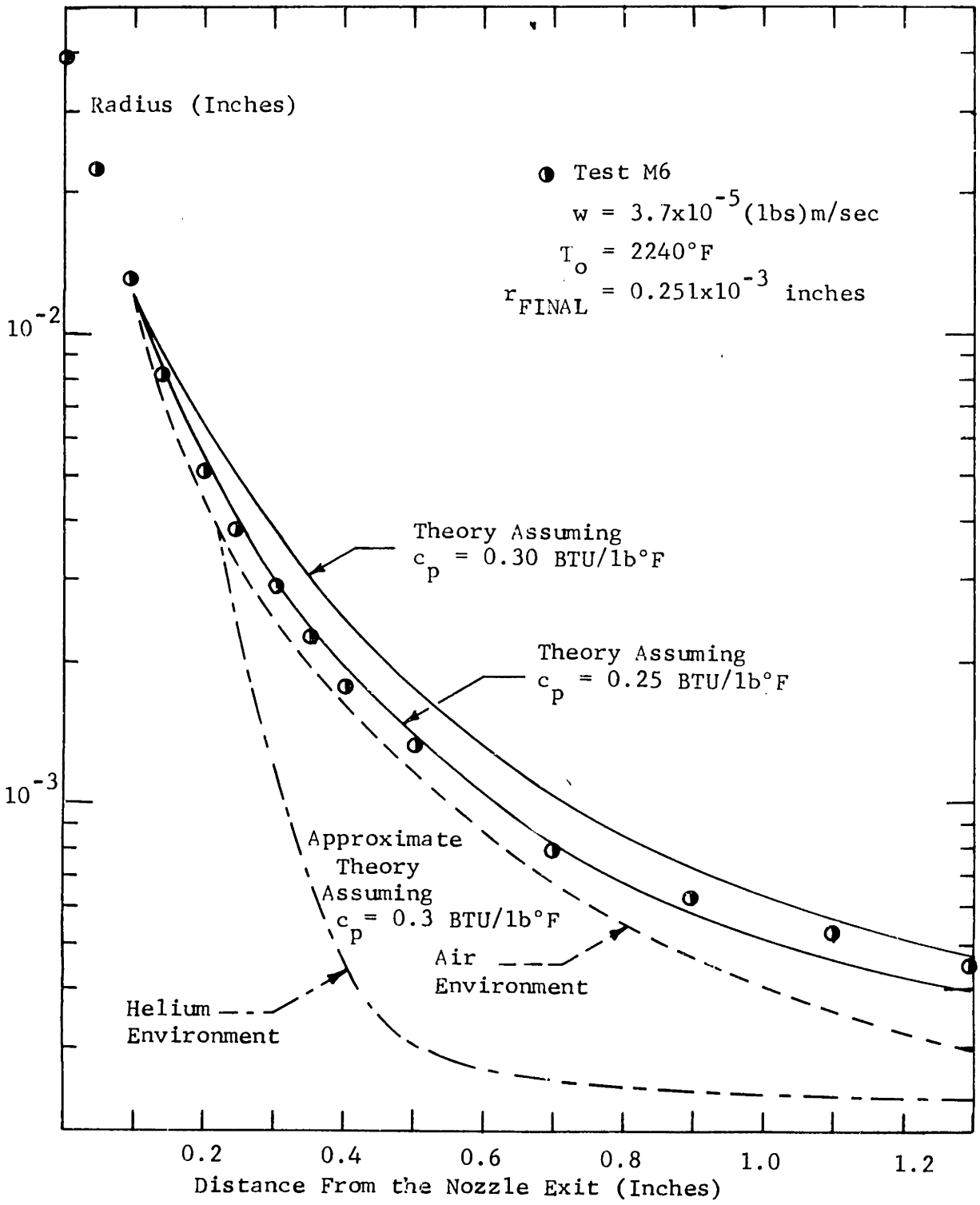

JET RADIUS VERSUS DISTANCE
THE EFFECT OF CHANGING THE ENVIRONMENT

Fig. 10.1

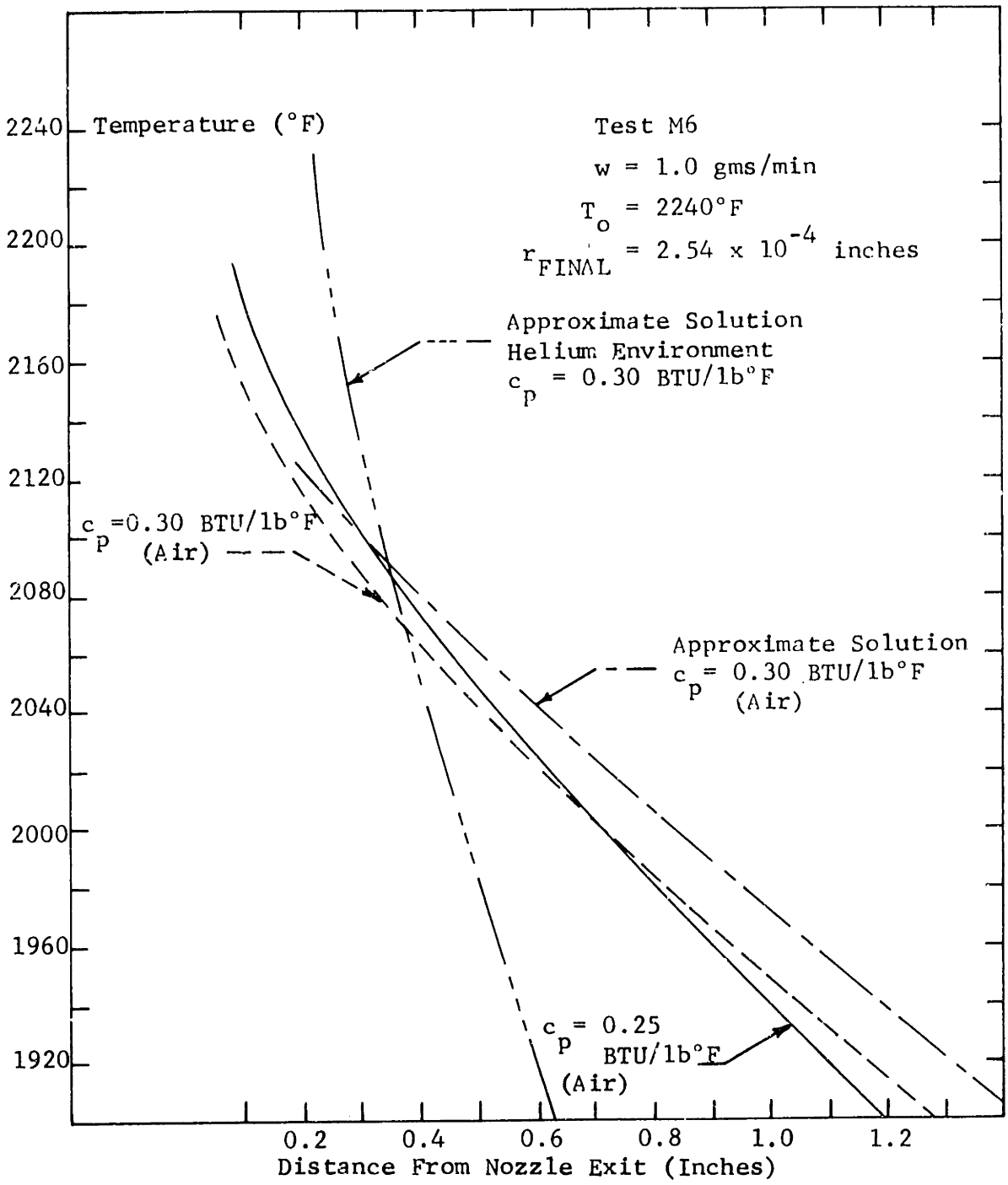

TEMPERATURE VERSUS DISTANCE
THE EFFECT OF CHANGING THE ENVIRONMENT

Fig. 10.2

When the environment is assumed to be helium instead of air the shape and temperature distribution are drastically altered as Figs. 10.1 and 10.2 illustrate. The change is primarily due to a change in the thermal conductivity of the environment since the film coefficient of heat transfer has been shown to be directly proportional to the thermal conductivity. The reason the initial temperature was raised for the case of the helium environment will be discussed in a later section.

It is important to know the effect of the environment on the tension increase in the jet. If the tension becomes too large, the solidified portion of the jet will fail by yielding. In the region of the jet where the radius reached its final value, the tension may be approximated by neglecting the tension increase necessary to accelerate the jet

$$\text{Tension} \approx (\text{Tension})_o = \left(\frac{d\ \text{Tension}}{dz}\right)_{\text{AIR DRAG}} z \qquad (10.1)$$

In order to find the effect of the environment on the tension increase it will be assumed that the boundary layer on the jet is turbulent. Sparrow, et al.'s turbulent theory, Fig. 9.16, in the region of present interest can be approximately represented by

$$\bar{C}_F = 0.4\ (Re_{r_o})^{-0.7} \tag{10.2}$$

or

$$\tau_\infty = \frac{0.2(U_\infty)^{1.3}}{(r_o)^{0.7}}\ (\rho_{ATM})^{0.3}\ (\mu_{ATM})^{0.7} \tag{10.3}$$

and the tension increase per unit length is

(10.4)

$$\frac{\Delta \text{Tension}}{\Delta z} = \tau_\infty 2\pi r_o = 0.4\pi (U_\infty)^{1.3} (r_o)^{0.3} (\rho_{ATM})^{0.3} (\mu_{ATM})^{0.7}$$

$$\frac{\Delta \text{Tension}}{\Delta z} = 0.284\ \frac{(Q)^{1.3}}{(r_o)^{2.3}}\ (\rho)^{0.3}_{ATM}\ (\mu)^{0.7}_{ATM} \tag{10.5}$$

Therefore, for a given flow rate and final jet radius the tension increase is proportional to the density and viscosity

$$\frac{\Delta \text{Tension}}{\Delta z} = (\text{Constant})(\rho_{ATM})^{0.3} (\mu_{ATM})^{0.7} \tag{10.6}$$

If one assumed the environment was helium rather than air and evaluated the density and viscosity at the same film temperature, 212°F, the tension increase with length for the helium environment is only 58 per cent as large as for the air environment. This is due to the small helium density. For an environment where the air pressure has been reduced to one half an atmosphere, the tension increase with length is 82 per cent as large as an environment of air at one atmosphere.

The optimum environment would be one in which the gas density and viscosity were low. A low viscosity gas would also have a low thermal conductivity. The following section will indicate why this is an advantageous property if, at one extreme, a jet with a very small final radius is desired.

10.2 Criterion for Producing Jets of a Given Final Radius

It has been shown that the simplified solution for the shape of the central jet region although not strictly correct, does give results which predict the radius versus distance relationship within 25 per cent for the jet. The results of the simplified solution will be used to predict the effect of various fluid properties, environmental properties, etc., on the ability to produce a given final radius.

From the simplified solution for the shape of the jet, see Eq. (4.32)

$$r_{FINAL} \quad \frac{0.6\mu_E Q}{(Tension)_o} \; e^{-\left[\frac{\rho\, c_p\, (Tension)_o}{6a_2(T_E-T_{ATM})\mu_E k_{ATM} C_L}\right]} \qquad (10.7)$$

Position E is the point where the one-dimensional solution commences, the slope of the jet is minus one-tenth at position E, and a_2 is a physical property of the fluid which relates the viscosity to the temperature

$$\ln \mu = a_1 - a_2 T \tag{10.8}$$

As explained in Chapter 4, when the flow rate, initial jet radius, slope, and temperature, and the physical properties of the jet fluid and the environment are held constant, the final jet radius changes as the viscosity, and temperature, at position E change. In practice, the final jet radius can be varied by simply changing the speed of the pulling wheel while the flow rate is held constant. However, when the final radius is changed, Eq. (10.7) must be satisfied; if it is not satisfied, steady flow is not possible.

Equation (10.7) indicates that as μ_E decreases the final jet radius decreases. The effect of increasing T_E with decreasing μ_E can be disregarded in Eq. (10.7) since the latter quantity changes much more rapidly than the former as seen from Eq. (10.8). Obviously, there is a lower limit to the minimum value of the final jet radius which corresponds to the smallest possible value of μ_E, i.e., the largest possible value of T_E. The smallest possible value of μ_E occurs when the temperature decrease in the upper jet, $T_o - T_E$, is a minimum. The temperature decrease in the upper jet can not be predicted at present since a solution of the governing equations in the upper jet has not been made. Certainly, in the limit, the value of T_E can not be higher than

the initial temperature, T_o. Therefore, as T_o is increased, a smaller final jet radius is possible.

It also may be concluded from Eq. (10.7) that a fluid of higher specific heat or an environment with a lower thermal conductivity will also allow the steady state jet to achieve a smaller final radius.

For example, consider the case where the environment is helium rather than air, Figs. 10.1 and 10.2. For a helium environment, the thermal conductivity is three times that of an air environment while C_L calculated from the laminar boundary layer theory remains approximately a constant. In order to achieve the same final jet radius at the same flow rate using helium in place of air, the calculated temperature at position E increased from 2140°F for air to 2350°F for helium. Since the initial temperature for the experiment with air was 2240°F, if helium is substituted for air the initial jet temperature must be raised by more than one hundred degrees.

Alternatively, a jet with a large final radius may be desired. In this case, the viscosity at point E must have a large value, T_E must be as small as possible. The largest possible final radius is now limited by the largest temperature difference which can occur in the upper jet. Lowering the initial

jet temperature will allow an increase in the size of the final jet radius.

The effect of the initial temperature on the smallest or largest final radius attainable presupposes that the initial tension does not change when the initial temperature has changed. The initial tension written as

$$(\text{Tension})_o = -\frac{6\mu_o Q}{R_o}\left(\frac{dr_o}{dz}\right)_o + \gamma_T \pi R_o \cos\theta_o \qquad (10.9)$$

does not change with temperature changes when the surface tension is the dominant term, assuming θ_o and R_o stay constant. If the viscous force is the dominate term in the tension

$$(\text{Tension})_o \approx -\frac{6\mu_o Q}{R_o}\left(\frac{dr_o}{dz}\right)_o \qquad (10.10)$$

then Eq. (10.7) must be written as

$$r_{FINAL} - \frac{R_o (dr_o/dz)_o}{10(\mu_o/\mu_E)}\, e^{-\left[\frac{\rho C_p Q(\mu_o/\mu_E)(dr_o/dz)_o}{a_2 (T_E - T_{ATM}) k_{ATM} C_L R_o}\right]} \qquad (10.11)$$

In this case, it is the viscosity ratio, a function of the temperature ratio over the upper jet which is controlling, rather than the temperature level.

The results of the foregoing analysis can be alternatively explained by rewriting the basic equations. The simplified analysis assumed that

$$-\frac{6\mu Q}{r_o}\left(\frac{dr_o}{dz}\right) = (\text{Tension})_o = \text{Constant} \tag{10.12}$$

Integrating the above expression

$$\ln(r) = -\frac{1}{6Q}\int \frac{(\text{Tension})_o}{\mu}\, dz \tag{10.13}$$

it can be seen that the lower the value of the viscosity is over a given length, the greater the radius can be attenuated. The value of the viscosity may be kept small over a given length by slow changes of jet temperature with distance or by a high initial temperature.

The limiting case occurs when the viscosity is held constant, produced, for example, by enclosing a portion of the jet within heated walls; the tension being supplied mechanically to the cooled jet below the heated walls. In this case, the solution for the jet radius, assuming a constant tension, is

$$r/(r)_{z=o} = e^{-\left[\frac{(\text{Tension})_o}{6\mu Q}\, z\right]} \tag{10.14}$$

Notice that the solution does not asymptotically approach a final radius, rather the radius continues to decrease. If the length of the heated section is not kept short, the radius will continue to attenuate beyond the desired final radius causing the jet velocity to increase until the jet breaks up due to instabilities, which occur when the viscosity of the jet is low.

There is one constant viscosity case which is stable and it occurs when no mechanical tension is applied, rather the jet is attenuated by gravity. In this case, the tension decreases with distance so that a final radius is asymptotically approached. The final radius in this case occurs when the gravity force on the jet is balanced by the air drag.

10.3 Upper Jet Instability

By the above analysis, one method to achieve large radius reductions in the jet is to increase the initial jet temperature. It has been found experimentally that an instability occurs in the upper jet region at high initial jet temperatures. The instability is a pulsing of the jet, a swelling and decreasing of the jet size. First, small fluctuations of the jet which start and then are damped out occur. As the temperature is increased, the fluctuations become unstable causing the jet to break. The fluctuations also increase at a constant temperature when the flow rate is increased.

One possible explanation of the fluctuations is that a disturbing force, possible an air current normal to the jet, cools the upper jet. When the jet cools, the fluid in the nozzle also cools since the fluid in the nozzle exchanges radiant energy with the jet. A small cooling of the nozzle fluid can cause a marked

increase in its viscosity, e.g., at 2400°F a 20° temperature drop causes the viscosity to rise by 15 per cent. The increase of viscosity of the fluid in the nozzle causes the flow rate to fall. For lower flow rates the upper jet decreases in size. This can be seen from Eq. (10.13) if the flow is considered one-dimensional; lower flow rates cause higher rates of attenuation in the jet if the ratio of the initial tension to viscosity is considered constant.

The smaller upper jet size provides less area for surface radiation, an important heat transfer mechanism in this region. In addition, a small temperature decrease can strongly affect the emmissive power proportional to the temperature to the forth power. Assuming the disturbing force is now absent, the reduced heat transfer from the upper jet is not high enough to maintain equilibrium at the new, lower temperature so that the jet heats up, heating the fluid in the nozzle, increasing the flow rate, etc. The initial disturbance might be a single impulse or of a periodic nature. Depending upon the interaction between the cooling of the upper jet and the cooling of the fluid in the nozzle, the amount the shape of the upper jet changes with flow rate, etc., the disturbance will be damped out or will cause an instability of increasing amplitude. The above mentioned effects

can only be estimated after a steady state analysis of the fluid dynamics and heat transfer in the upper jet and in the nozzle has been made.

CHAPTER 11

CONCLUSIONS

A one-dimensional analysis has been developed which accurately predicts the shape, temperature distribution, and tension in the viscous Newtonian jet as a function of fluid and environmental properties, flow rate, initial jet temperature, initial jet radius and slope and the final jet radius. The one-dimensional analysis has been found to be invalid within two or three nozzle diameters of the nozzle exit where the slope of the jet boundary is greater than one-tenth.

The heat transfer from the jet is by radiation and forced convection near the nozzle exit and by forced convection in the one-dimensional region. The Nusselt number for the boundary layer, which has been found to be laminar in the region where the jet radius is being attenuated, can be accurately calculated from a shear stress analysis by Glauert and Lighthill (11) combined with Reynolds analogy.

It has been found that the tension is constant in the region near the nozzle exit, increases to accelerate the attenuating jet and in the region where the jet has reached its final radius the tension increases due to the air shear stress on the jet. The

air shear stress can be predicted by an extension of a turbulent boundary layer analysis of Sparrow, et al. (14).

The attenuation of the jet is controlled by the flow rate, initial tension, and the viscosity gradient in the jet which, in turn, is dependent upon the gradient of the jet temperature in the axial direction. For a large attenuation of the jet radius, a small flow rate or a high initial jet temperature is required. The increase of the jet temperature has been found to be limited by an instability which occurs in the upper jet at high temperatures. This instability can not be adequately predicted at present.

CHAPTER 12

RECOMMENDATIONS

As pointed out in Chapter 10, in order to predict the onset of upper jet stability a solution of the steady state temperature and velocity distribution for flow in the nozzle and in the upper jet is necessary. As the first step, the assumption of a two-dimensional temperature distribution and a one-dimensional velocity distribution in the upper jet region might yield accurate results.

In order to solve for the temperature distribution in the upper jet the absorption coefficient versus wavelength of the glass must be known. At present the absorption coefficient has only been accurately measured for low wavelengths where the absorption coefficient is less than 10 (cm^{-1}). An accurate measurement of the specific heat versus temperature is also necessary.

Once the absorption coefficient has been found for high wavelengths a measurement of the temperature at the surface of the jet could be made. If a filter could be found which would only transmit infared radiation at wavelengths for which the jet is opaque, where the product of the absorption coefficient and the jet radius is much greater than one, the filter could be placed in front of a total radiation pyrometer. The modified pyrometer

would only be sensitive to radiation from the glass surface. At high glass temperatures, a significant fraction of the total radiation from the jet surface would still be received by the pyrometer to give an accurate measurement of the temperature, e.g., at 2000°F, 15 per cent of the total radiation energy is found between the wavelengths four microns to six microns.

An investigation of the transition region between laminar and turbulent boundary layers on a cylinder moving axially would be in order. The value of the drag coefficient for turbulent flow at low radius Reynolds numbers is presently in doubt and should be found experimentally.

The drag tests could be conducted by using a wire or fiber moving in still air. The use of unheated wires would exclude any thermal interactions with the dynamic boundary layer.

The wire could be unwound from one spool and wound on another or it could be formed into a continuous loop guided by pulleys to run along a long, straight test section.

REFERENCES

1. Pai, Shih-I, Fluid Dynamics of Jets, D. Van Nostrand
Inc., New York, 1954.

2. Rupe, J.H., "On the Dynamic Characteristics of Free-L
and a Partial Correlation with Orifice Geometry," Jet
sion Laboratory Technical Report 32-207, 1962.

3. Ziabicki, Andrzej and Krystyna, Kedzierska, "Mechanic
of Fibre Spinning Process in Molten Polymers," Kolloi
Zeitschrift, Band 171, Heft 1, 51-61.

4. Von Emil Deeg and Dietzel, Adolf, "Über die Ursache d
anomalen mechanischen Eigenschaften der Glasfaser,"
Glastechnische Berichte, 28, 221-232, 1955.

5. Gardon, Robert, "Calculation of Temperature Distribut
Glass Plates Undergoing Heat Treatment," Journal of t
American Ceramic Society, 41, #6, 200-209.

6. Gardon, Robert, "The Emissivity of Transparent Materi
Journal of the American Ceramic Society, 39, #8, 278-

7. Jahnke, E. and Enade, F., Tables of Higher Functions,
McGraw-Hill Cook Company, New York, 1960.

8. Federal Works Agency, W.P.A., Tables of Sine, Cosine
Exponent Integrals, Vol. I, New York.

9. Seban, R.A. and Bond, R., "Skin Friction and Heat Tra
Characteristics of a Laminar Boundary Layer on a Cyli
in Axial Incompressible Flow," Journal of Aeronautica
Science, 18, 671, 1951.

10. Kelly, H.R., "A Note on the Laminar Boundary Layer on
Circular Cylinder in Axial Incompressible Flow," Jour
of Aeronautical Sciences, 21, 634, 1954.

11. Glauert, M.B. and Lighthill, M.J., "The Axi-symmetric Boundary Layer on a Long Thin Cylinder," Proceedings Royal Society of London, Series A, 230, 188-203, 1955.

12. Jakob, M. and Dow, W.M., "Heat Transfer From a Cylindrical Surface to Air in Parallel Flow With and Without Unheated Starting Sections," Transactions of the ASME, 68, 123-134, February, 1946.

13. Sandborn, V.A. and Lawrence, J.C., "Heat Loss From Yawed Hot Wires at Subsonic Mach Numbers," NACA TN 3563, September, 1955.

14. Sparrow, E.M., Eckert, E.R.G. and Minkowycz, W.J., "Heat Transfer and Skin Friction for Turbulent Boundary Layer Flow Longitudinal to a Circular Cylinder," ASME Paper 62-WA-7, November, 1962.

15. Schlichting, H., Boundary Layer Theory, McGraw-Hill Book Company, Inc., New York, 1955.

16. Sakiadis, B.C., "Boundary Layer Behavior on Continuous Solid Surfaces," Journal of American Institute of Chemical Engineers, 7, #3, 467-472, September, 1961.

17. Landweber, L., "Effect of Transverse Curvature on Frictional Resistance," David W. Taylor Model Basin, United States Navy, Report 687, 1949.

18. Eckert, H.U., "Simplified Treatment of the Turbulent Boundary Layer Along a Cylinder in Compressible Flow," Journal of the Aeronautical Sciences, 19, 23-29, 1952.

19. Ginevskii, A.S. and Salodkin, E.E., "The Effect of Lateral Surface Curvature on the Characteristics of Axially-Symmetric Turbulent Boundary Layers," Journal of Applied Mathematics and Mechanics, 22, 1169-1179, 1958.

20. Selwood, A., Letters to the Editor: "The Axial Air-Drag of Monofilaments," Transactions of Journal of the Textile Institute, 53, 1962.

21. Hildebrand, F.B., Introduction to Numerical Analysis, McGraw-Hill Book Company, Inc., New York, 1956.

22. Milne, W.E., Numerical Solutions of Differential Equations, John Wiley and Sons, Inc., New York, 1953.

23. Birkhoff and Farantonello, Jets, Wakes and Cavities, Academic Press, New York, 1957.

24. Lord Rayleigh, "On the Instability of a Cylinder of Viscous Liquid under Capillary Forces," Philosophical Magazine, August, 1892.

25. Lord Rayleigh, The Theory of Sound, Dover Publications, 1929.

26. Milne-Thompson, Theoretical Hydrodynamics, Macmillan, 1950.

27. Goldstein, Modern Developments in Fluid Mechanics, Vol. I, Clarendon Press, Oxford, 1938.

28. Miller and Nemeuk, "Coefficients of Discharge of Short Pipe Orifices for Incompressible Flow at Reynolds Numbers Less Tahn One," ASME Paper 58-A-106.

29. McMahon, Howard O., "Thermal Radiation Characteristics of Some Glasses," The Journal of the American Ceramic Society, 34, #3, 91-96, 1951.

30. Adamson, A.W., Physical Chemistry of Surfaces, Interscience Publishers, Inc., New York, 1960.

APPENDIX A

TABULATED RESULTS AND ERROR ANALYSIS

The results of the variable viscosity glass tests are tabulated below. The experimental apparatus as described in Chapter 8 was not altered during the tests.

The values for the flow rate, initial temperature and pulling wheel speed show the mean value and the maximum amount any single measurement deviated from the mean value. Since the errors are so small, a more refined error analysis was not employed. The final radius was calculated using the continuity equation.

For the radius measured from the photographs, the error reported is plus or minus one standard deviation from the mean value. A solid fiber was also mounted and photographed using the telemicroscope. The magnification of telemicroscope was 18.95X and the fiber diameter was calculated from the continuity equation to be 0.905×10^{-3} inches. The mean value of the diameter measured from the photographs was 2.07 per cent lower than the calculated diameter.

The error in the slope of the tension line is calculated assuming each point had the same error limits and also assuming the true tension versus distance curve is a straight line, see reference (21). The film temperature used to calculate the air

properties needed for the determination of the drag coefficient and Reynolds number was assumed to be 212°F. It was found that varying the air temperature did not affect the data's agreement with Sparrow's turbulent theory.

Test M1

$w = 0.992 \pm .030$ gms/min $= 3.65 \times 10^{-5} \pm 0.11 \times 10^{-5}$ (lbs)m/sec

$T_o = 2240°F \pm 20°F$

Pulling Wheel Speed = 1508 ± 10 rpm

Pulling Speed = 42.5 ± 0.28 ft/sec

r_{FINAL}(Calculated) $= 0.5 \times 10^{-3} \pm 0.012 \times 10^{-3}$ inches

θ_o(@ $r = R_o$) $= 15.75° \pm 0.05°$

Jet Radius Vs. Distance
(Measured From Photographs)

Film Roll No.	Frame No.	Microscope Magnification	z, Distance From Nozzle Exit (Inches)	r_o, Radius (Inches)
1	6	5.487X	0.0	34.1×10^{-3}
			0.0228	27.8
			0.0456	21.7
			0.0683	17.2
			0.0911	13.8
			0.1139	11.2
1	13	5.487X	0.0309	24.6
			0.0764	15.5
			0.0992	12.6
			0.1220	10.2
			0.1448	8.93
			0.1676	7.64
			0.1903	6.74

Film Roll No.	Frame No.	Microscope Magnification	z, Distance From Nozzle Exit (Inches)	r_o, Radius (Inches)
1	14	5.487X	0.2274	5.55×10^{-3}
			0.2501	4.98
			0.2729	4.38
			0.2957	3.96
			0.3185	3.55
			0.3413	3.21
			0.3640	2.90
1	19	5.487X	0.5632	1.525
			0.5997	1.33
			0.6362	1.165
1	26	19.04X	0.9570	0.765
1	30	19.04X	1.1540	0.723
2	3A	19.04X	1.3490	0.585
1	33	19.04X	1.3510	0.593
1	36	19.04X	1.6310	0.571
2	7A	19.04X	2.349	0.490

Tension

z, Distance From Nozzle Exit (Inches)	Average Tensometer Reading (Degrees)	Tensometer Reading (Dynes)	Tensometer Reading +WxV (Dynes)
8.72	82.0	207.38	228.97
12.72	83.5	211.17	232.76
14.72	84.67	214.13	235.72
16.72	87.67	221.72	243.31
18.72	89.50	226.35	247.94
20.72	92.33	233.50	255.09
22.72	94.00	237.73	259.32
23.72	94.83	239.83	261.42

All tension reading $\pm$ 2°, or $\pm$ 5 dynes
By theory of least squares.

Tension = 225.2 +(2.36)x z

Slope = 2.36 $\pm$ .38 dynes/inch = $5.31 \times 10^{-6} \pm .85 \times 10^{-6}$ (lbs)F/in

For $r = r_{FINAL}$ (Calculated) and T_{FILM} = 212°F, L = 20 inches

$(Re)_r = 7.18$; $(Re)_L = 2.86 \times 10^5$

$\overline{C}_F = 0.148 \pm .024$

Test M2

$w = 1.000 \pm .005$ gms/min $= 3.68 \times 10^{-5} \pm .0184 \times 10^{-5}$ (lbs)m/sec

$T_o = 2240°F \pm 20°F$

Pulling Wheel Speed = 2682 ± 10 rpm

Pulling Speed = 75.5 ± 0.28 ft/sec

r_{FINAL}(Calculated) $= 0.376 \times 10^{-3} \pm 0.004 \times 10^{-3}$ inches

θ_o(@ $r = R_o$) $= 16.23° \pm .08°$

$R_o = 34.5 \times 10^{-3}$ inches

Jet Radius Vs. Distance

Film Roll No.	Frame No.	Microscope Magnification	z, Distance From Nozzle Exit (Inches)	r_o, Radius (Inches)
3	22	19.022X	0.176	$.9855 \times 10^{-3}$
	25	19.022X	0.341	.860
	30	19.022X	0.588	.6125
	32	19.022X	1.088	.51
4	9	37.309X	1.088	.523
	21	37.309X	4.088	.427
	36	37.309X	7.558	.3955

No accurate pictures of the upper jet region were taken

Tension

z, Distance From Nozzle Exit (Inches)	Average Tensometer Reading (Degrees)	Tensometer Reading (Dynes)	Tensometer Reading +WxV (Dynes)
7.75	88.5	226.5	264.5
10.72	88.7	227	265
12.72	94.8	243	281
14.72	97.3	249	287
16.72	100.0	256	294
18.72	103.7	264	302
20.72	108.3	276	314
22.72	109.8	280	318
23.72	113.5	289	327

Tension reading $\pm$ 2° = $\pm$5 dynes

By the theory of least squares

Tension = 259.26 + 4.04 z

Slope = 4.04 $\pm$ .32 dynes/inch = $9.09 \times 10^{-6} \pm .72 \times 10^{-6}$ (lbs)F/in

For r = r_{FINAL} (Calculated), T_{FILM} = 212°F, L = 20 inches

$\bar{C}_F = 0.106 \pm .008$

$(Re)_r = 9.64$

$(Re)_L = 5.09 \times 10^5$

Test M3

$w = 0.506 \pm .003$ gms/min $= 1.86 \times 10^{-5} \pm .011 \times 10^{-5}$ (lbs)m/sec

$T_o = 2240°F \pm 20°F$

Pulling Wheel Speed = 754 ± 5 rpm

Pulling Speed = 21.3 ± 0.14 ft/sec

r_{FINAL}(Calculated) $= 0.505 \times 10^{-3} \pm .005 \times 10^{-3}$ inches

Jet Radius Vs. Distance

(The photographs taken on Test M3 were not acceptable, See Test M4 which was run at the same test conditions)

Tension

z, Distance From Nozzle Exit (Inches)	Average Tensometer Reading (Degrees)	Tensometer Reading (Dynes)	Tensometer Reading +WxV (Dynes)
12.72	74.17	187.58	192.98
14.72	75.17	190.10	195.50
16.72	77.33	195.57	200.97
18.72	77.5	196.00	201.40
20.72	77.37	195.67	201.07
22.72	79.0	199.79	205.19
23.72	80.5	203.58	208.98

All tension reading $\pm 2° = \pm 5$ dynes

By the theory of least squares

Tension = $195.02 + 1.260\ z$

Slope $= 1.26 \pm 0.50$ dynes/in $= 2.83 \times 10^{-6} \pm 1.13 \times 10^{-6}$ (lbs)F/in

For $r = r_{FINAL}$(Calculated), $T_{FILM} = 212°F$, L = 20 inches

$\bar{C}_F = 0.316 \pm .125$

$(Re)_r = 3.6$

$(Re)_L = 1.43 \times 10^5$

Test M4

$w = 0.496 \pm .008$ gms/min $= 1.85 \times 10^{-5} \pm .0294 \times 10^{-5}$ (lbs)m/sec

$T_o = 2240°F \pm 20°F$

Pulling Wheel Speed $= 754 \pm 5$ rpm

Pulling Speed $= 21.3 \pm 0.14$ ft/sec

r_{FINAL}(Calculated) $= 0.500 \times 10^{-3} \pm .008 \times 10^{-3}$ inches

θ_o(@ $r = R_o$) $= 32.27° \pm 1.01°$

Jet Radius Vs. Distance

Film Roll No.	Frame No.	Microscope Magnification	z, Distance From Nozzle Exit (Inches)	r_o, Radius (Inches)
7	7	5.409X	0	34.09×10^{-3}
			.0231	21.81
			.0462	14.26
			.0693	9.87
			.0924	7.17
			.1155	5.49
			.0595	13.65
7	9	5.409X	.0826	9.23
			.1288	4.93
			.1519	3.93
			.1750	3.22
			.1981	2.69
			.2212	2.27
			.2443	2.00
			.2674	1.83
7	13	5.409X	.2126	2.5
			.2357	2.17
			.2588	1.91
			.2819	1.68
			.3050	1.48
			.3281	1.36
			.3512	1.22

Film Roll No.	Frame No.	Microscope Magnification	z, Distance From Nozzle Exit (Inches)	r_o, Radius (Inches)
7	17,18	19.082X	.405	$.9902 \times 10^{-3} \pm .0327 \times 10^{-3}$
	20,21		.505	$.8375 \times 10^{-3} \pm .0205 \times 10^{-3}$
	24,27		.695	$.6497 \times 10^{-3} \pm .0094 \times 10^{-3}$
	28,29		.895	$.5629 \times 10^{-3} \pm .0243 \times 10^{-3}$
	32,33		1.095	$.5432 \times 10^{-3} \pm .0132 \times 10^{-3}$
8	2,3		1.295	$.5445 \times 10^{-3} \pm .0152 \times 10^{-3}$
	10,11		1.695	$.5257 \times 10^{-3} \pm .0158 \times 10^{-3}$

Tension

z, Distance From Nozzle Exit (Inches)	Average Tensometer Reading (Degrees)	Tensometer Reading (Dynes)	Tensometer Reading +WxV (Dynes)
12.72	74.17	187.58	192.98
14.72	75.67	191.37	196.77
16.72	78.67	198.96	204.36
18.72	77.50	196.00	201.40
20.72	79.50	201.06	206.46
22.72	82.00	207.38	212.78
23.72	80.33	203.15	208.55

All tension measurements $\pm$ 2° = $\pm$ 5 dynes

By the theory of least squares

Tension = 197.49 + 1.55 z

Slope = 1.55 $\pm$ .5 dynes/in = $3.48 \times 10^{-6} \pm 1.12 \times 10^{-6}$ (lbs) F/in

r_{FINAL} (Calculated), T_{FILM} = 212°F, L = 20 inches

$C_F = 0.389 \pm .125$

$(Re)_r = 3.6$

$(Re)_L = 1.43 \times 10^5$

Test M5

$w = 0.483 \pm .012$ gms/min $= 1.78 \times 10^{-5} \pm .044 \times 10^{-5}$ (lbs)m/sec

$T_o = 2240°F \pm 20°F$

Pulling Wheel Speed = 3016 $\pm$ 20 rpm

Pulling Speed = 84.9 $\pm$ 0.56 ft/sec

r_{FINAL}(Calculated) $= 0.246 \times 10^{-3} \pm .005 \times 10^{-3}$ inches

θ_o(@ $r = R_o$) $= 31.825° \pm 0.4°$

Jet Radius Vs. Distance

Film Roll No.	Frame No.	Microscope Magnification	z, Distance From Nozzle Exit (Inches)	r_o, Radius (Inches)
9	6	5.424X	0.0	33.93×10^{-3}
			0.0230	22.12
			0.0461	14.23
			0.0691	9.63
			0.0922	6.81
	10	5.424X	0.07550	9.52×10^{-3}
			0.09850	6.86
			0.1446	3.92
			0.1677	3.00
			0.1907	2.40
			0.2137	1.99
			0.2368	1.72
			0.2598	1.42
			0.2829	1.22
	13	5.424X	0.2055	2.10×10^{-3}
			0.2285	1.75
			0.2516	1.51
			0.2746	1.30
			0.2977	1.10
			0.3207	1.04
			0.3437	0.934
			0.3668	0.832

Film Roll No.	Frame No.	Microscope Magnification	z, Distance From Nozzle Exit (Inches)	r_o, Radius (Inches)
	19,20	19.052A	0.4207	$0.688\times10^{-3}\pm.0194\times10^{-3}$
	21,22		0.5207	$0.569\times10^{-3}\pm.023\times10^{-3}$
	27,28		0.7107	$0.401\times10^{-3}\pm.011\times10^{-3}$
	30,31		0.9107	$0.343\times10^{-3}\pm.010\times10^{-3}$
	33,34		1.1107	$0.304\times10^{-3}\pm.008\times10^{-3}$
10	1,2	33.774X	1.1107	$0.314\times10^{-3}\pm.007\times10^{-3}$
	11,12		1.5107	$0.285\times10^{-3}\pm.013\times10^{-3}$
	19,20		2.1107	$0.289\times10^{-3}\pm.015\times10^{-3}$

Tension

z, Distance From Nozzle Exit (Inches)	Average Tensometer Reading (Degrees)	Tensometer Reading (Dynes)	Tensometer Reading +WxV (Dynes)
12.72	78.50	198.53	220.12
14.72	82.38	208.34	229.93
16.72	84.0	212.44	234.03
18.72	86.5	218.76	240.35
20.72	87.75	221.92	243.59
22.72	89.25	225.71	247.30
23.72	91.67	231.83	253.42

All tension measurements $\pm$ 2° = $\pm$ 5 dynes

By the theory of least squares

Tension = 222.5 + 2.71 z

Slope = 2.71 $\pm$ .50 dynes/in = $6.09\times10^{-6}\pm1.12\times10^{-6}$ (lbs)F/in

$r = r_{FINAL}$ (Calculated), T_{FILM} = 212°F, L = 20 inches

$\bar{C}_F = 0.086 \pm .016$

$(Re)_r = 7.05$

$(Re)_L = 5.72\times10^5$

Test M6

$w = 1.004 \pm .021$ gms/min $= 3.7 \times 10^{-5} \pm .077 \times 10^{-5}$ (lbs)m/sec

$T_o = 2240°F \pm 20°F$

Pulling Wheel Speed = 6034 ± 10 rpm

Pulling Speed = 170.1 ± 0.28 ft/sec

r_{FINAL}(Calculated) $= 0.251 \times 10^{-3} \pm .004 \times 10^{-3}$ inches

θ_o(@ $r = R_o$) $= 33.55° \pm 2.05°$

Jet Radius Vs. Distance

Film Roll No.	Frame No.	Microscope Magnification	z, Distance From Nozzle Exit (Inches)	r_o, Radius (Inches)
11	9	5.355X	0.0	39.06×10^{-3}
			.0233	30.68
			.0467	22.59
			.0700	16.93
			.0934	13.02
			.1170	10.26
			.1400	8.16
11	14	5.355X	.0833	14.29×10^{-3}
			.1067	11.10
			.1300	8.90
			.1534	7.26
			.1767	6.06
			.2000	5.08
			.2234	4.43
			.2467	3.83
			.2701	3.39
11	17	5.355X	.2600	3.55×10^{-3}
			.2834	3.19
			.3067	2.90
			.3300	2.52
			.3534	2.25
			.3767	2.05
			.4004	1.87

Film Roll No.	Frame No.	Microscope Magnification	z, Distance From Nozzle Exit (Inches)	r_o, Radius (Inches)
11	21	19.013X	.4067	$1.614 \times 10^{-3} \pm 0.02 \times 10^{-3}$
	28		.5067	$1.301 \times 10^{-3} \pm 0.062 \times 10^{-3}$
	31,32		.6967	$0.794 \times 10^{-3} \pm 0.017 \times 10^{-3}$
	34,35		.8967	$0.626 \times 10^{-3} \pm .023 \times 10^{-3}$
12	1,4		1.0967	$0.530 \times 10^{-3} \pm .026 \times 10^{-3}$
	7,8		1.2967	$0.453 \times 10^{-3} \pm .013 \times 10^{-3}$
	11,12	32.43X	1.2967	$0.450 \times 10^{-3} \pm .039 \times 10^{-3}$
	13,16		1.4967	$0.372 \times 10^{-3} \pm .008 \times 10^{-3}$
	19,20		1.6967	$0.391 \times 10^{-3} \pm .011 \times 10^{-3}$
	23,24		2.0967	$0.295 \times 10^{-3} \pm .010 \times 10^{-3}$
	31,32		3.5967	$0.2637 \times 10^{-3} \pm .011 \times 10^{-3}$

Tension

It was impossible to measure the tension for Test M6. The jet continually broke when it was threaded in the tensometer.

Test M7

$w = 0.495 \pm .010$ gms/min - $1.82 \times 10^{-5} \pm .037 \times 10^{-5}$ (lbs)m/sec

$T_o = 2160°F \pm 20°F$

Pulling Wheel Speed = 3016 ± 10 rpm

Pulling Speed = 84.9 ± 0.56 ft/sec

r_{FINAL} (Calculated) = $0.2495 \times 10^{-3} \pm .0045 \times 10^{-3}$ inches

θ_o (@ $r = R_o$) = $37.38° \pm 0.41°$

Jet Radius Vs. Distance

Film Roll No.	Frame No.	Microscope Magnification	z, Distance From Nozzle Exit (Inches)	r_o, Radius (Inches)
13	12A-13	5.421X	0.0	33.26×10^{-3}
			.0231	18.61
			.0461	11.63
			.0692	7.85
			.0922	5.58
13	14A	5.421X	.0580	8.77×10^{-3}
			.0793	6.32
			.1023	4.52
			.1254	3.94
			.1484	2.77
			.1715	2.32
			.1946	1.97
			.2176	1.68
			.2407	1.39
13	18A	5.421X	.2323	1.48×10^{-3}
			.2554	1.29
			.2784	1.12
			.3015	1.00
			.3246	0.945
			.3476	0.922

Film Roll No.	Frame No.	Microscope Magnification	z, Distance From Nozzle Exit (Inches)	r_o, Radius (Inches)
13	21A, 22A	19.223X	.4036	0.622×10^{-3}
	26A, 29A		.5036	0.471
	31A, 32A		.6936	0.368
	35A, 36A		.8936	0.331
14	3A, 4A		1.0936	0.313
	7A, 8A	32.355X	1.0936	0.328×10^{-3}
	10A, 11A		1.2936	0.282
	16A, 17A		1.4936	0.291
	20A		1.6936	0.248

Tension

z, Distance From Nozzle Exit (Inches)	Average Tensometer Reading (Degrees)	Tensometer Reading (Dynes)	Tensometer Reading +WxV (Dynes)
8.72	128.0	323.71	345.30
10.72	135.5	342.68	364.27
12.72	138.83	351.10	372.69
14.72	140.33	354.95	376.54
16.72	141.50	357.86	379.45
18.72	149.80	378.84	400.43
20.72	153.13	387.27	408.86
22.72	156.4	395.53	417.12
23.72	160.17	405.07	426.66

All tension measurements $\pm$ 2° = $\pm$ 5 dynes

By the theory of least squares

Tension = 348.5 + 4.99 z

Slope = 4.99 $\pm$ .33 dynes/in = $11.22 \times 10^{-6} \pm .74 \times 10^{-6}$ (lbs)F/in

$r = r_{FINAL}$ (Calculated), T_{FILM} = 212°F, L = 20 inches

$\overline{C}_F = 0.155 \pm 0.010$

$(Re)_r = 7.22$

$(Re)_L = 5.72 \times 10^5$

Test M8

$w = 0.498 \pm .005$ gms/min $= 1.83 \times 10^{-5} \pm .0184$ (lbs)m/sec

$T_o = 2160°F \pm 20°F$

Pulling Wheel Speed = 754 ± 5 rpm

Pulling Speed = 21.3 ± 0.14 ft/sec

r_{FINAL}(Calculated) $= 0.4995 \times 10^{-3} \pm .0065 \times 10^{-3}$ inches

θ_o(@ $r = R_o$) $= 37.63° \pm 0.48°$

Jet Radius Vs. Distance

Film Roll No.	Frame No.	Microscope Magnification	z, Distance From Nozzle Exit (Inches)	r_o, Radius (Inches)
15	10	5.503X	0	33.88×10^{-3}
			.0228	19.91
			.0454	12.84
			.0681	8.89
			.0909	6.44
15	12	5.503X	.0784	8.23×10^{-3}
			.1011	6.03
			.1239	4.50
			.1466	3.56
			.1692	2.91
			.1920	2.50
			.2140	2.20
			.2374	1.87
			.2601	1.61
15	16	5.503X	.2766	1.58×10^{-3}
			.2992	1.40
			.3220	1.31
			.3448	1.20
			.3674	1.09

Film Roll No.	Frame No.	Microscope Magnification	z, Distance From Nozzle Exit (Inches)	r_o, Radius (Inches)
15	22,23	19.055X	.4220	0.98×10^{-3}
	24,25		.5220	0.774
	28,29		.7120	0.619
	32,34		.9120	0.546
16	1,2		1.1120	0.502
	7,8		1.3120	0.478

Tension

z, Distance From Nozzle Exit (Inches)	Average Tensometer Reading (Degrees)	Tensometer Reading (Dynes)	Tensometer Reading +WxV (Dynes)
8.72	121.5	306.01	311.41
10.72	127.75	323.08	328.48
12.72	126.67	320.35	327.75
14.72	128.67	325.41	330.81
16.72	130.33	329.60	335.00
18.72	131.83	333.40	338.80
20.72	133.17	336.79	342.19
22.72	134.75	340.78	346.18
23.72	135.12	341.72	347.12

All tension measurements $\pm$ 2° = $\pm$ 5 dynes

By the theory of least squares

Tension = 317.7 + 2.045 z

Slope = 2.045 $\pm$ 0.33 dynes/in = $4.6 \times 10^{-6} \pm .74 \times 10^{-6}$ (lbs)F/in

$r = r_{FINAL}$ (Calculated), T_{FILM} = 212°F, L = 20 inches

$\overline{C}_F = 0.513 \pm 0.083$

$(Re)_r = 3.6$

$(Re)_L = 1.43 \times 10^5$

Test M9

$w = .967 \pm .010$ gms/min $= 3.56 \times 10^{-5} \pm .037 \times 10^{-5}$ (lbs)m/sec

$T_o = 2240°F \pm 20°F$

Pulling Wheel Speed $= 4500 \pm 10$ rpm

Pulling Speed $= 127 \pm 0.28$ ft/sec

r_{FINAL}(Calculated) $= 0.2855 \times 10^{-3} \pm .0015 \times 10^{-3}$ inches

θ_o(@ $r = R_o$) $= 32.5° \pm 1.30$

$R_o = 39.11 \times 10^{-3} \pm 0.57 \times 10^{-3}$ inches

The jet shape was not photographed for Test M9.

Tension

z, Distance From Nozzle Exit (Inches)	Average Tensometer Reading (Degrees)	Tensometer Reading (Dynes)	Tensometer Reading +WxV (Dynes)
10.72	123.67	312.8	377.2
12.72	124.67	315.3	379.7
14.72	129.0	326.24	390.64
16.72	133.83	338.45	402.85
18.72	137.5	347.7	412.1
20.72	143.83	363.7	428.1
22.72	148.75	376.2	440.6
23.72	150.0	379.4	443.8

All tension measurements $\pm 2° = \pm 5$ dynes

By the theory of least squares

Tension $= 371.3 + 5.54\ z$

Slope $= 5.54 \pm 0.40$ dynes/in $= 12.46 \times 10^{-6} \pm 0.9 \times 10^{-6}$ (lbs)F/in

$\bar{r} = r_{FINAL}$(Calculated), $T_{FILM} = 212°F$, $L = 20$ inches

$\bar{C}_F = 0.0678 \pm 0.0050$

$(Re)_r = 12.2$

$(Re)_L = 8.54 \times 10^5$

Properties of Glass

Some of the properties of the glass have been presented in the report, μ versus T and γ_λ versus λ. Other properties which were needed in the theoretical analysis are:

$$\gamma_T = 330 \text{ dynes/cm}$$

$$\rho = 158.5 \text{ (lbs)m/ft}^3$$

$$(K)_{MAX} = 0.1 \text{ BTU/hr-ft}^2\text{-}^\circ\text{F/ft}$$

The values of the initial jet radii do not always agree with the nozzle inner radius since in some cases the jet spread along the external surface of the nozzle. No satisfactory explanation of the large change in the initial jet angle, θ_o, from a small value for Tests M1 and M2 to a much larger value for Tests M4 and beyond can be proposed. There was a lapse of ten days between the completion of Test M3 and the beginning of M4.

For all tests the circumference of the pulling wheel was 1.69 feet.

APPENDIX B

GOVERNING EQUATIONS, TWO DIMENSIONAL EQUATIONS AND BOUNDARY CONDITIONS FOR A CONSTANT VISCOSITY JET

B.1 Governing Equation

For a very low Reynolds Number, steady, incompressible, axi-symmetric, constant viscosity fluid flow where inertia forces can be neglected (creeping flow), the Navier-Stokes equations in cylindrical co-ordinates are:

$$0 = F_r - \frac{\partial p}{\partial r} + \mu\left(\frac{\partial^2 v_r}{\partial r^2} + \frac{1}{r}\frac{\partial v_r}{\partial r} - \frac{v_r}{r^2} + \frac{\partial^2 v_r}{\partial z^2}\right) \tag{B-1}$$

$$0 = F_z - \frac{\partial p}{\partial z} + \mu\left(\frac{\partial^2 v_z}{\partial r^2} + \frac{1}{r}\frac{\partial v_z}{\partial r} + \frac{\partial^2 v_z}{\partial z^2}\right) \tag{B-2}$$

and the continuity equation is:

$$\frac{\partial v_r}{\partial r} + \frac{v_r}{r} + \frac{\partial v_z}{\partial z} = 0 \tag{B-3}$$

Defining the stream function φ:

$$v_r \equiv -\frac{1}{r}\frac{\partial \varphi}{\partial z} \tag{B-4}$$

and

$$v_z \equiv \frac{1}{r}\frac{\partial \varphi}{\partial r} \tag{B-5}$$

Putting the definition of φ into the Navier-Stokes equations and differentiating the r equation with respect to z and the z equation with respect to r, one finds:

$$0 = \frac{\partial F_r}{\partial z} - \frac{\partial^2 p}{\partial r \partial z} - \mu \left[\frac{1}{r} \frac{\partial^4 \varphi}{\partial r^2 \partial z^2} + \frac{1}{r} \frac{\partial^4 \omega}{\partial z^4} - \frac{1}{r^2} \frac{\partial^3 \omega}{\partial z^2 \partial r} \right] \tag{B-6}$$

$$0 = \frac{\partial F_z}{\partial r} - \frac{\partial^2 p}{\partial r \partial z} + \mu \left[\frac{1}{r} \frac{\partial^4 \varphi}{\partial r^4} - \frac{2}{r^2} \frac{\partial^3 \varphi}{\partial r^3} + \frac{3}{r^3} \frac{\partial^2 \omega}{\partial r^2} - \frac{3}{r^4} \frac{\partial \varphi}{\partial r} + \frac{1}{r} \frac{\partial^4 \omega}{\partial z^2 \partial r^2} - \frac{1}{r^2} \frac{\partial^3 \varphi}{\partial z^2 \partial r} \right] \tag{B-7}$$

The stream function by its definition automatically satisfys the continuity equation. Subtracting one of the above equations from the other to eliminate the pressure, one finds

$$0 = \frac{\partial F_r}{\partial z} - \frac{\partial F_z}{\partial r} - \mu r \left[\frac{\partial^4 \varphi}{\partial z^4} - \frac{2}{r} \frac{\partial^3 \varphi}{\partial z^2 \partial r} + \frac{\partial^4 \varphi}{\partial r^4} - \frac{2}{r} \frac{\partial^3 \omega}{\partial r^3} + \frac{3}{r^2} \frac{\partial^2 \omega}{\partial r^2} - \frac{3}{r^3} \frac{\partial \varphi}{\partial r} + 2 \frac{\partial^4 \varphi}{\partial z^2 \partial r^2} \right] \tag{B-8}$$

For the case of constant body forces the equation can be reduced to:

$$\frac{\partial^4 \omega}{\partial z^4} - \frac{2}{r} \frac{\partial^3 \varphi}{\partial z^2 \partial r} + 2 \frac{\partial^4 \varphi}{\partial z^2 \partial r^2} - \frac{3}{r^3} \frac{\partial \omega}{\partial r} + \frac{3}{r^2} \frac{\partial^2 \omega}{\partial r^2} - \frac{2}{r} \frac{\partial^3 \varphi}{\partial r^3} + \frac{\partial^4 \varphi}{\partial r^4} = 0 \tag{B-9}$$

The equation can also be written as

$$E^2(E^2\psi) = 0 \tag{B-10}$$

where the operator E^2 is defined as

$$E^2 \equiv \frac{\partial^2}{\partial z^2} - \frac{1}{r}\frac{\partial}{\partial r} + \frac{\partial^2}{\partial r^2} \tag{B-11}$$

The above equation is the governing differential equation to be solved.

B.2 Boundary Conditions

Since the governing differential equation is of the fourth order in both r and z, two boundary conditions at each boundary are needed.

For the case of an axi-symmetric jet by symmetry considerations at r = 0

$$v_r = 0 \tag{B-12}$$

$$\frac{\partial v_z}{\partial r} = 0 \tag{B-13}$$

Or in terms of the stream function

$$-\frac{1}{r}\frac{\partial \psi}{\partial z} = 0 \tag{B-14}$$

$$\frac{1}{r}\frac{\partial^2 \psi}{\partial r^2} - \frac{1}{r}\frac{\partial \psi}{\partial r} = 0 \tag{B-15}$$

at z = 0 and at z = L, the boundary conditions are:

at z = 0

$$v_z = \frac{1}{r}\frac{\partial \varphi}{\partial r} = F_o(r) \tag{B-16}$$

$$v_r = -\frac{1}{r}\frac{\partial \varphi}{\partial z} = g_o(r) \tag{B-17}$$

and at $z \rightarrow \infty$

$$v_z = \frac{1}{r}\frac{\partial \varphi}{\partial r} = F_\infty(r) \tag{B-18}$$

$$v_r = -\frac{1}{r}\frac{\partial \varphi}{\partial z} = 0 \tag{B-19}$$

The boundary conditions at $z \rightarrow \infty$ are derived from the fact that if the constant viscosity jet, falling under gravity does not break up due to instabilities it reaches a constant radius steady state solution. At this point the velocities of the jet are no longer functions of z, hence, Eq. (B-18). Since the radius is constant, the outside slope, dr_o/dz, is zero and therefore the radial velocity is zero. From the continuity equation where $z \rightarrow \infty$

$$\frac{\partial v_r}{\partial r} = -\frac{v_r}{r} - \frac{\partial v_z}{\partial z} \tag{B-20}$$

and since

$$\frac{\partial v_z}{\partial z} = 0 \quad \text{everywhere} \tag{B-21}$$

$$v_r = v_r(r) \tag{B-22}$$

therefore,

$$\frac{\partial v_r}{\partial r} = - \frac{v_r}{r} \tag{B-23}$$

The solution of this equation is

$$\ln v_r = - \ln r + C \tag{B-24}$$

$$v_r = \frac{C_1}{r} + C_2 \tag{B-25}$$

Since the radial velocity is zero at $r = 0$ and $r = r_o$, both C_1 and C_2 are zero, therefore the radial velocity is zero at $z \rightarrow \infty$, Eq. (B-19).

The remaining boundary conditions are those at the outside surface of the jet. Since the outside surface of the jet is a free surface the fluid velocity at the surface does not have to be zero. At the free surface the normal force of the liquid must balance the normal force of the air (air pressure) and the tangential force in the fluid at the free boundary must be balanced by the shear force of the air on the boundary.

In symbolic form these boundary conditions are:

$$(\sigma_n)_{liq} = \sigma_{ww} = p_{air} \tag{B-26}$$

$$(\tau)_{liq} = \tau_w = - \tau_\infty \tag{B-27}$$

B.3 Free Surface Boundary Conditions

In the derivation of the free surface boundary conditions, the liquid jet will be assumed to be axi-symmetric and inertial forces will be neglected.

First, the relations for the shear and normal forces on an outside face of arbitrary orientation will be derived.

Figures B1 and B2 show a differential element of fluid at the surface with the forces acting on it.

Summing the forces on the element in the z direction and setting the sum equal to zero

$$\Sigma F_z = 0$$

$$- \tau_{rz} \cdot r_o \, d\alpha \cdot dz + \sigma_{zz} \cdot (r_o + \frac{1}{2} \frac{dr_o}{dz} dz) \cdot d\alpha \cdot \frac{dr_o}{dz} dz \qquad (B\text{-}28)$$

$$+ \tau_w \cdot (r_o + \frac{1}{2} \frac{dr_o}{dz} dz) \cdot d\alpha \cdot ds \cdot \cos\theta - \sigma_{ww} \cdot (r_o + \frac{1}{2} \frac{dr_o}{dz} dz) \cdot d\alpha \cdot ds \cdot$$

$$\cdot \sin\theta + \rho \, g \, d(\text{Volume})$$

Using the approximations

$$d(\text{Volume}) \approx dz \cdot r_o \, d\alpha \cdot \frac{1}{2} \frac{dr_o}{dz} dz \qquad (B\text{-}29)$$

$$ds \approx dz/\cos\theta \qquad (B\text{-}30)$$

$$\tan\theta = dr_o/dz \qquad (B\text{-}31)$$

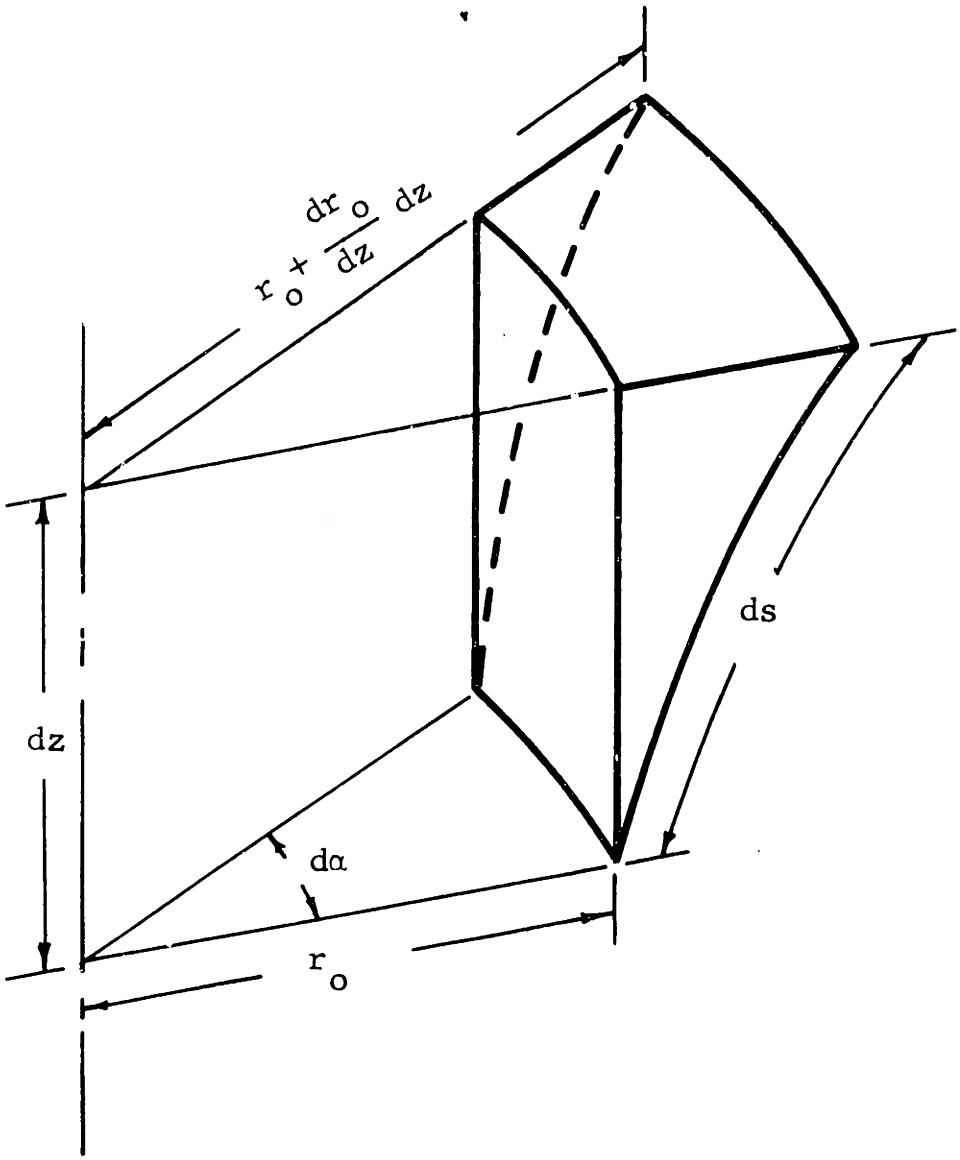

AN ELEMENT OF FLUID AT THE SURFACE

Fig. B-1

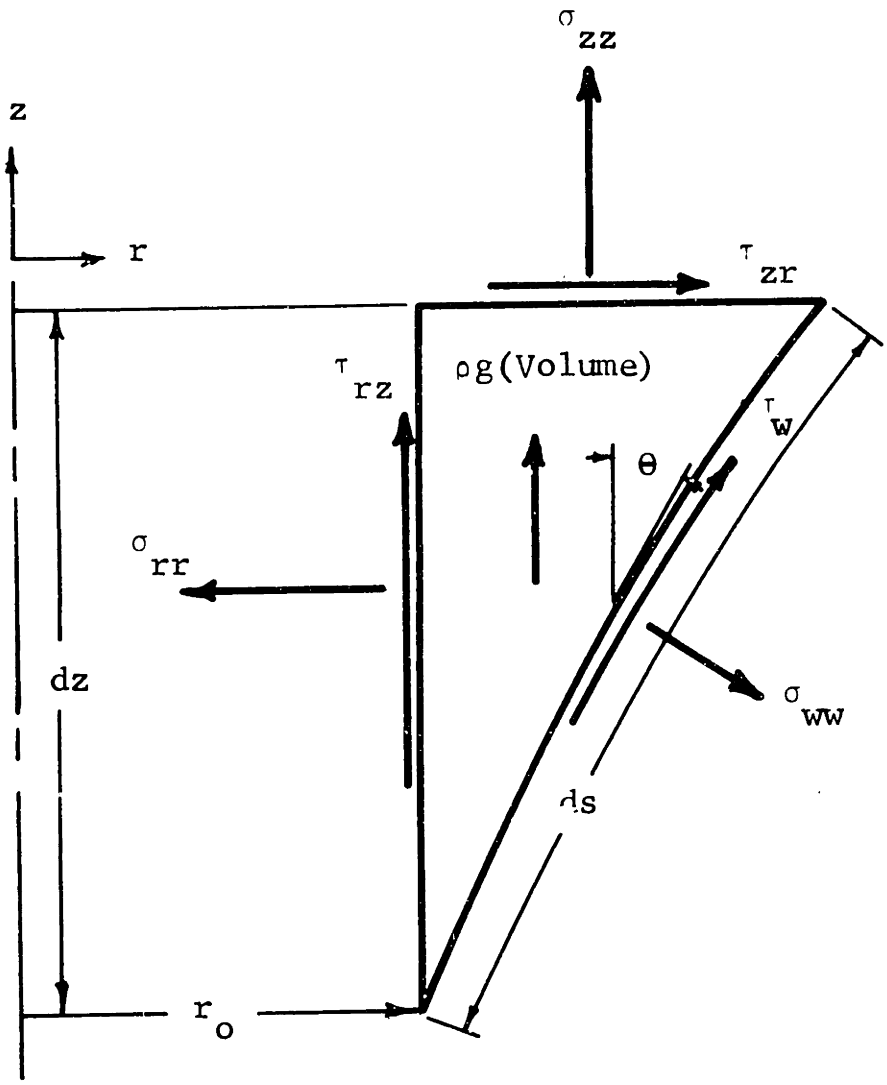

THE FORCES ACTING ON A FLUID ELEMENT

Fig. B-2

Equation (B-28) becomes

$$- \tau_{rz} \cdot r_o \, d\alpha \cdot dz + \sigma_{zz} \cdot (r_o + \frac{1}{2} \frac{dr_o}{dz} dz) \cdot d\alpha \cdot \frac{dr_o}{dz} dz \qquad (B-32)$$

$$+ \tau_w \cdot (r_o + \frac{1}{2} \frac{dr_o}{dz}) \cdot d\alpha \cdot dz - \sigma_{ww} \cdot (r_o + \frac{1}{2} \frac{dr_o}{dz} dz) \cdot d\alpha \cdot dz \cdot \frac{dr_o}{dz}$$

$$+ \rho \, g \cdot dz \cdot r_o d\alpha \cdot \frac{1}{2} \frac{dr_o}{dz} dz = 0$$

Canceling $d\alpha dz$ and retaining terms of the highest order only:

$$- \tau_{rz} \cdot r_o + \sigma_{zz} \cdot r_o \cdot \frac{dr_o}{dz} + \tau_w \cdot r_o - \sigma_{ww} \cdot r_o \cdot \frac{dr_o}{dz} = 0 \qquad (B-33)$$

Canceling r_o and rearranging

$$\tau_w = \tau_{rz} - \sigma_{zz} (\frac{dr_o}{dz}) + \sigma_{ww} (\frac{dr_o}{dz}) \qquad (B-34)$$

Summing the forces on the element in the r direction:

$$\Sigma F_r = 0$$

$$\tau_{zr} \cdot (r_o + \frac{1}{2} \frac{dr_o}{dz} dz) \cdot d\alpha \cdot \frac{dr_o}{dz} dz - \sigma_{rr} \cdot r_o d\alpha \cdot dz \qquad (B-35)$$

$$+ \sigma_{ww} \cdot ds \cdot (r_o + \frac{1}{2} \frac{dr_o}{dz} dz) d\alpha \cdot \cos\theta + \tau_w \cdot ds \cdot (r_o + \frac{1}{2} \frac{dr_o}{dz}) d\alpha \cdot$$

$$\cdot \sin\theta = 0$$

Dividing by $dz \cdot d\alpha$ and using Eqs. (B-30) and (B-31):

$$\tau_{zr} (r_o + \frac{1}{2} \frac{dr_o}{dz} dz) \cdot \frac{dr_o}{dz} - \sigma_{rr} \cdot r_o + \sigma_{ww} (r_o + \frac{1}{2} \frac{dr_o}{dz} dz) \qquad (B-36)$$

$$+ \tau_w \cdot \frac{dr_o}{dz} \cdot (r_o + \frac{1}{2} \frac{dr_o}{dz} dz) = 0$$

Neglecting higher order terms, dividing by r_o, and rearranging:

$$\sigma_{ww} = \sigma_{rr} - \tau_{zr}\left(\frac{dr_o}{dz}\right) - \tau_w\left(\frac{dr_o}{dz}\right) \tag{B-37}$$

Substituting Eq. (B-37) into Eq. (B-34) to eliminate σ_w:

$$\tau_w = \tau_{rz} - \sigma_{zz}\frac{dr_o}{dz} + \sigma_{rr}\frac{dr_o}{dz} - \tau_{zr}\left(\frac{dr_o}{dz}\right)^2 - \tau_w\left(\frac{dr_o}{dz}\right)^2 \tag{B-38}$$

$$\tau_w\left[1+\left(\frac{dr_o}{dz}\right)^2\right] = \tau_{rz} + \frac{dr_o}{dz}(\sigma_{rr} - \sigma_{zz}) - \tau_{zr}\left(\frac{dr_o}{dz}\right)^2 \tag{B-39}$$

In the limit as the size of the fluid element approaches zero,

$$\tau_{rz} = \tau_{zr}$$

$$\tau_w\left[1+\left(\frac{dr_o}{dz}\right)^2\right] = \tau_{rz}\left[1-\left(\frac{dr_o}{dz}\right)^2\right] + \left(\frac{dr_o}{dz}\right)(\sigma_{rr} - \sigma_{zz}) \tag{B-40}$$

Substituting Eq. (B-34) into Eq. (B-37) to eliminate τ_w:

$$\sigma_{ww} = \sigma_{rr} - \tau_{zr}\left(\frac{dr_o}{dz}\right) - \frac{dr_o}{dz}\left(\tau_{rz} - \sigma_{zz}\frac{dr_o}{dz} + \sigma_{ww}\frac{dr_o}{dz}\right) \tag{B-41}$$

$$\sigma_{ww}\left[1+\left(\frac{dr_o}{dz}\right)^2\right] = \sigma_{rr} - 2\,\tau_{zr}\left(\frac{dr_o}{dz}\right) + \sigma_{zz}\left(\frac{dr_o}{dz}\right)^2 \tag{B-42}$$

To find the boundary conditions, consider an element of the liquid jet boundary or "skin" of infinitesimal thickness as shown in Fig. B3. Note that τ_∞ is the drag from air on the liquid when the liquid flows in the positive z direction.

Equating forces in the normal (n) direction

$$-\sigma_{ww}(dA) = \left[p_{AMB} + \gamma_T\left(\frac{\cos\theta}{r_o} - \frac{1}{R_1}\right)\right] dA \tag{B-43}$$

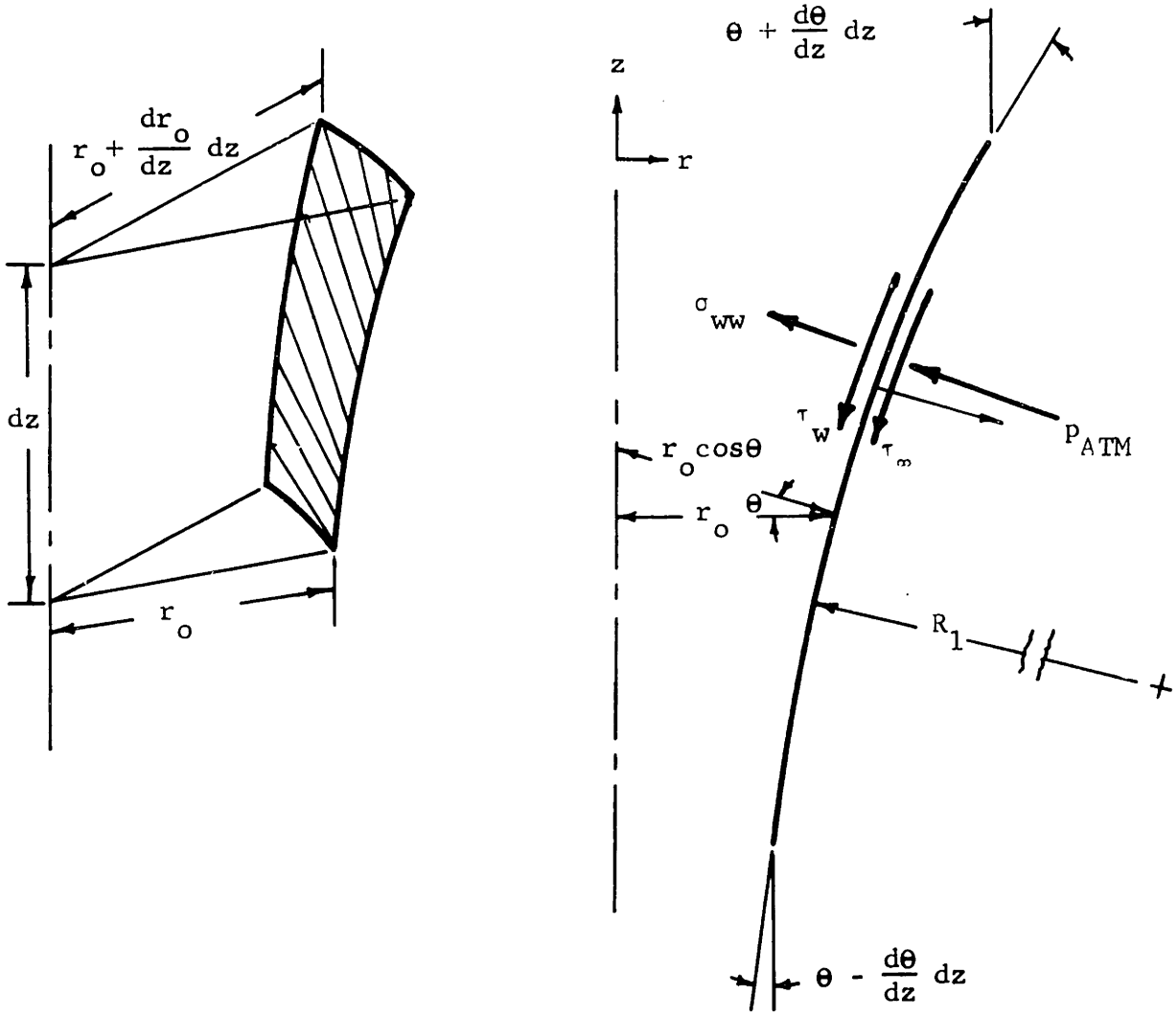

THE SURFACE "SKIN" SHOWING THE FORCES THAT ACT ON IT

Fig. B-3

Using Eq. (B-42) yields the boundary condition in the normal direction

$$-\left[\sigma_{rr} - 2\tau_{zr}\left(\frac{dr_o}{dz}\right) + \sigma_{zz}\left(\frac{dr_o}{dz}\right)^2\right] = \left[1 + \left(\frac{dr_o}{dz}\right)^2\right]\left[p_{AMB} + \gamma_T\left(\frac{\cos\theta}{r_o} - \frac{1}{R_1}\right)\right] \tag{B-44}$$

For the boundary condition in the tangential direction a section of the "skin" completely around the circumference is taken.

Summing the forces in the z direction

$$\Sigma F_z = 0$$

$$-(\tau_w + \tau_{\infty})2\pi\left(r_o + \frac{1}{2}\frac{dr_o}{dz}\,dz\right)ds\,\cos\theta + (\gamma_T + d\gamma_T)2\pi\left(r_o + \frac{dr_o}{dz}\,dz\right)\cos\left(\theta + \frac{1}{2}\frac{d\theta}{dz}\,dz\right) \tag{B-45}$$

$$-\gamma_T\,2\pi\,r_o\cos\left(\theta - \frac{1}{2}\frac{d\theta}{dz}\,dz\right)$$

$$+(\sigma_{ww} + p_{AMB})\sin\theta(2\pi)\left(r_o + \frac{1}{2}\frac{dr_o}{dz}\,dz\right)ds = 0$$

$$\cos\left(\theta \pm \frac{1}{2}\frac{d\theta}{dz}\,dz\right) = \cos\theta\cos\left(\frac{1}{2}\frac{d\theta}{dz}\,dz\right) \mp \sin\theta\sin\left(\frac{1}{2}\frac{d\theta}{dz}\,dz\right) \tag{B-46}$$

$$\approx \cos\theta \mp (\sin\theta)\left(\frac{1}{2}\frac{d\theta}{dz}\,dz\right)$$

For dz approaching 0, using Eqs. (B-30), (B-42), (B-45) and (B-46)

$$
\begin{aligned}
&-(\tau_w + \tau_\infty)\,2\pi\left(r_o + \frac{1}{2}\frac{dr_o}{dz}\,dz\right) \\
&+ \gamma_T\,2\pi\left(r_o + \frac{dr_o}{dz}\,dz\right)\left[\cos\theta - \sin\theta\left(\frac{1}{2}\frac{d\theta}{dz}\,dz\right)\right] \\
&+ d\gamma_T 2\pi\left(r_o + \frac{dr_o}{dz}\,dz\right)\left[\cos\theta - \sin\theta\left(\frac{1}{2}\frac{d\theta}{dz}\,dz\right)\right] \qquad \text{(B-47)} \\
&- \gamma_T\,2\pi r_o\left[\cos\theta + \sin\theta\left(\frac{1}{2}\frac{d\theta}{dz}\,dz\right)\right] \\
&+ (\sigma_{ww} + p_{AMB})\frac{dr_o}{dz}\,2\pi\left(r_o + \frac{1}{2}\frac{dr_o}{dz}\,dz\right)\,dz
\end{aligned}
$$

Using Eq. (B-43) for σ_{ww} one finds, after canceling common terms:

$$
\begin{aligned}
&-(\tau_w + \tau_\infty)\,2\pi\left(r_o + \frac{1}{2}\frac{dr_o}{dz}\,dz\right)\,dz \\
&\gamma_T\,2\pi\left(\frac{dr_o}{dz}\,dz\right)\left[\cos\theta - \sin\theta\left(\frac{1}{2}\frac{d\theta}{dz}\,dz\right)\right] - 2\gamma_T\pi\, r_o \sin\theta\left(\frac{d\theta}{dz}\right)dz \\
&+ d\gamma_T 2\pi\left(r_o + \frac{dr_o}{dz}\,dz\right)\left[\cos\theta - \sin\theta\left(\frac{1}{2}\frac{d\theta}{dz}\,dz\right)\right] \qquad \text{(B-48)} \\
&+ \left[-\gamma_T\left(\frac{\cos\theta}{r_o} - \frac{1}{R_1}\right)\right]\left(\frac{dr_o}{dz}\right)2\pi\left(r_o + \frac{1}{2}\frac{dr_o}{dz}\,dz\right)\,dz = 0
\end{aligned}
$$

Dividing Eq. (B-48) by 2π and retaining terms of order (1) and (dz):

$$
\begin{aligned}
&-(\tau_w + \tau_\infty)\, r_o\, dz + \gamma_T \cos\theta\,\frac{dr_o}{dz}\,dz \\
&- \gamma_T\, r_o \sin\theta\,\frac{d\theta}{dz}\,dz + d\gamma_T\left[r_o\cos\theta\right] \\
&- \gamma_T \cos\theta\left(\frac{dr_o}{dz}\right)\,dz + \gamma_T 1/R_1\,\left(\frac{dr_o}{dz}\right)r_o\,dz = 0
\end{aligned}
$$

Dividing by $r_o\, dz$

$$-(\tau_w + \tau_\infty) - \nu_T \sin\theta \frac{d\theta}{dz} + \frac{d\gamma_T}{dz} (\cos\theta) + \frac{1}{R_1} \left(\frac{dr_o}{dz}\right) = 0 \tag{B-49}$$

Noting

$$\frac{dz}{\cos\theta} \approx ds \approx R_1 \left(\frac{d\theta}{dz}\, dz\right) \tag{B-50}$$

$$\frac{1}{R_1} \approx \frac{d\theta}{dz} \cos\theta \tag{B-51}$$

$$\therefore \quad -(\tau_w + \tau_\infty) - \nu_T \sin\theta \frac{d\theta}{dz} + \frac{d\gamma_T}{dz} (\cos\theta) + \frac{d\theta}{dz} \cos\theta \left(\frac{dr_o}{dz}\right) \gamma_T \tag{B-52}$$

$$\cos\theta \frac{dr_o}{dz} = \cos\theta \tan\theta = \sin\theta \tag{B-53}$$

$$+ (\tau_w + \tau_\infty) = \frac{d\gamma_T}{dz} \cos\theta \tag{B-54}$$

Substituting from Eq. (B-40):

$$\tau_{rz} \left[1 - \left(\frac{dr_o}{dz}\right)^2\right] + \frac{dr_o}{dz} (\sigma_{rr} - \sigma_{zz}) = \left[1 + \left(\frac{dr_o}{dz}\right)^2\right] \left[-\tau_\infty + \frac{d\gamma_T}{dz} \cos\theta\right] \tag{B-55}$$

Using the relationships between stresses and velocity gradients:

$$\sigma_{rr} = -p + 2\mu \frac{\partial v_r}{\partial r} \quad ; \quad \sigma_{zz} = -p + 2\mu \frac{\partial v_z}{dz}$$
$$\tau_{zr} = \mu \left(\frac{\partial v_r}{dz} + \frac{\partial v_z}{\partial r}\right) \tag{B-56}$$

The normal direction boundary condition, (B-44), becomes:

$$-\left[-p + 2\mu \frac{\partial v_r}{\partial r} - 2\left(\frac{dr_o}{dz}\right)(\mu)\left(\frac{\partial v_r}{\partial z} + \frac{\partial v_z}{\partial r}\right) + \left(-p + 2\mu \frac{\partial v_z}{\partial z}\right)\left(\frac{dr_o}{dz}\right)^2\right]$$

$$= \left[1 + \left(\frac{dr_o}{dz}\right)^2\right]\left[p_{AMB} + \gamma_T\left(\frac{\cos\theta}{r_o} - \frac{1}{R_1}\right)\right] \qquad \text{(B-57)}$$

$$p\left[1 + \left(\frac{dr_o}{dz}\right)^2\right] + 2\mu\left[-\frac{\partial v_r}{\partial r} + \frac{dr_o}{dz}\left(\frac{\partial v_r}{\partial z} + \frac{\partial v_z}{\partial r}\right) - \frac{\partial v_z}{\partial z}\left(\frac{dr_o}{dz}\right)^2\right] \qquad \text{(B-58)}$$

$$= \left[1 + \left(\frac{dr_o}{dz}\right)^2\right]\left[p_{AMB} + \gamma_T\left(\frac{\cos\theta}{r_o} - \frac{1}{R_1}\right)\right]$$

For the tangential boundary condition:

$$\mu\left(\frac{\partial v_r}{\partial z} + \frac{\partial v_z}{\partial r}\right)\left[1 - \left(\frac{dr_o}{dz}\right)^2\right] + \mu\,\frac{dr_o}{dz}\left[\frac{\partial v_r}{\partial r} - \frac{\partial v_z}{\partial z}\right] \qquad \text{(B-59)}$$

$$= -\left[1 + \left(\frac{dr_o}{dz}\right)^2\right]\left[-\tau_\infty + \frac{d\gamma_T}{dz}\cos\theta\right]$$

In terms of the stream function, the two free surface boundary conditions are:

$$p\left[1 + \left(\frac{\partial\varpi/\partial z}{\partial\varphi/\partial r}\right)^2\right] + 2\mu\left[+\frac{1}{r}\frac{\partial^2\varpi}{\partial r\partial z} - \frac{1}{r^2}\frac{\partial\varpi}{\partial r} - \left(\frac{\partial\varpi/\partial z}{\partial\varpi/\partial r}\right)\left(\frac{1}{r}\frac{\partial^2\varpi}{\partial r^2} - \right.\right.$$

$$\left.\left. - \frac{1}{r}\frac{\partial^2\varphi}{\partial z^2} - \frac{1}{r^2}\frac{\partial\varpi}{\partial r}\right) - \left(\frac{\partial\varpi/\partial z}{\partial\varpi/\partial r}\right)^2\left(\frac{1}{r}\frac{\partial^2\varphi}{\partial r\partial z}\right)\right] = \qquad \text{(B-60)}$$

$$= \left[1 + \left(\frac{\partial\varphi/\partial z}{\partial\varpi/\partial r}\right)^2\right]\left[p_{AMB} + \gamma_T\left(\frac{\cos\theta}{r_o} - \frac{1}{R_1}\right)\right]$$

$$\mu\left[\frac{1}{r}\frac{\partial^2\varpi}{\partial r^2} - \frac{1}{r^2}\frac{\partial\varpi}{\partial r} - \frac{1}{r}\frac{\partial^2\varpi}{\partial z^2}\right]\left[1 - \left(\frac{\partial\varpi/\partial z}{\partial\varphi/\partial r}\right)^2\right]$$

$$-\mu\left[\frac{\partial\varpi/\partial z}{\partial\varphi/\partial r}\right]\left[\frac{1}{r^2}\frac{\partial\varphi}{\partial z} - \frac{2}{r}\frac{\partial^2\varpi}{\partial r\partial z}\right] = -\left[1 + \left(\frac{\partial\varphi/\partial z}{\partial\varpi/\partial r}\right)^2\right] x \qquad \text{(B-61)}$$

$$x\left[-\tau_\infty + \frac{d\gamma_T}{dz}\cos\theta\right]$$

B.4 Simplifications of the Boundary Conditions

For the case where $dr_o/dz \rightarrow 0$ and the surface tension is a constant, the boundary conditions become:

$$p - 2\mu\left(\frac{\partial v_r}{\partial r}\right) = p_{ATM} + \gamma_T\frac{\cos\theta}{r_o} \qquad \text{(B-62)}$$

$$\mu\left(\frac{\partial v_r}{\partial z} + \frac{\partial v_z}{\partial r}\right) = +\tau_\infty \qquad \text{(B-63)}$$

From the equation of continuity, Eq. (B-62) can be rewritten as:

$$p + 2\mu\left(\frac{v_r}{r} + \frac{\partial v_z}{\partial z}\right) = p_{ATM} + \frac{\gamma_T\cos\theta}{r_o} \qquad \text{(B-64)}$$

and since

$$\frac{dr_o}{dz} = \left(\frac{v_r}{v_z}\right)_{r_o}$$

$$p + 2\mu\left(\frac{v_z}{r_o}\left(\frac{dr_o}{dz}\right) + \frac{\partial v_z}{\partial z}\right) = p_{ATM} + \frac{\gamma_T\cos\theta}{r_o} \qquad \text{(B-65)}$$

APPENDIX C

A CONSIDERATION OF VARIOUS METHODS TO SOLVE THE GENERAL CONSTANT VISCOSITY DIFFERENTIAL EQUATION AND BOUNDARY CONDITIONS

C.1 A Closed Form Solution

The governing differential equation to be solved is

$$E^2(E^2\psi) = 0 \qquad \text{(C-1)}$$

where

$$E^2 = \frac{\partial^2}{\partial z^2} - \frac{1}{r}\frac{\partial}{\partial r} + \frac{\partial^2}{\partial r^2}$$

as given in Appendix B. The boundary conditions for this equation are also derived in Appendix B.

A closed form solution of Eq. (C-1) was attempted assuming $\psi = F(r) \cdot g(z)$. The solution of this form is

$$\psi = C_1 r^4 + C_2 r^2 + C_3 r^2 z^3 + C_4 r^2 z^2 + C_5 r^2 z + \qquad \text{(C-2)}$$

$$+ C_6 z^3 + C_7 z^2 + C_8 z + C_9$$

Since the differential equation is linear any combination of the above equations is also a solution. Notice the first two terms are simply the Hagen-Poiseuille solution for steady flow in a constant radius circular tube.

The other terms in Eq. (C-2) represent either radial flow with no component of axial velocity or one-dimensional axial flow where the axial velocity does not vary in the radial direction.

Unfortunately, the solution given in Eq. (C-2) is too simple to satisfy the free surface boundary conditions. Although the terms in the boundary conditions are not all of the same order of magnitude, when the outside slope of the boundary is of order of magnitude one tenth, the terms of small magnitude in the boundary conditions have the same order of magnitude as the larger terms in the differential equation. Therefore, the small magnitude terms in the boundary conditions cannot be neglected. In other words, it is the rate of change of quantities along the boundary (pressure for example) which actually influence the flow in the interior of the jet. In addition, since the fluid pressure appears in the boundary condition, for each solution assumed the pressure field inside the jet must be calculated from the Navier-Stokes equations. Probably other closed form solutions of the differential equation could be found but this line of investigation was abandoned in favor of approximation solutions.

C.2 Solution by Finite Differences Using the Relaxation Method

The method of finite differences is ideally suited to the computer. In the present problem there are two definite drawbacks. First, the finite difference solution of the fourth order equation converges very slowly. Secondly, since the location of the boundaries is not known, the complexity of the solution is increased by an order of magnitude.

For example, to solve this problem an initial guess for the boundary and internal stream function distribution is put into the computer. The internal net is relaxed so that the differential equation is satisfied within the jet for the particular boundary shape, the result is then checked to see if it satisfies the boundary conditions. If the boundary conditions cannot be satisfied, a new guess for the boundary shape is made and the above process is repeated. Since a series of solutions for varying values of the flow rate, surface tension, etc., is wanted the time necessary to do the above even on a high speed computer seems prohibitive.

The relaxation method might be useful when used in combination with the series approximation for the shape or the one-dimensional solution for the shape of the jet described earlier in the report. Using the approximate jet shape, one

would attempt to satisfy the differential equation and boundary conditions using relaxation methods. If the boundary conditions were not exactly satisfied, the shape of the jet could be altered slightly until the boundary conditions were satisfied. The above process also seems quite lengthy.

C.3 Solution by Calculus of Variations

For this method a form of the velocity distribution in terms of unknown coefficient(s) is assumed and an integral is minimized over the region in question (physically, the integral is the viscous dissipation throughout the jet). In the solution of the most general constant viscosity case, the complexity becomes overwhelming. The cause of the trouble is the fact that the region in question is unknown, that is, the position of the jet boundaries is part of the solution we are attempting to find. In such a case, one must also take into account the "variation of the boundaries" which bring in parts of the physical boundary conditions at the fluid air interface.

The method of the calculus of variations would prove to be as lengthy as the relaxation method.

C.4 Solution By Series

Assume the stream function is of the form

$$\varphi = F_0(r) + F_1(r)/z + F_2(r)/z^2 + F_3(r)/z^3 + \qquad \text{(C-3)}$$

$$+ F_4(r)/z^4 + F_5(r)/z^5 + F_6(r)/z^6 + \ldots$$

where F is an arbitrary function of the radius. The series is assumed in inverse powers of z (the axial distance) because it agrees with the physically observed shape of the jet. That is, at large distances from the nozzle, the jet diameter changes very slowly and the diameter finally becomes constant. Also, selecting a series in inverse powers of z should converge nicely for large values of z.

Substituting the series given in Eq. (C-3) into the governing differential equation, Eq. (C-1), one finds after grouping the result by powers of z

$$
\begin{aligned}
&F_0^{IV} - \frac{2}{r} F_0''' + \frac{3}{r^2} F_0'' - \frac{3}{r^3} F_0' \\
&+ z^{-1}\left(F_1^{IV} - \frac{2}{r} F_1''' + \frac{3}{r^2} F_1'' - \frac{3}{r^3} F_1'\right) \\
&+ z^{-2}\left(F_2^{IV} - \frac{2}{r} F_2''' + \frac{3}{r^2} F_2'' - \frac{3}{r^3} F_2'\right) \qquad \text{(C-4)} \\
&+ z^{-3}\left[F_3^{IV} - \frac{2}{r} F_3''' + \frac{3}{r^2} F_3'' - \frac{3}{r^3} F_3' + 4\left(F_3'' - \frac{1}{r} F_3'\right)\right] \\
&+ z^{-4}\left[F_4^{IV} - \frac{2}{r} F_4''' + \frac{3}{r^2} F_4'' - \frac{3}{r^3} F_4' + 12\left(F_2'' - F_2'/r\right)\right] \\
&+ z^{-5}\left[F_5^{IV} - \frac{2}{r} F_5''' + \frac{3}{r^2} F_5'' - \frac{3}{r^3} F_5' + 24\left(F_3'' - \frac{1}{r} F_3'\right) + 24\, F_1\right] \\
&+ z^{-6}\left[F_6^{IV} - \frac{2}{r} F_6''' + \frac{3}{r^2} F_6'' - \frac{3}{r^3} F_6' + 40\left(F_4'' - \frac{F_4'}{r}\right) + 120\, F_2\right] \\
&+ z^{-7}(\ldots) + \ldots = 0
\end{aligned}
$$

Equating the terms with the same power of z to zero, the solution for F_0 and F_2 are

$$F_0 = C_{10} r^4 + C_{20} r^2 + C_{30} r^2 \ln(r) + C_{40} \qquad \text{(C-5)}$$

$$F_1 = C_{11} r^4 + C_{21} r^2 + C_{31} r^2 \ln(r) + C_{41} \qquad \text{(C-6)}$$

The boundary condition at the centerline of an axi-symmetric flow at any value of z is

$$\frac{\partial v_z}{\partial r} = 0 = \frac{\partial}{\partial r}\left(\frac{1}{r}\frac{\partial \varphi}{\partial r}\right)_r = 0 \qquad (C-7)$$

which gives

$$C_{30} = C_{31} = 0 \qquad (C-8)$$

The other boundary condition to be satisfied at the centerline for any value of z is

$$v_r = -\left(\frac{1}{r}\frac{\partial \varphi}{\partial z}\right)_{r=0} = 0 \qquad (C-9)$$

This can be satisfied by

$$C_{41} = 0 \qquad (C-10)$$

One can arbitrarily make $\varphi = 0$ at $r = 0$ by setting C_{40} equal to zero. Solving for $F_2, F_3, F_4, F_5, F_6, F_7$ and F_8 one finds, after satisfying the centerline boundary conditions

$$F_2 = C_{12}r^4 + C_{22}r^2 \qquad (C-11)$$

$$F_3 = C_{13}r^4 + C_{23}r^2 - \frac{1}{6}C_{11}r^6 \qquad (C-12)$$

$$F_4 = C_{14}r^4 + C_{24}r^2 - \frac{C_{12}}{2}r^6 \qquad (C-13)$$

$$F_5 = C_{15}r^4 + C_{25}r^2 - (C_{13} + \frac{1}{8} C_{21})r^6 + \frac{C_{11}}{16} r^8 \qquad (C-14)$$

$$F_6 = C_{16}r^4 + C_{26}r^2 - (\frac{5}{3} C_{14} + \frac{5}{8} C_{22})r^6 + \frac{5}{16} C_{12}r^8 \qquad (C-15)$$

$$F_7 = C_{17}r^4 + C_{27}r^2 - r^6(+\frac{5}{2} C_{15} + \frac{C_{21}}{8}) \qquad (C-16)$$

$$+ r^8(\frac{C_{11}}{48} - \frac{5}{4} C_{13} - \frac{5}{32} C_{21}) - r^{10}(\frac{9}{172})C_{11}$$

$$F_8 = C_{18}r^4 + C_{28}r^2 - \frac{7}{2} C_{16}r^6 \qquad (C-17)$$

$$+ r^8(\frac{35}{12} C_{14} + \frac{105}{96} C_{22}) - \frac{63}{192} C_{12}r^{10}$$

Notice that if $C_{20} = -2\, C_{10}$ the axial velocity tends toward a parabolic profile as z grows larger and if $C_{10} = 0$, the axial velocity will approach a uniform one-dimensional profile.

The series solution is suited to a computer where the coefficients of each term can be adjusted by trial and error until the boundary conditions are satisfied at a given number of discrete points.

C.5 Discussion of the Solution of the Differential Equation and Boundary Conditions

For the constant viscosity case as can be seen in the previous sections, any method beyond a simple approximate technique would require considerable effort in programming a computer. The actual problem to be solved considers the case of a variable

viscosity flow where the governing equation is now non-linear. Also, to find the velocity distribution at the mouth of the nozzle to be used as the upper boundary conditions, the flow inside the nozzle, near the exit would also have to be considered. In view of the complexity incurred above, it was decided to omit the detailed solution of the differential equations and boundary conditions for the upper jet.

APPENDIX D

THE EXPERIMENTS USING CONSTANT VISCOSITY FLUID

D.1 General

In conjunction with the efforts to solve the governing two-dimensional equations of motion for the jet, see Appendices B and C, experiments were performed using fluids which were kept at a constant temperature so that the viscosity of the fluid remained constant.

Originally, the experiments were intended to serve as a means to verify the results of the two-dimensional analysis. Although the two-dimensional equations were not solved, see Appendices B and C, the experiments were continued to gain a qualitative insight into the characteristics of low speed jets.

D.2 Qualitative Results

The experiments were designed so that the Reynolds number based upon the nozzle exit diameter would be less than one. It was found in many cases that rather than flow in a continuous jet, the fluid dripped from the nozzle exit. Accordingly, an analysis was made which predicted the onset of dripping, see Appendix E.

One of the controlling parameters was found to be the wetting of the jet on the outside surface of the nozzle. It was found that the contact angle and the distance the fluid crept out on the nozzle surface, which faced vertically downward, would vary from day to day even though all the other test conditions were kept constant. If the flow was suddenly begun at a high value and then lowered to the value for the experiment the fluid would not appear to spread out beyond the nozzle exit diameter in many cases. However, if there was an interruption in the flow rate or if the flow was begun at a low value, the fluid would spread out beyond the nozzle exit.

In some cases the outside surface of the nozzle was Teflon coated and the fluid which was used, glycerine, does not wet Teflon in static cases. However, it was found that the fluid did spread out on the Teflon when a nozzle with a small inner diameter was used. Obviously, the wetting phenomena must depend upon the dynamic conditions of the flow rather than just a static contact angle condition.

D.3 Description of the Experimental Apparatus

The constant viscosity apparatus simply consisted of a constant head tank connected by flexible tubing to a small closed

reservoir. The nozzle was mounted on the bottom of the reservoir so that it pointed vertically downward. The nozzle had a hole of constant diameter through which the fluid flowed. The length to diameter ratio of the nozzle was at least three for all cases. The bottom surface of the nozzle was flat and in some cases was coated with Teflon. By raising or lowering the head tank relative to the nozzle exit, the flow rate could be altered. The fluid and apparatus were kept at the ambient temperature.

A microscope and attached camera were mounted horizontally so that the jet could be photographed. The microscope was mounted on a vertical traversing device. Since the jet was not heated, the working distance of the microscope could be small, therefore, a standard Baush and Lamb microscope was used. The flow rate of the jet was measured by weighing the amount of fluid which had flowed for a known time. The surface tension, viscosity and density of the fluid was measured before and after the experiment.

Because the viscosity of the fluid was high, air bubbles entrained in the reservoir or connecting tubing would not surface immediately. Therefore, the apparatus was filled and allowed to stand at least an hour before the experiment was begun.

D.4 Further Results

As mentioned previously, the experiments were principally performed to yield qualitative results. However, the data of one test is compiled below. Notice that the jet expands and then contracts after leaving the nozzle exit.

An attempt was made to predict the jet shape using the one-dimensional dynamical equation given in Chapter 3, with the viscosity gradient equated to zero. The attempt was unsuccessful leading to the conclusion that the initial jet "bulge" must be a two-dimensional effect.

Tabulated Results

Fluid: Glycerine Test F2

Nozzle Exit Diameter: $0.0636 \pm .0006$ inches

Distance From Nozzle Exit to Collecting Cup: 9.5 inches

Surface Tension of Fluid:

Before Experiment: 67.2 dynes/cm

After Experiment: 66.5 dynes/cm

Kinematic Viscosity of Fluid

Before Experiment: 3.722 Stokes

After Experiment: 3.787 Stokes

Density of Fluid: $1.2489\ gm/cm^3$

Flow Rate: 0.5475 ± 0.0025 gms/min

Reynolds Number (based on nozzle exit diameter) = 0.92

Radius Versus Distance

Frame No.	z, Distance From Nozzle Exit (Inches)	r_o, Jet Radius (Inches)
28	0.0	3.50×10^{-2}
	0.0157	3.56×10^{-2}
25	0.0	3.52×10^{-2}
	0.0349	3.56×10^{-2}
	0.0603	3.46×10^{-2}
24	0.0440	3.53×10^{-2}
	0.0758	3.365×10^{-2}
21,22	0.190	2.925
19,20	0.390	2.501
17,18	0.790	2.041
15,16	1.790	1.638
12,13,14	2.490	1.492
10,11	4.490	1.261
7,8,9	5.490	1.225
4,5	6.593	1.124

APPENDIX E

A STABILITY CRITERION FOR THE CONSTANT VISCOSITY JET

It has been found in performing low Reynolds number constant viscosity experiments that rather than flowing continuously in many cases the liquid dripped from the nozzle. An analysis which predicts the limits of the flow-drip regimes follows.

Consider the case of a nozzle initially dripping which has the head above it increased, consequently, the flow rate increases. A drop forms at the nozzle and then moves downward forming a jet of liquid behind it. The radius of the jet immediately above the drop is designated r*. Assume a system to consist of the drop with a constant mass, M. Assume the velocity of the drop equals the average velocity of the fluid at r*. Then, for the drop to have a constant mass, the acceleration of the drop must equal the acceleration of the fluid at r*. If the drop acceleration is greater than the fluid acceleration at r*, then r* must contract or neck and a disturbance is caused. This disturbance is assumed to be the source of the instability which causes dripping.

Writing the equation of motion for the drop, $F = Ma$

$(a)_{drop} = (a)$ fluid at r* is the limiting condition for stability of a jet forming behind the drop.

The forces on the drop are surface tension, gravity, pressure forces, and viscous restraining forces.

$$-\gamma_T\, 2\pi r^* \cos\theta + \int_{\substack{\text{surface}\\ \text{area}}} p\,dA \;-\; \int_{\substack{\text{area}\\ \text{at } r^*}} (\text{Viscous Forces})\,dA \qquad \text{(E-1)}$$

$$+ Mg = M \frac{d}{dt} (V_{drop})$$

The viscous force per unit area is $3\mu \frac{\partial v_z}{\partial z}$ at r^*

$$\text{at } r^* \text{ , } p_{liquid} = p_A + \frac{\gamma_T}{r^*} \cos\theta \qquad \text{(E-2)}$$

$$\frac{dV}{dt} = \frac{dV}{dz}\frac{dz}{dt} = V \frac{dV}{dz} = v_z \frac{dv_z}{dz} \qquad \text{(E-3)}$$

From the technique used to measure surface tension by measuring the weight of drop formed from a nozzle it has been found that

$$M = C \left(\frac{2\pi R_o \gamma_T}{g}\right) \qquad \text{(E-4)}$$

Assuming the velocity is uniform at r^*, i.e., $v_z = \frac{w}{\rho\pi (r^*)^2}$

one finds, from Eq. (E-1),

$$0 = \left(\frac{2R_o \gamma_T C}{\rho\pi g \mu (r^*)^4}\right) w^2 + \frac{3}{2} w + \frac{\gamma_T (r^*)^2 \rho\pi}{2\mu \left(\frac{dr_o}{dz}\right)_{r^*}} \left(2\frac{R_o C}{r^*} + 1 - 2\cos\theta\right) \qquad \text{(E-5)}$$

where $(dr_o/dz)_{r^*}$ is the slope at r^*

$$(Re)_{R_o} = \frac{w}{\mu\pi R_o} = -\frac{3g\rho(r^*)^4}{8\nu_T R_o{}^2 C} + \sqrt{\left(\frac{3g\rho r^{*4}}{Cg\nu_T R_o{}^2}\right)^2 - \frac{g\rho^2(r^*)^6\left(\frac{2R_o C}{r^*} - 1 - 2\cos\theta\right)}{4\mu^2 R_o{}^3\left(\frac{dr_o}{dz}\right)_{r^*} C}} \qquad (E\text{-}5)$$

For the actual cases considered, $(3g\rho(r^*)^4/8C\,\nu_T R_o{}^2)^2$ can be neglected compared to

$$\frac{g\rho^2(r^*)^6}{4\mu^2 R_o{}^3\left(\frac{dr_o}{dz}\right)_{r^*} C}$$

So,

$$(Re)_{R_o} = \frac{w}{\mu\pi R_o} = \sqrt{\frac{g\rho^2(r^*)^6\left(2\,\frac{R_o}{r^*}\,C + 1 - 2\cos\theta\right)}{4\mu^2 R_o{}^3\left(\frac{dr_o}{dz}\right)_{r^*} C}} \qquad (E\text{-}6)$$

or,

$$\frac{w}{\pi R_o{}^{5/2}\rho g^{1/2}} = \text{constant} = \sqrt{\text{Froude Number}} \qquad (E\text{-}7)$$

To evaluate the constant, assume

$$r_o = \frac{C_1}{C_2 + z} \qquad (E\text{-}8)$$

where C_1 and C_2 are found by matching the conditions at $z = o$, namely $r_o = R_o$ and $dr_o/dz = (dr_o/dz)_{R_o}$.

The value of the mass flow rate, w, is the value which just satisfies F = Ma. For a value of the flow rate less than the calculated value, the fluid acceleration at r* will be less than the drop acceleration meaning that a disturbance, dripping, occurs. Therefore, the value of w or Reynolds number calculated above is the transition value.

A value of z where r* is to be evaluated also must be known. At present z is assumed equal to one-half the critical wave length of a pertibation on the surface of a constant radius cylindrical jet which will grow rather than die out as predicted by Rayleigh. Undoubtedly, a more accurate analysis of the stability of a variable radius jet will yield a more accurate value for z.

Figure 1 shows the experimental values of the Froude and Reynolds numbers at which transition from dripping to a steady stream occurs. Physically, the validity of the analysis is doubtful since it indicates that surface tension effects are unimportant. Further experimentation using a wider range of fluids and larger nozzle radii, the largest used in the present work was 1/8 inch, are necessary before any definite conclusions can be made regarding the present analysis.

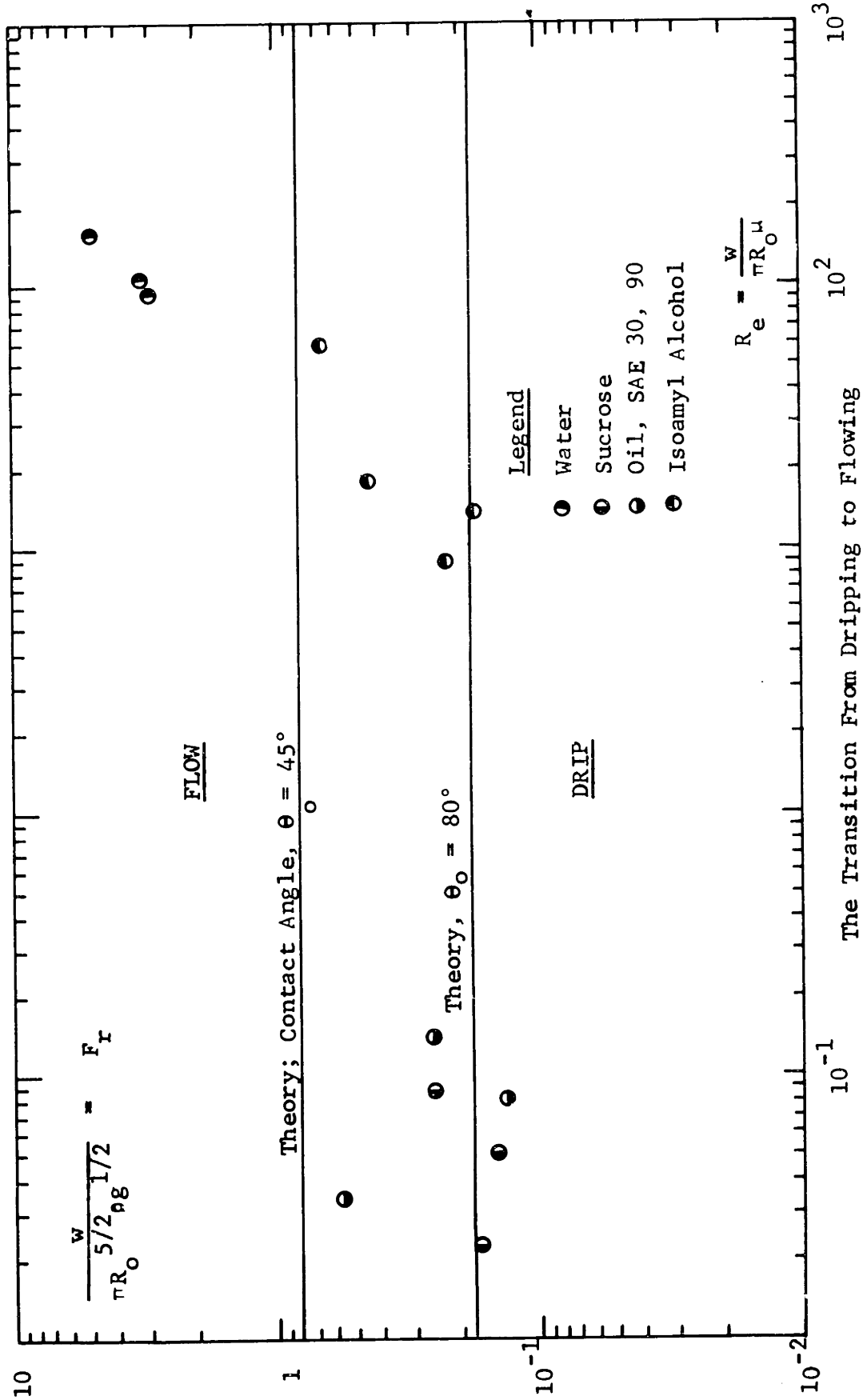

The Transition From Dripping to Flowing
Reynolds Number Versus
Square Root of Froude Number

Fig. E-1

APPENDIX F

COMPUTER PROGRAMS

The computer programs used to solve for the shape, temperature distribution and tension of the jet, are given below. The programs solve the general one-dimensional equations, 3.15 and 3.23. The boundary layer is assumed to be laminar for all cases.

The differential equations are converted to difference equations and solved using the Newton backward difference formula retaining forth differences. The starting procedure involves an iteration process (refer to pp. 188-191 and 195-197 of reference (21) or see reference (22)). The main program is listed first followed by two subroutines utilized by the main program.

The program lists the radius, temperature, tension, and viscous normal force at a given distance. The value of RE given does not correspond to r_E defined previously as the radius where dr_o/dz is minus one-tenth. Regard RE only as an arbitrary starting point for the program.

The variables which must be furnished to the program are explained below along with the units the variables must be written in.

DATA CARD 1, FORMAT (4E15.6)

W : The flow rate (gm/sec)

GAMMA : The absorption coefficient (gm/sec)
If GAMMA is greater than 0.01 the program assumes the absorption coefficient is a constant for all values of wavelength, if GAMMA is less than 0.01 three additional data cards are needed, see cards 5, 6, and 7.

THETA : Corresponds to θ_o defined previously (degrees)

FINDZ : The value of Δz used in the difference equations, a value of 4.0 has been found to give accurate results

DATA CARD 2, FORMAT (4E15.6)

RO : Corresponds to R_o defined previously (cm)

RW : Corresponds to r_{FINAL} defined previously (cm)

TO : Corresponds to T_o defined previously (°F not °R)

TAMB : Corresponds to T_{ATM} defined previously (°F)

DATA CARD 3, FORMAT (I4, 2E15.6)

JUMP : Program control variable, if JUMP is 1 or 2 Δz is constant throughout the program, if JUMP is 2 or 3, SIGMAT is assumed equal to zero in the momentum equation. If JUMP = 0 neither of the above happens. Only values of z for r_o less than R_o will be printed when JUMP is 3 or less. When JUMP is 9, the program will be continued for values of r_o greater than R_E up to the point where r_o equals R_o, below R_E the program runs as if JUMP equaled 0.

AL : Corresponds to L defined previously (cm)
AL must be assumed. If the calculated value of L is greater than the assumed value of AL, an error in the program will result.

CLXFC : The program uses the values of h and τ_∞ equal to the values predicted by the laminar boundary layer analysis multiplied by CLXFC. In the usual case CLXFC is 1.0

DATA CARD 4, FORMAT (5E14.5)

CP : Corresponds to c_p defined previously (BTU/lb°F)

RHO : Corresponds to ρ defined previously (gm/cm^3)

SIGMAT : Corresponds to γ_T defined previously (dynes/cm)

GLASSK : Corresponds to k defined previously (gm-cal/sec-cm°C)

GUESS : If the initial part of the program fails, GUESS will provide the first value of $(dr_o/dz)_{RE}$ to be used in the solution, normally GUESS is set equal to 10^{-2}.

DATA CARDS 5,6, and 7, FORMAT (6E11.3/6E11.3/5E11.3)

If GAMMA given in data card 1 is greater than 0.01 do not include data cards 5,6, and 7. If GAMMA is less than 0.01 data cards 5,6, and 7 give the absorption coefficient (cm^{-1}) versus wavelength distribution to be used by the program. The values of the absorption coefficient at intervals of 0.5 microns are given from 0 microns through 8.0 microns on cards 5,6, and 7.

08/09 1329.9

```
C       ALL INPUT DATA SHOULD BE IN CGS UNITS, TEMPERATURES IN DEGREES F, NOT
C       ABSOLUTE DEGREES
C       FINDZ SPECIFIES THE INITIAL VALUE OF DZ
C       GUESS WILL BE USED AS THE FIRST VALUE OF DR/DZ AT RE IF RITAL FAILS
C       JUMP=1,2 - DZ STAYS CONSTANT DURING A GIVEN RUN, JUMP=2,3 - SIGMAT=0 IN
C       THE CALCULATION OF DDRAD, JUMP=0 - NEITHER OF THE ABOVE OCCURS
C       IF JUMP=9, CALCULATION ABOVE RE TAKES PLACE WITH JUMP=4
C       THEATA IS IN DEGREES FROM THE VERTICAL
C       IF GAMMA IS LESS THAN 0.01 (1/CM), 17 VALUES OF GAMMA VS. LAMBDA ARE
C       USED) LAMBDA IS IN STEPS OF 0.5 MICRONS STARTING AT 0 MICRONS
  1     READ 3,(W,GAMMA,THEATA,FINDZ)
        DIMENSION R(11),T(12),DR(11),DT(11),DDR(11),FR(3),FDR(3),G(20)
        IGAM=0
        NUP=0
        READ 3,(RC,RW,TO,TAMB)
  3     FORMAT(4E15.6)
  2     READ 4,(JUMP,AL,CLXFC)
  4     FORMAT(I4,2E15.6)
        IF(JUMP-9)220,800,800
 800    NUP=1
        JUMP=4
 220    READ 221,(CP,RHC,SIGMAT,GLASSK,GUESS)
 221    FORMAT(5E14.5)
 240    Q=W/RHC
        NOPRNT=0
        TEMP=TO
        RWO=RW
        U=EXPF(-(9.827E-3)*TEMP+28.7415)
        UO=U
        TFILM=(TEMP-100.0+TAMB)/3.6+255.38
  5     VISKIN=(1.149E-5)*(TFILM**1.672)-0.0132
        X=AL
        Y=VISKIN*X*12.56637/Q
  6     CL=6.78575*((2.0/(LOGF(Y)))-6.0/(LOGF(Y))**3.0)
  7     UAIR=(145.8E-7)*(TFILM**1.5)/(TFILM+110.4)
  8     RE=((CL*Q*UAIR)/(9576.1819*RHO))**0.25
        THEATO=THEATA*0.017453
        DRO=-TANF(THEATO)
  9     B1=UO*RE*DRO/RO
        B2=SIGMAT*RE*0.7854/(Q*1.5)
        B3=RHO*Q*RE/(12.56637*1.5)
 10     PROD=B1-B2*(COSF(THEATO)*RO-RE)-B3*((1.0/(RE*RE))-1.0/(RO*RO))
        W=Q*RHO
 11     PRINT 12
 12     FORMAT(1H1,5X,7HRO (CM),8X,7HRE (CM),3X,14HTO (DEGREES F),1X,17H T
       1HEATA (DEGREES),2X,12HPROD (POISE),5X,7HRW (CM),2X,16HQ (CUBIC CM/
       2SEC),1X,16HCP (GM CAL/GM C))
 13     FORMAT(1H ,8G15.6)
 14     PRINT 13,(RO,RE,TO,THEATA,PROD,RW,Q,CP)
 15     PRINT 16
 16     FORMAT(1HC,1X,12HGAMMA (1/CM),6X,17HRHO (GM/CUBIC CM),3X,17HSIGMAT
       1 (DYNES/CM),2X,24HGLASSK (GM CAL/SEC CM C),2X,13HGUESS FORDRE,9X,1
       22HTAMB (DEG F))
 17     PRINT 18,(GAMMA,RHO,SIGMAT,GLASSK,GUESS,TAMB)
 18     FORMAT(1H ,G15.6,5X,G15.6,5X,G15.6,10X,G15.6,5X,G16.6,4X,G16.6)
```

```
      PRINT 802,(AL)
  802 FORMAT(1HC,20HLENGTH FROM RC TO RE,G15.6,4H(CM))
      PRINT 860,(CLXFC)
  860 FORMAT(1HO,59HTHEORETICAL VALUES OF DRAG AND FILM COEF. ARE MULTIP
     1LIED BY,G12.3)
  846 IF(GAMMA-C.C1)841,841,840
  841 READ 842,(G(J),J=1,17)
      IGAM=1
  842 FORMAT(6E11.3/6E11.3/5E11.3)
      PRINT 843
  843 FORMAT(1HO,86H VALUES OF GAMMA (1/CM) FOR WAVELENGTH INTERVALS OF
     1C.5 MICRONS STARTING AT 0 MICRONS )
      PRINT 845,(G(J),J=1,17)
  845 FORMAT(6G11.3/6G11.3/5G11.3)
  840 NCDDR=C
   20 NCDRE=0
      TFILM=(TFILM+TAMB/1.8)/2.C
      AIRK=(C.6325E-5*(TFILM)**C.5)/(1.0+245.4/(TFILM*(10.0)**(12.0/TFIL
     1M)))
  200 RITA1=+(AIRK*RE*CL)/(W*CP)
      RITA2=(9.827E-3)*(TO-2CC.0-TAMB)
  201 IF(RITA2-7.C)202,204,204
  202 DRE=GUESS
      NCTNSN=C
      GC TO 21
  204 DRE=-(RITA1)*(RITA2**4.C)*LOGF(RE/RW)/(((RITA2)**3.C)+((RITA2)**2.
     10)+(2.C*RITA2)+6.0)
      NCTNSN=C
   21 FDZ=FINDZ
      NODZ=0
      TGAVG=3CCC.C
      IF(NOPRNT)23,23,700
  7CC PRINT 22,(FDZ,DRE)
   22 FORMAT(1HC,4HDZ= ,F7.3,5X,5HDRE= ,F11.8)
   23 N=2
      DRAD=DRE
      I=0
      Z=0.0
      AIRDRG=C.C
      IF(DRAD)25,805,805
   25 IF(NUP-1)27,27,804
  804 IF(DRAD+3.0)805,805,27
  805 PRINT 26
   26 FORMAT(3CHO  DR IS POSITIVE STATEMENT 25)
      GO TO 16C
   27 RAD=1.C
      TEMP=1.G
      U=1.0
      UE=PROD/DRAD
      DZ=FDZ
      TE=(28.7415-LOGF(UE))/(C.9827E-2)
      IF(NOPRNT)7C2,7C2,701
  701 PRINT 3CC,(UE,TE)
  300 FORMAT(1HC,4HUE= ,G15.7,16H (POISE)     TE= ,G15.7,11H(DEGREES F))
  702 II=-1
   28 TFILM=((TE*TEMP)+TAMB)/3.6+255.38
```

```
      AIRK=(0.6325E-5*(TFILM)**0.5)/(1.0+245.4/(TFILM*(10.0)**(12.0/TFIL
     1M)))
831   X=AL+Z*RF
      IF(X)832,832,833
832   CL=0.0
      FVIEW=1.0
      GO TO 834
833   UAIR=(145.8E-7*(TFILM)**1.5)/(TFILM+110.4)
      FVIEW=0.5*(1.0-1.0/((1.0+(RO/X)**2.0)**0.5))
      VISKIN=(1.149E-5)*(TFILM**1.672)-0.0132
      GAMMAO=GAMMA
      XY=(VISKIN*X*12.5664)/G
      IF(XY-40.0)930,930,920
930   XY=XY/4.0
      IF(XY-1.0)910,909,909
910   IF(XY-0.1)901,900,900
909   CL=5.01/(XY)**(1.0/4.5)
      GO TO 834
900   CL=5.01/(XY)**(1.0/3.31)
      GO TO 834
901   IF(XY)902,902,903
902   CL=0.0
      GO TO 834
903   CL=6.2834*(0.332/(XY)**0.5+0.697-0.797*(XY)**0.5)
      GO TO 834
920   CL=6.78575*((2.0/(LOGF(XY)))-6.0/(LOGF(XY))**3.0)
834   IF(IGAM)850,850,999
999   IF(NUP-2)997,851,851
997   IF(TGAVG-TEMP*TE-10.0)998,998,851
998   GAMMA=GAVG1
      GO TO 850
851   NN=0
      CALL GAMAVG(G,TEMP,TE,RAD,RE,GAVG,NN)
      GAMMA=GAVG
      GAVG1=GAVG
      TGAVG=TEMP*TE
      IF(X)861,861,862
862   X=X/RE
      TO=TO/TE
      CALL VIEWFC(X,RE,TO,RO,G,TE,RAD,FVIEWG)
      TO=TO*TE
      X=X*RE
      GO TO 850
861   FVIEWG=GAMMA*(TO+459.6/TE)**4.0
850   ENG1=(6.28319*GLASSK*RE)/(W*CP)
      CL=CL*CLXFC
      ENG2=(2.9199E-12*GAMMA)*((TE*RE)**3.0)/(W*CP)*(1.0-FVIEWG/GAMMA)/(
     1TEMP+459.6/TE)**4.0
      ENG3=AIRK*CL*RE/(W*CP)
30    U=(1.0/UE)*EXPF((-0.9827E-2)*TEMP*TE+28.7415)
      DTEMP=(1.0/(1.0-ENG1*RAD*DRAD))*(-ENG2*RAD*RAD*(TEMP+459.4/TE)**4-
     10-ENG3*(TEMP-TAMB/TE))
835   RDIMEN=RAD*RE/2.54
      TDIMEN=TEMP*TE
      ZDIMEN=Z*RE/2.54
      UI=U*UE
```

```
      AIRDRG=AIRDRG+CL*Q*UAIR*CZ/(3.1417*RAD*RAD*RE)
      IF(NOTNSN)31,31,136
31    DLNU=-((0.9827E-2)*DTEMP)*TE
      THEATO=ATANF(-CRAD)
      XX=COSF(THEATO)
      TENSN=-(6.0*UE*Q/RE)*(U/RAD)*DRAD
      PRD=PRCC
      TENSN1=-PRD*6.0*Q/RE+SIGMAT*3.1417*RE*(COSF(ATANF(-DRE))-RAD*XX)+(
     1RHO/3.1417)*((Q/RE)**2.0)*(1.0/(RAD*RAD)-1.0)+AIRDRG
      TENSN2=TENSN1+SIGMAT*3.1417*RE*RAD*XX
      IF(JUMP-2)400,401,401
401   A1=0.0
402   IF(JUMP-3)403,403,400
400   A1=((0.7854*SIGMAT*RE*RE)/(UE*Q))*XX**3.0
403   A2=RHO*769.85*((RE)**4.0)/(UE*Q*1.5)
      A3=CL*UAIR/(12.5664*UE*1.5)
      A1=A1/1.5
      A4=W/(6.28319*RE*UE*1.5)
720   IF(II-7)32,32,705
32    CCRAD=(1.0/(1.0+A1*RAD*RAD*CRAD/U))*(A2*(RAD**3.0)/U-A3/(RAD*U)+DR
     1AD*(DRAD/RAD-DLNU+A1*RAD/(U*XX*XX)+A4/(U*RAD*RAD)))
      IF(CCRAD)302,33,33
302   NCCCR=NCCCR+1
303   PRINT 304
304   FORMAT(1HC,17HCCRAD IS NEGATIVE)
      IF(NCCCR-3)305,305,1
305   DRE=DRE/2.0
      GO TO 21
33    IF(II)34,59,70
34    R(N)=RAD
      T(N)=TEMP
      DT(N)=DTEMP
      DR(N)=DRAD
      CCR(N)=CCRAD
      N=N+1
      IF(N-7)40,41,41
40    Z=Z+DZ
      TEMP=TEMP+DTEMP*DZ
      RAD=RAD+DRAD*DZ
      DRAD=DRAD+DDRAD*DZ
      GO TO 28
41    J=0
42    AR6=R(6)
      AT6=T(6)
      ADR6=DR(6)
      R(3)=R(2)+(DZ/720.0)*(251.0*DR(2)+646.0*DR(3)-264.0*DR(4)+106.0*DR
     1(5)-19.0*DR(6))
      R(4)=R(2)+(DZ/90.0)*(29.0*DR(2)+124.0*DR(3)+24.0*DR(4)+4.0*DR(5)-D
     1R(6))
      R(5)=R(2)+(DZ/80.0)*(27.0*DR(2)+102.0*DR(3)+72.0*DR(4)+42.0*DR(5)-
     13.0*DR(6))
      R(6)=R(2)+(DZ/22.5)*(7.0*DR(2)+32.0*DR(3)+12.0*DR(4)+32.0*DR(5)+7.
     10*DR(6))
43    DR(3)=DR(2)+(DZ/720.0)*(251.0*DDR(2)+646.0*DDR(3)-264.0*DDR(4)+106
     1.0*DDR(5)-19.0*DDR(6))
      DR(4)=DR(2)+(DZ/90.0)*(29.0*DDR(2)+124.0*DDR(3)+24.0*DDR(4)+4.0*DD
```

```
     1R(5)-CDR(6))
      DR(5)=DR(2)+(DZ/80.0)*(27.0*CDR(2)+102.0*CDR(3)+72.0*CDR(4)+42.0*C
     1DR(5)-3.0*CDR(6))
      DR(6)=DR(2)+(DZ/22.5)*(7.0*CDR(2)+32.0*CDR(3)+12.0*CDR(4)+32.0*CDR
     1(5)+7.0*CDR(6))
      T(3)=T(2)+(DZ/720.0)*(251.0*DT(2)+646.0*DT(3)-264.0*DT(4)+106.0*DT
     1(5)-19.0*DT(6))
      T(4)=T(2)+(DZ/90.0)*(29.0*DT(2)+124.0*DT(3)+24.0*DT(4)+4.0*DT(5)-0
     1T(6))
      T(5)=T(2)+(DZ/80.0)*(27.0*DT(2)+102.0*DT(3)+72.0*DT(4)+42.0*DT(5)-
     13.0*DT(6))
      T(6)=T(2)+(DZ/22.5)*(7.0*DT(2)+32.0*DT(3)+12.0*DT(4)+32.0*DT(5)+7.
     10*DT(6))
      J=J+1
51    IF(J-8)52,63,63
52    IF(ABSF((R(6)-AR6)/R(6))-0.001)53,53,57
53    IF(ABSF((DR(6)-ADR6)/DR(6))-0.001)55,55,57
55    IF(ABSF((T(6)-AT6)/T(6))-0.001)63,63,57
57    N=2
58    II=0
      RAD=R(N)
      CRAD=DR(N)
      TEMP=T(N)
      AAA=N-2
      Z=AAA*DZ
      GO TO 28
59    CDR(N)=CDRAD
      DT(N)=CTEMP
      N=N+1
      IF(N-6)58,58,42
63    IF(NOPRNT)710,710,704
704   PRINT 133
133   FORMAT(1H4,17HDISTANCE BELOW RE,2X,6HRADIUS,5X,11HTEMPERATURE,4X,1
     12HNON DIMEN. Z,3X,12HNON DIMEN. R,3X,12HNON DIMEN. T,4X,9HVISCOSITY
     2Y,6X,7HTENSION,3X,14HVISCOUS NORMAL)
      PRINT 137
137   FORMAT(1H ,4X,1CHZ (INCHES),3X,10HR (INCHES),3X,13HT (DEGREES F),6
     1X,4HZ/RE,11X,4HR/RE,11X,4HT/TE,9X,7H(POISE),7X,7H(DYNES),4X,13HFOR
     2CE (DYNES))
      AIRDRG=0.0
      DO 705 N=2,6
      RAD=R(N)
      CRAD=DR(N)
      TEMP=T(N)
      AAA=N-2
      Z=AAA*DZ
      II=9
      GO TO 28
705   PRINT 406,(ZDIMEN,RDIMEN,TDIMEN,Z,RAD,TEMP,UI,TENSN2,TENSN1)
      II=0
406   FORMAT(7G15.6,2G13.4)
710   N=6
      III=0
65    R(N+1)=R(N)+(DZ/720.0)*(1901.0*DR(N)-2774.0*DR(N-1)+2616.0*DR(N-2)
     1-1274.0*DR(N-3)+251.0*DR(N-4))
      DR(N+1)=DR(N)+(DZ/720.0)*(1901.0*CDR(N)-2774.0*CDR(N-1)+2616.0*CDR
```

```
      1(N-2)=1274.0*CDR(N-3)+251.0*DDR(N-4))
      T(N+1)=T(N)+(DZ/720.0)*(1901.0*DT(N)-2774.0*DT(N-1)+2616.0*DT(N-2)
     1-1274.0*DT(N-3)+251.0*DT(N-4))
      II=1
   68 Z=Z+DZ
      TEMP=T(N+1)
      RAD=R(N+1)
      CRAD=CR(N+1)
      IF(NUP-1)28,28,820
  820 IF(RAD*RE-RO)28,146,146
   70 CDR(N+1)=CDRAD
      DT(N+1)=DTEMP
      IF(NOPRNT)72,72,715
  715 PRINT 406,(ZDIMEN,RDIMEN,TDIMEN,Z,RAD,TEMP,C1,TENSN2,TENSN1)
   72 IF(N-10)75,76,76
   75 N=N+1
      GO TO 65
   76 CC=CRAD
      IF(CC+5.0E-3)78,80,80
   78 N=10
      DO 79 N=2,10
      R(N)=R(N+1)
      DR(N)=DR(N+1)
      CDR(N)=CDR(N+1)
      T(N)=T(N+1)
   79 DT(N)=DT(N+1)
      GO TO 65
   80 IF(I-1)82,84,85
   82 IF(JUMP-1)81,90,405
  405 IF(JUMP-2)90,90,81
   81 DO 83 N=1,5
      R(N+1)=R(2*N)
      DR(N+1)=DR(2*N)
      CDR(N+1)=CDR(2*N)
      T(N+1)=T(2*N)
   83 DT(N+1)=DT(2*N)
      I=I+1
      DZ=DZ*2.0
12    N=6
      GO TO 65
11 84 IF(CC+1.0E-3)78,82,82
   85 IF(I-3)86,88,90
10 86 IF(CC+5.0E-4)78,82,82
   88 IF(CC+1.0E-4)78,82,82
 9 90 IF(CC-GRE/100.0)78,94,94
   94 IF(CC)98,98,95
 8 95 PRINT 96
   96 FORMAT(30H0 DR IS GREATER THAN ZERO STEP 95)
      GO TO 150
   98 NCCZ=NCCZ+1
 6    RW=RWO/RE
      IF(NOPRNT)105,105,135
 5 105 IF(ABSF((RAD-RW)/RW)-0.005)134,134,106
  106 NODRE=NODRE+1
 4    FR(NODRE)=RAD
      FDR(NCCRE)=CRE
 3
 2
```

F-10

```
      108  IF(NCDRE-2)11C,124,130
      110  XFACTR=C.01
      112  DRE=(RW-FR(1))/(XFACTR*Z)+FDR(1)
           IF(DRE)116,114,114
      114  XFACTR=XFACTR*2.0
           GO TO 112
      116  IF(ABSF((DRE-FDR(1))/FDR(1))-C.5)118,114,114
      118  GO TO 21
      124  CC2=(FDR(1)-FDR(2))/(FR(1)-FR(2))
           CC1=FDR(1)-CC2*FR(1)
           DRE=CC1+CC2*RW
      126  IF(DRE)118,127,127
      127  PRINT 128
      128  FORMAT(29HO DRE IS POSITIVE AT STEP 126)
           GO TO 165
      130  IF(NCDRE-8)603,134,134
      603  CC2=(FDR(NCDRE-1)-FDR(NCDRE))/(FR(NCDRE-1)-FR(NCDRE))
           CC1=FDR(NCDRE-1)-CC2*FR(NCDRE-1)
           DRE=CC1+CC2*RW
           GO TO 126
      134  NOPRNT =1
           PRINT 119
      119  FORMAT(1HO)
           GO TO 21
      135  NOTNSN=1
           GO TO 28
      136  N=11
           Z=Z+DZ
           DZ=100.0
           DT(11)=DTEMP
           TENSN1=-PRD*6.0*G/RE+SIGMAT*3.1417*RE*(COSF(ATANF(-DRE))-RAD*XX)+(
          1RHO/3.1417)*((G/RE)**2.0)*(1.0/(RAD*RAD)-1.0)+AIRDRG
           TENSN2=TENSN1+SIGMAT*3.1417*RE*RAD*XX
           T(N+1)=T(N)+(DZ/720.0)*(1901.0*DT(N)-2774.0*DT(N-1)+2616.0*DT(N-2)
          1-1274.0*DT(N-3)+251.0*DT(N-4))
      140  T(11)=T(12)
           TEMP=T(11)
           DO 141 N=7,10
      141  DT(N)=DT(N+1)
           PRINT 406,(ZDIMEN,RDIMEN,TDIMEN,Z,RAD,TEMP,U1,TENSN2,TENSN1)
           IF(TEMP*TE/TAMB-3.0)810,144,144
      144  IF(Z-300000.0)135,810,810
      810  IF(NUP)146,146,811
      811  NUP=2
           FINDZ=-FINDZ/2.0
           NOTNSN=0
           GO TO 21
      146  PRINT 147
      147  FORMAT(52HO THE PROGRAM HAS BEEN COMPLETED FOR ONE VALUE OF RW)
      150  GO TO 1
      160  PRINT 161,TU,TFILM,VISKIN,CL,CAIR,B1,B2,B3)
      161  FORMAT(1HO,8E15.6)
      162  GO TO 1
      165  IF(NODRE-2)166,166,170
      166  PRINT 167,(CC1,CC2,FDR(1),FDR(2),FR(1),FR(2),DRE,NODRE)
      167  FORMAT(1HO,7E15.6,I5)
```

```
      GO TO 1
  170 PRINT 171,(CRE,RW)
  171 FORMAT(1HC,2E15.6)
      GO TO 1
```

```
*      LABEL
CGAMAVG1
       SUBROUTINE GAMAVG(G,TEMP,TE,RAD,AL,GAVG,N)
       DIMENSION G(20)
       DO 1 J=18,20
 1     G(J)=G(17)
       GAVG=0.0
       DO 520 J=1,19
       GA=(G(J)+G(J+1))/2.0
       DLAM=J
       DLAM=DLAM/2.0-0.5
       IR=0
       GO TO 530
 506   IR=1
       P1=P
       DLAM=DLAM+0.5
       GO TO 530
 507   P=P-P1
 508   IF(GA*RAD*AL-1.0)509,510,510
 509   TOTRD1=P*GA
       GO TO 520
 510   TOTRD1=P*0.44/(RAD*AL)
       IF(N)520,520,500
 500   TOTRD1=0.0
 520   GAVG=GAVG+TOTRD1
       GO TO 560
 530   TABS=TEMP*TE+459.6
       TL=DLAM*TABS
       IF(TL-1.6E+03)531,532,532
 532   IF(TL-3.4E+03)533,534,534
 531   P=0.0
       GO TO 550
 534   IF(TL-14.4E+03)535,536,536
 533   XT=0.01*TL-16.0
       P=+0.01*(0.01-0.132*XT+0.02292*(XT)**2.0)
       GO TO 550
 535   XT=0.001*TL-3.4
       P=.01*(5.06+12.029*XT-0.059177*XT*XT-0.054597*(XT)**3.0+0.001918*(
      1XT)**4.0)
       GO TO 550
 536   XT=0.001*TL-14.4
       P=1.08361-0.0037916*XT-0.22731*EXPF(-XT/10.0)
 550   IF(IR)506,506,507
 560   RETURN
       END
```

```
*       LABEL
CVIEW
        SUBROUTINE VIEWFC(A,AL,T0,R0,G,TE,RAD,FVIEWG)
        DIMENSION G(20),FVIEW(4)
        N=1
        NN=1
        R01=R0
        TEMP=T0
 1      Z=A*AL
 4      FVIEWA=0.5*(1.0-1.0/((1.0+(R0/Z)**2.0)**0.5))
        FVIEW(N)=FVIEWA
 6      CALL GAMAVG(G,TEMP,TE,RAD,AL,GAVG,NN)
        IF(N-2)10,20,40
 10     N=2
        NN=0
        FVWG1=FVIEWA*GAVG*(TEMP+459.6/TE)**4.0
 12     TEMP=T0+50.0/TE
        R0=0.476
        Z=Z+0.381
        GO TO 4
 20     N=3
        IF(FVIEW(2)-FVIEW(1))30,30,25
 25     FVWG2=(FVIEW(2)-FVIEW(1))*GAVG*(TEMP+459.6/TE)**4.0
        GO TO 32
 30     FVWG2=0.0
 32     TEMP=T0-300.0/TE
        R0=0.889
        Z=Z+0.178
        GO TO 4
 40     IF(FVIEW(3)-FVIEW(2))41,41,42
 41     FVWG3=0.0
        GO TO 50
 42     IF(FVIEW(3)-FVIEW(1))41,41,45
 45     FVWG3=(FVIEW(3)-FVIEW(2))*GAVG*(TEMP+459.6/TE)**4.0
 50     FVIEWG=FVWG1+FVWG2+FVWG3
        R0=R01
 100    RETURN
        END
```

APPENDIX G

ADDITIONAL FIGURES

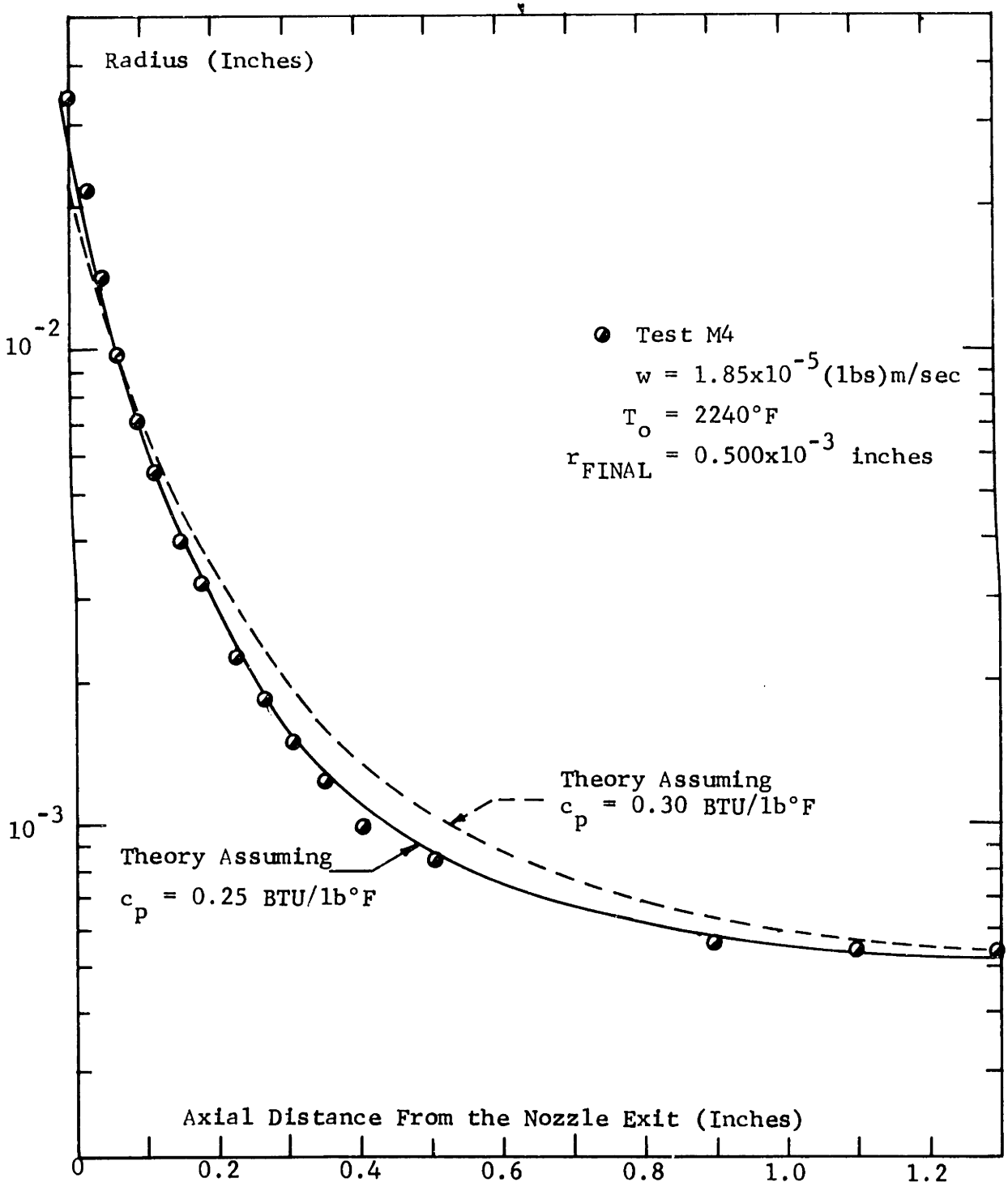

Fig. G-1

JET RADIUS VERSUS DISTANCE
THEORETICAL AND EXPERIMENTAL RESULTS

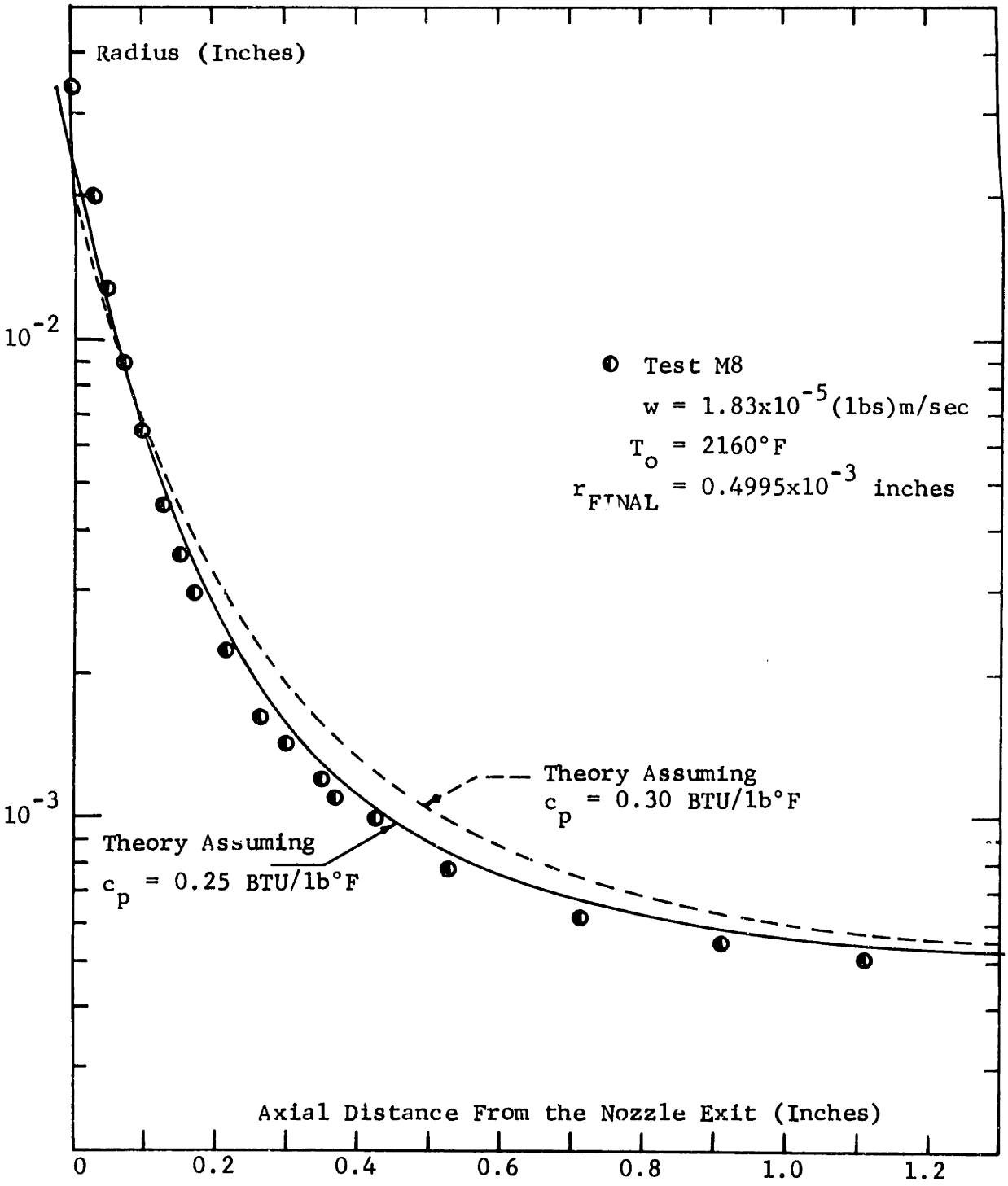

Fig. G-2

JET RADIUS VERSUS DISTANCE
THEORETICAL AND EXPERIMENTAL RESULTS

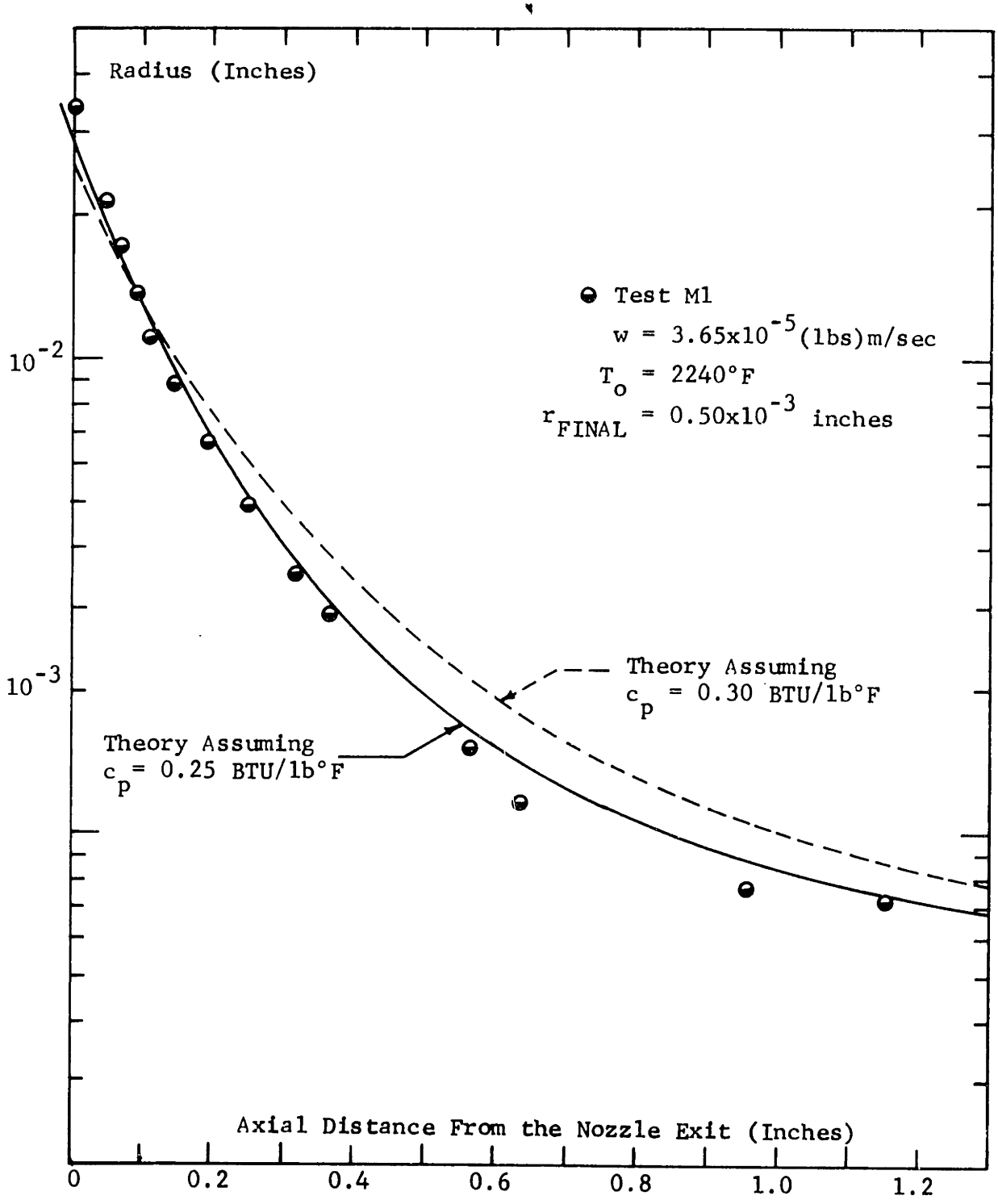

Fig. G-3

JET RADIUS VERSUS DISTANCE
THEORETICAL AND EXPERIMENTAL RESULTS

BIOGRAPHICAL NOTE

The author, Leon Robert Glicksman, was born May 12, 1938 in Chicago, Illinois. He attended Thomas Jefferson High School in San Antonio, Texas, graduating in 1955.

He entered the Massachusetts Institute of Technology in 1955 and graduated in 1959 with the degree of Bachelor of Science in Mechanical Engineering.

He entered Stanford University in 1959 and graduated in 1960 with the degree of Master of Science in Mechanical Engineering.

Returning to the Massachusetts Institute of Technology in 1960, he served as a research assistant for one year and as a teaching assistant the following year in the Department of Mechanical Engineering. From 1962 to the present the author has been an Instructor in the Department of Mechanical Engineering.

He was elected to the Society of the Sigma Xi in 1963. He has worked for Curtis-Wright Corporation and General Electric Corporation.